DEVELOPMENT OF DESIGN AID FOR SLENDER REINFORCED CONCRETE BEARING WALL

BY ANDUALEM DERESSE

MASTER OF SCIENCE

ADDIS ABABA SCIENCE AND TECHNOLOGY UNIVERSITY

ADDIS ABABA, OCTOBER 2018

DEVELOPMENT OF DESIGN AID FOR SLENDER REINFORCED CONCRETE BEARING WALL

A thesis

Submitted by

ANDUALEM DERESSE

(GSR 0086/08)

In partial fulfillment of the requirements for

the award of the degree

of

MASTER OF SCIENCE

In

STRUCTURAL ENGINEERING

Under the Guidance of: Dr. Temesgen Wondimu

ADDIS ABABA SCIENCE AND TECHNOLOGY UNIVERSITY

DEPARTMENT OF CIVIL ENGINEERING

DECLARATION

I hereby declare that this thesis entitled "**Development of Design Aid for Slender Reinforced Concrete Bearing Wall**" was composed by myself, with the guidance of my advisor, that the work contained herein is my own except where explicitly stated otherwise in the text, and that this work has not been submitted, in whole or in part, for any other degrees or processional qualification.

Andualem Deresse

Addis Ababa Science and Technology University

CERTIFICATE

This is to certify that the thesis prepared by **Andualem Deresse** entitled "**Development of Design Aid for Slender Reinforced Concrete Bearing Wall"** and submitted to Addis Ababa science and Technology University for the award of the degree of Master of Science complies with the regulations of the University and meets the accepted standards with respect to originality and quality. The contents of this thesis, in full or in parts, have not been submitted to any other Institute or University for the award of any other degree.

Date of Defense: October 20, 2018

Principal Advisor

Dr. Temesgen Wondimu	_____	_____
	Signature	Date

Members of the Examining board:

1. Dr. Nigatu Chaffo	_____	_____
External Examiner	Signature	Date
2. Dr. Tesfaye Alemu	_____	_____
Internal Examiner	Signature	Date
3. Mr. Seifu Sisay	_____	_____
Head, Civil Eng'g Department	Signature	Date
4. Dr. Brook Abate	_____	_____
Dean, College of Architecture And Civil Engineering	Signature	Date
5. Dr. Melaku Sisay	_____	_____
ERA.PG Program coordinator	Signature	Date

ABSTRACT

Non-rectangular shaped reinforced concrete members subjected to uniaxial or biaxial bending with axial compression are frequently used in different structures like tall buildings and bridge piers.

This thesis is concerned with finite element modeling of axially loaded reinforced concrete L-shaped and C-shaped walls in both concentric and eccentric loading conditions to determine walls' axial load carrying capacity. Finite element modelling is carried out by ABAQUS software with concrete damaged plasticity constitutive relation for concrete material. Concrete stress-strain relation for nonlinear analysis specified in EBCS EN 1992-1-1 2013 is used. Reinforcement steel is modelled up to plastic stage.

Validation of the software is conducted by comparing empirical equation answers with analysis results (primary validation) and by comparing test results of RC column with that of analysis results (supportive validation) to insure the accuracy of the outcomes.

The considered reinforced concrete member is pin ended with embedded constraint condition between concrete and reinforcement steel. To reduce convergence problem, rigid body constraint is used between the member and the reference point at which the load is applied.

Axial load capacity of the wall for different loading condition is extracted from analysis. Then moment capacity is calculated by multiplying the axial load with eccentricity including mid height lateral deflection.

The reduction of axial load capacity with increment of slenderness ratio is found to be observable. The axial stress variation with eccentricity is also significantly observed from the axial stress distribution.

Finally smooth P-M interaction diagram of considered bearing walls are plotted for different slenderness ratio and steel ratio. Concrete grade of (fck=25MPa) and steel grade of (fy=420MPa) are used for modelling material in this thesis.

AKNOWLEDGMENT

Thanks to God for each and every success in my life and being hopeful of proceeding my future endeavor.

I would like to express my sincere gratitude to my advisor Dr. Temesgen Wondimu who has advised me determinedly throughout the progress of doing this thesis. Being my instructor, he also inspired me to be interested in the profession of structural engineering.

I am deeply grateful to my families and friends for their motivation to accomplish this thesis.

Besides, I would like to express the gratefulness of Ethiopian Roads Authority (ERA) to sponsor me this master education in collaboration with Addis Ababa Science and Technology University.

Table of Contents

ABSTRACT iv
AKNOWLEDGMENT v
List of Tables viii
List of Figures ix
Notations xii
CHAPTER ONE 1
1. INTRODUCTION 1
1.1. Back ground 1
1.2. Statement of problem 2
1.3. Objective 2
1.4. Scope 3
1.5. Thesis outline 3
CHAPTER TWO 4
2. LITERATURE REVIEW 4
2.1. Introduction 4
2.2. Slenderness classification of core walls 7
2.3. Capacity of bearing walls 10
2.4. Previous work reviews 12
2.5. Concrete constitutive model relations 28
CHAPTER THREE 32
3. METHODOLOGY 32
3.1. General 32
3.2. Stress-strain relation for non-linear structural analysis 32
3.3. Reinforcement provision of walls as per EBCS EN 1992-1-1:2013 39
3.4. Slenderness criterion for isolated members 40
3.5. Boundary conditions and Constraints 43
CHAPTER FOUR 45
4. VALIDATION 45
4.1. Definition of validation 45
4.2. Validation one 46
4.3. Validation two 48

CHAPTER FIVE 55
5. RESULT AND DISCUSSION 55
5.1. Load-mid height lateral displacement curve variation 56
5.2. Variation of axial stress distribution with variation of eccentricities 56
5.3. Effect of slenderness ratio on the P-M interaction diagram 63
CHAPTER SIX 66
6. CONCLUSION AND RECOMMENDATION 66
6.1. Conclusion 66
6.2. Recommendation 66
References 67
Appendix 70
Appendix A:P-M interaction diagrams of L-shaped walls for different cases 70
Appendix B: Material properties used to model reinforced concrete column and walls .. 82
Appendix C: Sample illustrations for concrete compression damage and axial stress distribution of C-shaped wall with variation of eccentricities. 90
Appendix D: Sample P-M interaction diagram plotting illustration for biaxial bending of L-shaped wall of klu/r=22 and ρ=0.032 94

List of Tables

Table 2-1. Thickness of structural component and material strength used in CSCSW test and FE modelling 19
Table 3-1. Fracture energy test results 35
Table 3-2. Aggregate sized based fracture energy coefficients 35
Table 4-1.Axial load capacity of short L-shaped wall from equation. 47
Table 4-2: Axial load capacity of short L-shaped wall from analysis for pin-pin end case 47
Table 4-3. Axial load capacity of short L-shaped wall from analysis for fixed-fixed end case. 47
Table 4-4. Comparison of axial load capacity from equation and analysis. 48
Table 4-5. Description of columns used for validation. 50
Table 4-6. Material properties of column used for validation. 50
Table 4-7. Comparison of maximum axial load capacities of columns used for validation. 51
Table 5-1. Considered walls for plotting P-M interaction diagram. 55

List of Figures

Figure 2-1. Typical moment-axial force interaction relationship for a channel-shaped shear wall 5
Figure 2-2. Interaction Diagram for axial compression and biaxial bending of rectangular reinforced concrete column..... 6
Figure 2-3. Examples of core lay out 9
Figure 2-4. End moments of wall from analysis (Mi) and from minimum eccentricity and slenderness effect (Madd) 9
Figure 2-5. Resistance of an axially loaded column 12
Figure 2-6. Cross section and stress-strain relation of channel section core wall at rotated neutral axis 14
Figure 2-7. (a) Wall cross section (b) elevation 16
Figure 2-8. (a) Labelling of different wall sections and line of action of the actuators (b) bidirectional displacement loading history 16
Figure 2-9. Geometric and Components detail of test specimen composite steel concrete shear wall (CSCSW-1)..... 18
Figure 2-10. (a) Comparison between Experimental and Numerical envelope curves (b) Comparison between Experimental and Numerical hysteretic response in terms of skeleton curve. 20
Figure 2-11. (a) MVLEM element (b) MVLEM rotation and displacement 21
Figure 2-12. Orackal and Wallace model details..... 21
Figure 2-13. Results of Orackal and Wallace model 22
Figure 2-14. Specimen detailing..... 22
Figure 2-15. Concrete constitutive model 23
Figure 2-16. Dodd-restrepo steel model 23
Figure 2-17. Analytical bilinear steel model 24
Figure 2-18. Meneggoto-pinto steel model 24
Figure 2-19. (a) dimension and detailing of tested and modeled beam (b) force-displacement curves of test result and analysis result 25
Figure 2-20. (a) Test specimens (b) Finite element models 26
Figure 2-21. Uniaxial concrete behavior 29

Figure 2-22. Fracture energy cracking model of concrete 29
Figure 2-23. Damage Plasticity uniaxial concrete compressive behavior 30
Figure 2-24. Damage plasticity tension response of concrete 31
Figure 2-25. Post failure stress-fracture energy curve 31
Figure 3-1. Schematic representative of the stress-strain relation of structural analysis (the use 0.4fcm for the definition of Ecm is approximate) 33
Figure 3-2. Post failure stress-fracture energy curve 34
Figure 3-3. Idealized (nominal) and design stress-strain diagram for reinforcing steel (for tension and compression)..... 37
Figure 3-4. (a) C3D8 element (b) T3D2 element 38
Figure 3-5. Examples of different buckling modes and corresponding effective lengths for isolated members 41
Figure 3-6. Direction of moments due to eccentrically loaded columns 42
Figure 3-7. Forces in deflected column 42
Figure 3-8. Boundary conditions notation in ABAQUS..... 43
Figure 3-9. Behavior of rigid body constraints 44
Figure 4-1.L-shaped wall detailing used for validation and to develop P-M interaction charts..... 46
Figure 4-2. Cross section and reinforcement detailing of column used for validation 49
Figure 4-3. Column setup, demec points and details 49
Figure 4-4. Axial load and mid height displacement relation comparison of (Hany A.Kottb et al., 2015) test result and analysis result for column S1-R..... 51
Figure 4-5. Axial load and mid height displacement relation comparison of (Hany A.Kottb et al., 2015) test result and analysis result for column S8-St8. 52
Figure 4-6. Axial load and mid height displacement relation comparison of (Hany A.Kottb et al., 2015) test result and analysis result for column S9-St10. 52
Figure 4-7. Axial load and mid height compressive strain relation comparison of (Hany A.Kottb et al., 2015) test result and analysis result for column S1-R..... 53
Figure 4-8. Axial load and mid height compressive strain relation comparison of (Hany A.Kottb et al., 2015) test result and analysis result for column S8-St8..... 53

Figure 4-9. Axial load and mid height compressive strain relation comparison of (Hany A. Kottb et al., 2015) test result and analysis result for column S9-St10. 54
Figure 5-1. Considered cross section and detailing of L-shaped reinforced concrete wall for analysis (all dimensions in mm). 55
Figure 5-2. Variation of load –mid height displacement with eccentricities for L-shaped wall with klu/r=22 and ρ=0.032 56
Figure 5-3.Variation of concrete compression damage location with location of axial load . for wall with klu/r=22 and ρ=0.032. 57
Figure 5-4. Reinforcement steel stress distribution for concentric loads of L-shaped wall taken below mid height section with klu/r=22 and ρ=0.032. 58
Figure 5-5. Variation of axial stress distribution with eccentricities of reinforcement steel at mid height of wall with klu/r=22 and ρ=0.032. 59
Figure 5-6. Concrete stress distribution for concentric load of considered wall at the mid height 60
.Figure 5-7.Concrete stress distribution for eccentric load of considered wall at balanced failure at the mid height of the wall. 61
Figure 5-8. Concrete stress distribution for eccentric load of considered wall at flexural failure at the mid height of the wall 62
Figure 5-9.Increment of mid height deflection at maximum axial load level of L-shaped wall loaded uniaxialy with variation of slenderness ration for equal eccentricities. 63
Figure 5-10. Illustration of P-δ moment and Pe moment contribution to total moment on P-M interaction diagram keeping all parameters constant for L-shaped wall loaded biaxialy at 45°. 64
Figure 5-11. Illustration of Pe moment and P-δ moment independently for different slenderness ratio keeping all parameters constant for L-shaped wall loaded biaxialy 45°. 64
Figure 5-12. Stanadard and scaled down channel shaped core wall considered for finite element analysis (all dimension in mm) 65

Notations

P-Applied axial load

δ-Lateral mid height deflection for braced frame

ρ-Longitudinal steel ratio

Δ-End deflection for sway frame

$P_n(P)$-Value of axial load

$M_{nx}(M_x)$-Uniaxial moment about x-axis

$M_{ny}(M_y)$-Uniaxial moment about y-axis

λ-Inclination angle from x-axis for biaxial moment/slenderness ratio

f_{ck}-Cubic characteristic strength of concrete

f_{cm}-Mean compressive strength of concrete

ε_{cu} -The limiting compressive strain of concrete

ε_{yd}-The yield strain of reinforcement steel

ε_b -Ttrain value of the least compressed steel.

$\varepsilon_c(y)$- The strain at 'y' distance from the x-axis

y_{max}- The perpendicular distance between the local x-axis and the most compressed fiber.

c - The perpendicular distance between the neutral axis (NA) and the most compressed fiber.

μ-Displacement ductility

f_c'-Cylinder compressive strength of concrete

σ_c-Concrete compressive strength

σ_s-Steel compressive and tensile strength

σ_{ult}-Ultimate stress

F_{cu}-Cubic strength of cocncrete

ε_{ult}-Ultimate strain

ϕ- Curvature

Φ-Represents rotation/diameter

φ_{ef}-Effective creep ratio

A_s-The total area of longitudinal reinforcement

A_C-The area of concrete cross section

n-Relative normal force

r_m-Moment ratio

G_f-Fracture energy

σ_{to}-Maximum tensile strength of cocncrete

CHAPTER ONE

1. INTRODUCTION

1.1. Back ground

Non-rectangular shaped reinforced concrete members subjected to uniaxial or biaxial bending with axial compression are frequently used in different structures like tall buildings and bridge piers. Some of reinforced concrete members that carry uniaxial or biaxial bending and axial compression includes rectangular concrete columns, L-shaped concrete columns at corner of buildings and channel section elevator core walls to carry lateral loads and vertical loads. The same design method for all reinforced concrete section subjected to uniaxial or biaxial bending and axial compression cannot be used for all types of cross sections since the distribution of stresses induced on the cross section due to the loads is varied. Now a day's construction of high rise buildings is becoming congested following the rapid rate of population and their desire of better services. Reaching to higher stories on foot is tiresome and time wasting. Resisting larger lateral forces by beam to column frames is also ineffective. To solve this problems insertion of reinforced concrete structural walls in the buildings structural element with respective of its efficient location is relevant.

This thesis specifically focused on developing P-M interaction charts for channel section reinforced concrete slender core walls and L-shaped bearing walls by finite element analysis. Even though these reinforced concrete core walls are assemblage of orthogonally oriented walls, the whole cross-section is taken as a single member since they are casted as single and carry the loads together. Partial closure of core wall by beams or slabs across the opening restrain the core section from warping and increases the cores torsional stiffness while reducing its rotation stress. Reinforced concrete core walls carry gravity and lateral loads coming from beam and suspended floors in addition to supporting casing lifts. Quantifying the cross section of reinforced concrete members is based on the magnitude of loads (axial loads and moments) that the member is desired to carry. The variation of magnitudes of loads (uniaxial or biaxial bending and axial loads) induces different stress concentration to the reinforcement and concrete section with respective of the neutral axis of the section. In this thesis provision of adequate reinforced concrete section to resist axial

loads such as where they are internal walls supporting approximately symmetrical arrangement of slabs in such a way that the resistance of the section will not be exceeded by the stresses induced will be investigated. Slenderness of core wall is occurred when the longitudinal dimension of member is much greater than the transverse dimensions of the member so that deflection of axis of the core wall away from the chord joining the ends of the core wall (P- δ effect) and relative displacement of story joints (P- Δ effect) is induced.

1.2. Statement of problem

Up to my knowledge, in context of Ethiopia, there is not such axial load-moment interaction diagrams for channel section core walls and L-shaped reinforced concrete slender bearing walls. They are designed by trial and error methods. Investigation of an accurate and rapid design method is expected to be existed to standardize our design technique.

1.3. Objective

1.3.1. General Objective

In design reinforced concrete section reinforcement pattern could be assumed and the reinforcement area successively corrected until the section capacity approached the required value. There for the direct use of the equation in design is tiresome and laborious. The general objective of this thesis is to investigate reinforced concrete core walls section capacity subjected to axial force and biaxial bending.

1.3.2. Specific Objective

The strength of reinforced concrete section with uniaxial and biaxial bending can be illustrated by interaction surfaces. The specific objective of this thesis is to develop P-M interaction chart for channel section reinforced concrete core walls and L-shaped bearing walls considering slenderness effect by extracting failure concentric and eccentric axial loads from ABAQUS finite element modeling and analysis software results. After completion of this thesis a smooth axial load and bending moment interaction curve is expected for slender reinforced concrete core wall which will later help as design aid. C-shaped and L-shaped slender core walls will be modeled and investigated.

1.4. Scope

The scope of the research is up to developing P-M interaction diagram for designing channel section slender reinforced concrete core walls and L-shaped bearing walls. Material properties and stress-strain relationship of both concrete and reinforcement steel for modelling will be as per EBCS EN 1992-1-1:2013.

1.5. Thesis outline

The second chapter discusses different theories of isolated reinforced concrete walls including their slenderness classification from different reviews. In this chapter concrete constitutive model relations for finite element modeling of reinforced concrete members is also discussed.

The third chapter presents how concrete and reinforcement steel are modeled for nonlinear finite element analysis in ABAQUS software. In this chapter the slenderness criterion for isolated rein forced concrete members with boundary conditions and constraints to be used specifically for this thesis is also presented.

The fourth chapter describes validation of ABAQUS software to insure the accuracy of its output. For validation tested reinforced concrete column results are compared with ABAQUS software results and the result are found to be approached well. Concentric load capacity L-shaped reinforced concrete walls are also compared with results from empirical formulas and finally the results became soundly agreed.

The fifth chapter explains results from finite element analysis. In this chapter how eccentricities and slenderness ratio affect the axial stress distribution and axial load capacity of reinforced concrete wall is illustrated.

The last chapter deals about conclusion and recommendation of this thesis.

CHAPTER TWO

2. LITERATURE REVIEW

2.1. Introduction

Reinforced concrete (RC) buildings often have vertical reinforced concrete walls in addition to slabs, beams and columns. These walls generally start at foundation level and are continuous throughout the building height. Their thickness can be determined by code requirement for minima to ensure pouring of wet concrete or to satisfy fire rating in addition to deflection requirements. When earthquake forces are significant, it may require to increase the thickness. These walls transfer both lateral and gravity loads to the foundation. Walls carrying vertical loads should be designed as columns (The Inistitution of Structural Engineers, 2000).

A single rectangular cantilever shear wall can be expected to behave essentially in the same way as a reinforced concrete beam. In narrower cross-section, problem of instability of the compression edge may arise. Normally, the floor slabs of the multi-story building act as horizontal diaphragm and will provide lateral support, thus the critical length with respect to buckling may be taken as being equal to the floor height (T.POULAY&R.PARK, 1974).The shear wall as large cantilever, will be subjected to bending moments and shear forces originating from lateral loads and axial compression caused by gravity. Accordingly the strength of the critical section across the wall can be evaluated from moment-axial force interaction relationship. There is no reason to expect slender flanged shear walls to behave differently from those having rectangular cross-sections (T.POULAY&R.PARK, 1974).When the axial compression is significant, the whole of the flange and part of the web may be in compression. In such cases it appears advisable to consider the flanges as axially tied columns.

Cross-section of flanged, angle or channel shapes often appear in shear walls, forming the cores of multi-story buildings. These may be subjected to axial loads of varying intensity including net tension together with bending moment about one or both principal axes. For practical reason, the cross-section remains constant over the full height of the structures. It is possible and it may be advantageous to evaluate the interaction relationship between flexure and axial force for such cantilever shear walls and pin ended wall like wall panels

at mid stories. Failure due to crushing is basically material failure whereas due to buckling is geometry instability. Buckling is a failure of compression member at much lower stress than yield value. Buckling is also called as elastic instability. In slender compression member like bearing wall or column under vertical load, as the axial load increases they buckled and fails. This all happens while stress in material are much less than their yield value hence material is not fully utilized. Wall buckling is a phenomenon that has generally been related with wall slenderness. Buckling of longitudinal bar is a common form of damage in reinforced concrete structures subjected to earth quakes. When parts of the wall are subjected to compressive strain, the possibility of lateral instability arises. Basically buckling tendency is assumed to depend mostly on the wall clear height to thick ness ratio (for rectangular reinforced wall) and loading history. When channel shaped cross section is subjected to axial load and flexure about its weak principal axis, there is an interaction between axial load and bending moment capacities with the location of applied axial load.

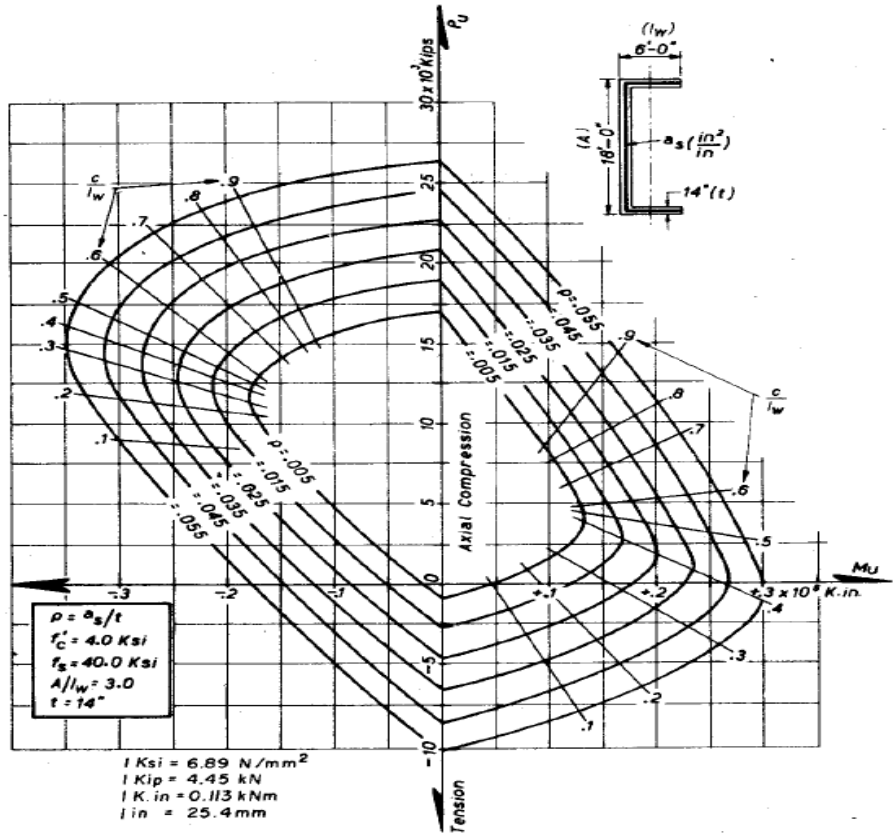

Figure 2-1. Typical moment-axial force interaction relationship for a channel-shaped shear wall *(T.POULAY&R.PARK, 1974)*

For structural analysis core walls can be modeled as vertical beam element (S.S.Ray, 1995). A typical axial load and bending moment interaction diagram depicts all combination of axial load and bending moments which correspond to prescribe limit state. Interaction diagrams can be plotted from finite element modeling and analyses results. Finite element modeling is an important tool in structural engineering that can eliminate the extensive physical resources and time requirement in experimental investigation.

Shear walls have been studied for a variety of conditions. However, analysis and experimental testing of shear walls has almost always assumed that a wall is supported by a rigid foundation, such as a block wall. Shear walls are also supported by non-rigid foundations, such as floor joists (horizontal supporting members that run between foundations, walls or beams to support the floor) and stud walls (vertical framing member in a building's wall of smaller cross-section than post), which would significantly reduce the stiffness at the foundation of the wall. This could have a significant effect on the stiffness of the entire wall system, possibly resulting in increased lateral displacement of the wall and variations in the dynamic base shear.

In case of rectangular solid column cross section subjected to both axial load and uniaxial or biaxial bending moment the failure surface of the cross section excluding slenderness effect is plotted as shown in Figure 2-2.

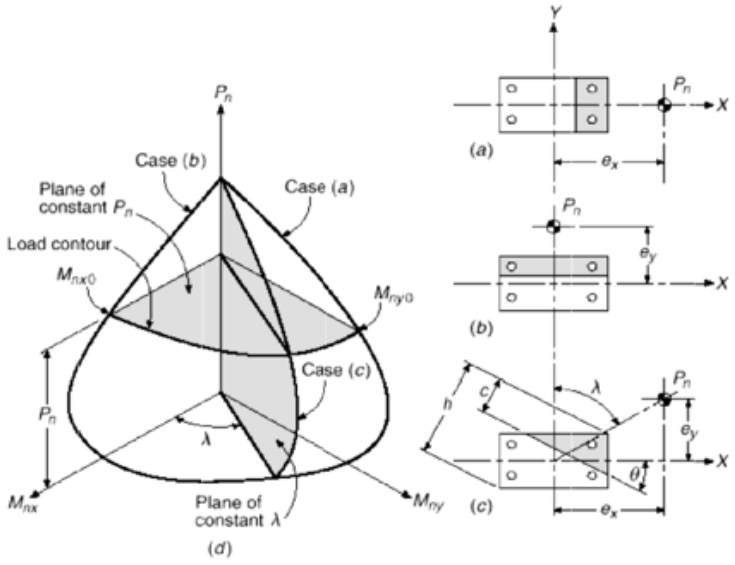

Figure 2-2. Interaction Diagram for axial compression and biaxial bending of rectangular reinforced concrete column *(Asnakew Abebe, 2009)*

In the illustration Figure 2-2:

Case a shows a failure envelope of axial force P_n and uniaxial moment M_{ny}

Case b shows a failure envelope of axial force P_n and uniaxial moment M_{nx}

Case c shows a failure envelope of axial force P_n and biaxial moment M_{nx} and M_{ny} for constant inclination angle λ, $\lambda = tan^{-1}\frac{M_{ny}}{M_{nx}} = tan^{-1}\frac{e_x}{e_y}$.

2.2. Slenderness classification of core walls

A reinforced concrete wall is a vertical load bearing member whose greater lateral dimension is more than four times its least lateral dimension and in which the reinforcement is taken in two accounts when considering its strength. Where there are no possibilities of using common shear wall due to the economic or structural and architectural issues, thin shear walls instead of column and common shear walls are used throughout the structure of the building (Sabetahd, Reza Bagerzadeh Karimi, & Sadeg bagerzadeh, 2012).

A wall may be considered short when the ratio of its effective height to its thickness does not exceed 7.It shall otherwise be considered slender (EBCS2, 1995).

Slender walls are those whose height to length ratio is greater than 2 (EBCS-8, 1995).

The ratio of the effective height of stocky walls to their thickness should be 15 or less. The thick ness should not be less than 150mm but to facilitate concreting 180mm is preferable (The Inistitutions of Structural Engineers, 1985).

Stocky wall is where the height divided by thickness does not exceed 15 for braced wall and 10 for an unbraced wall. Slender wall is a wall other than a stocky wall (S.S.Ray, 1995).

Shear walls with height of wall to length of wall ratio greater than or equal to 3 are referred to as slender or flexural walls (JAMES K.WIGHT & GAMES G.MACGREGOR, 2012).

If the ratio of the effective height of the wall to its thickness exceeds $7.2l\left(2-\frac{M_1}{M_2}\right)$, then the wall is slender (The Inistitution of Structural Engineers, 2000). Where M_2 is numerically larger end moment,M_1 numerically smaller end moment and l is height of the wall.

For flanged walls the depth of an outstand clearly has a considerable restraining effect on the stability of the adjacent planar section of a wall in compression. As described by

(A.W.Irwin, 1984), the instability of plate which is simply supported on all four sides is defined from classical buckling theory by an effective height (h_e) of:

$$h_e = \frac{h}{\sqrt{1 + \frac{kh^2}{L^2}}} \ldots\ldots\ldots\ldots\ldots\ldots\ldots\ldots\ldots\ldots\ldots\ldots\ldots\ldots 2.1$$

Where L is the length of the wall element and h is the wall height between floors.

The instability of a plate which is simply supported on three sides and free on one longitudinal edge (as for out stand of width) is defined by an effective height of:

$$h_e = \frac{h}{\sqrt{1 + \frac{0.46kh^2}{B^2}}} \ldots\ldots\ldots\ldots\ldots\ldots\ldots\ldots\ldots\ldots\ldots\ldots\ldots 2.2$$

B is the width of the wall if it is outstand.

Because reinforced concrete walls do not behave in an ideally elastic manner, an efficiency factor k (<1) is included in this formula. It is suggested that k should be taken as 0.5 for wall height up to about 30t (A.W.Irwin, 1984). Where t is thickness of the wall.

The small width of slender wall section causes the problem of instability. Consequently the thickness at the critical region near the base of the wall must be chosen accordingly when considering the floor height as buckling length. The strength of such wall can be simply evaluated from conventional axial load-bending moment interaction relationship (T.PAULAY*, 1972).

Flanged ,angle or channel shaped cross-sections often appear in shear walls forming the cores of multistory buildings such section will be subjected to axial force including tension as well as bending moments about either of the principal axes. Because the overall dimension of the core walls remain constant throughout the height of the structure and because more than one load combination may be considered, it could be advantageous to construct interaction curve for axial and bending moments. The core walls normally form structural element through which the lifts move. Each building has its own core layout.

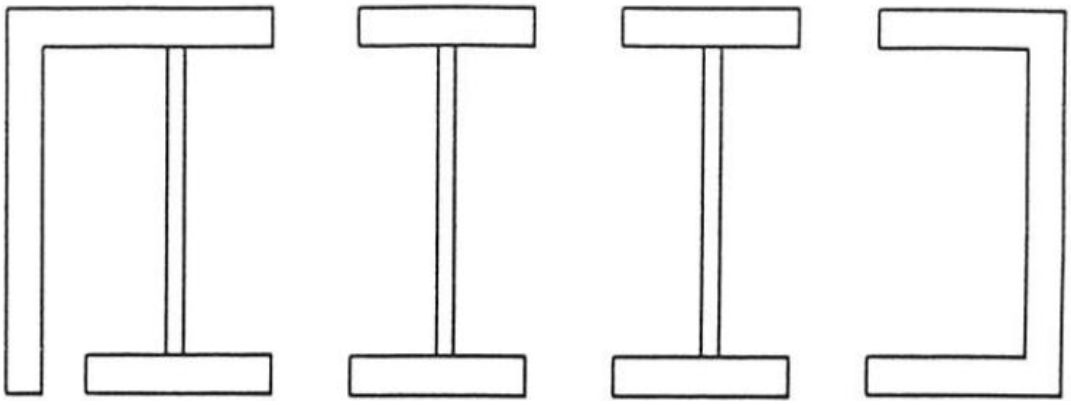

Figure 2-3. Examples of core lay out *(Mario M.Attard, 1994)*

The diaphragm walls of cores shown in figure 2-3 above are only restrained by interesting walls of their side (there are no intersecting floors).A diaphragm is a flat structural unit acting like a deep, thin beam. The term "diaphragm" is usually applied to roof and floors. A shear wall however is a vertical cantilevered diaphragm. The critical slenderness of these walls is therefore the horizontal span to thickness ratio. Australian standard for concrete structures (AS3600) limits the slenderness ratio of 30 (Mario M.Attard, 1994). Economic benefits can be gained by using high strength concrete and reducing thickness which results wall having greater slenderness that require assessment of amplification effect of buckling. To take the full advantage of high strength concrete a more detailed assessment of effect of buckling are required incorporating the two way nature of bending in core walls.

Unbraced wall is designed to carry lateral loads in addition to vertical loads while that of braced walls do not carry any lateral loads (S.S.Ray, 1995).

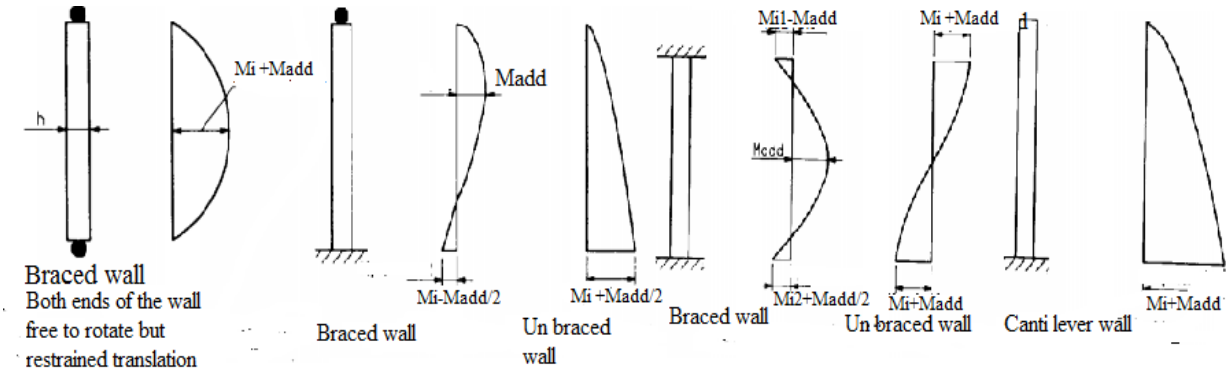

Figure 2-4. End moments of wall from analysis (Mi) and from minimum eccentricity and slenderness effect (Madd) *(S.S.Ray, 1995)*

2.3. Capacity of bearing walls

Bearing walls are primarily used to support gravity loads in buildings. As specified by (ACI committee 318, 2011),the design axial load capacity of rectangular reinforced concrete wall of eccentricity equal or less than one-sixth thickness of the wall is given by:

$$Øp_n = 0.55Øf_c' A_g \left(1 - \left(\frac{kl_c}{32h}\right)^2\right) \ldots\ldots\ldots\ldots\ldots\ldots\ldots\ldots\ldots 2.3$$

f_c' is specified compressive strength of concrete in psi.

l_c is clear vertical distance between supports in inch.

k is the effective length factor for a wall taken as 0.8 if the wall is braced against translation at both ends and top or bottom end is restrained against rotation, 1 if both ends are effectively hinged, 2 for walls which are not effectively braced against lateral translation at the top and therefore must be considered to be free standing.

h is the overall thickness of the wall in inch.

Ø is the strength reduction factor for compression centroid section taken equal to 0.65.

Thickness of bearing walls shall not be less than $\frac{1}{25}$ of he supported height or length whichever is shorter, nor less than 100mm.Thickness of non-bearing walls shall not be less than 100mm, nor less than $\frac{1}{30}$ of the least distance between members that provide lateral support (ACI committee 318, 2011). Minimum vertical ratio of reinforcement area to gross area is 0.0012 for deformed bar not less than No.16 with fy not less than 420 Mpa and 0.0015 for other deformed bar. Minimum horizontal ratio of reinforcement area to gross area is 0.002 for deformed bar not less than No.16 with fy not less than 420 Mpa and 0.0025 for other deformed bar.

As described by (Fragomeni, Doh, & Lee, 2012), for simplified design method, the ultimate design axial strength per unit length (N/mm) of a braced wall in compression is given by:

$$ØN_u = Ø(t_w - 1.2e - 2e_a)0.6f_c' \ldots\ldots\ldots\ldots\ldots\ldots\ldots 2.4$$

Where t_w is the thickness of wall (mm),e is the load eccentricity (mm) which has a minimum of $0.05t_w$,f_c' (Mpa) is concrete strength and $e_a = \frac{(H_{we})^2}{2500t_w}$.

$H_{we} = kH_w$is the effective height of the wall.

A. For one way buckling with floors providing lateral support at both ends, $k = 0.75$ when walls are restrained against rotation at both ends and $k = 1$ when the walls are not restrained against rotation at one or both ends.

B. For two way buckling with three side lateral support provided by floors and intersecting walls $k = \frac{1}{1+\left(\frac{H_w}{3L}\right)^2} \geq 0.3$ but less than obtained from A.

C. for two way buckling with four sides lateral support provided from floors and intersecting walls $k = \frac{1}{1+\left(\frac{H_w}{L}\right)^2}$ for H_w less than or equal to L or $k = \frac{L}{2H_w}$ for $H_w > L$ where H_w is floor to floor un supported height and L is horizontal length of the wall.

The strength reduction factor Ø is 0.6.The walls are required to have a minimum reinforcement ratios of 0.0015 vertically and 0.0025 horizontally.

When a symmetrical column is subjected to concentric axial load, longitudinal strains develop across the section, since concrete and steel are bonded together. Strain in concrete is similar to strain in steel.

As described in (JAMES K.WIGHT & GAMES G.MACGREGOR, 2012) the axial load capacity of tied column for well-defined yield strength is calculated as equation:

$$P_O = P_c + P_s = k_3 f_c'\left(A_g - A_{st}\right) + f_y A_{st} \ldots\ldots\ldots\ldots\ldots 2.5$$

Where $k_3 = 0.85$ as described in (ACI committee 318, 2011),$P_{c=}k_3 f_c'\left(A_g - A_{st}\right)$ is the load carried by concrete and $P_{S=}f_y A_{st}$ is the load carried by steel.

f_c' denotes compressive strength of concrete,f_y denotes yield strength of reinforcement steel,A_g represents gross area of concrete and A_{st} represents area of reinforcement steel.

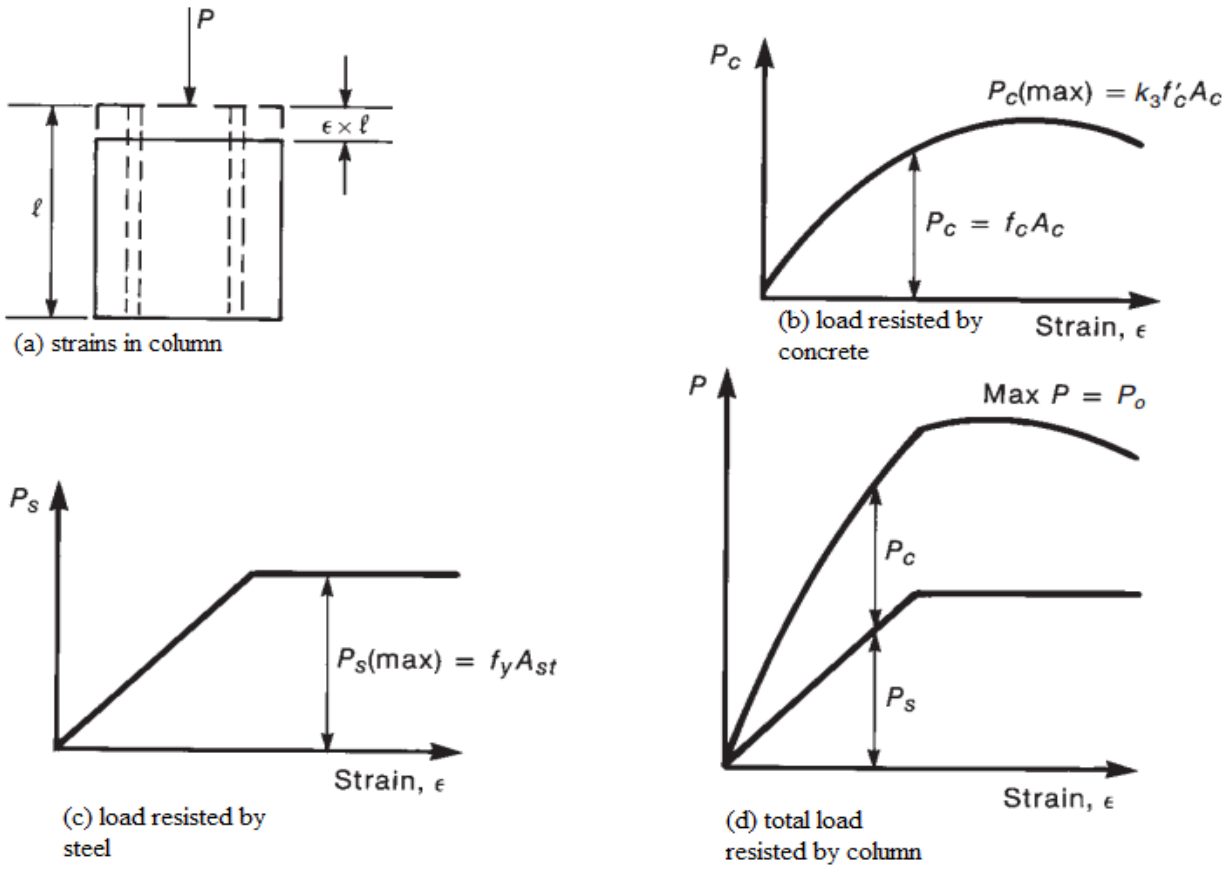

Figure 2-5. Resistance of an axially loaded column *(JAMES K.WIGHT & GAMES G.MACGREGOR, 2012)*

2.4. Previous work reviews

(Asnakew Abebe, 2009) Developed axial force and bending moment interaction diagram for channel shaped core walls based on the assumptions of EBCS 2-1995. Equilibrium equations and strain compatiplity equations were used to write general equation which can plot P-M interaction chart. After general equation were developed visual fortran-90 was used to develop a computer program. Assumptions taken in this research were:

a) The strain distribution in concrete and in the reinforcement whether in tension or compression, are derived from the assumption that plane sections normal to the axis remain plane after bending and there is no bond-ship between reinforcement steel and concrete, i.e. strain compatibility is assumed.

b) The tensile strength of concrete is ignored

c) The relationship between stress-strain distribution in concrete is assumed to be parabolic rectangular with maximum compressive stress equal to $\frac{0.67f_{ck}}{\gamma_c}$. where f_{ck} is characteristics compressive strength of concrete and γ_c is partial safety factor of concrete

d) The stresses in reinforcement are derived from the representative stress-strain curve for the type of steel used.

e) The maximum compressive strain in concrete in axial uniform compression is taken 0.002.

f) The maximum compression strain at the highly compressed extreme fiber in concrete subjected to axial compression and bending, but when there is no tension on the section, is taken, as 0.0035 minus 0.75 times the strain at the least compressed extreme fiber.

g) The maximum compressive strain at the highly compressed extreme fiber, when the neutral axis rests on the section in concrete subjected to axial compression and bending is taken as 0.0035. In the limiting case, when the neutral axis lies along one edge of the section, the strain varies from 0.0035 at the highly compressed edge to zero at the opposite edge.

h) The maximum strain in the reinforcement steel is 0.01.

In this research P-M interaction charts of channel section reinforced concrete core wall was developed by varying the neutral axis depth of a rotated section for different inclination angels ranging [0^0-180^0] from global X axis. Resultant stresses of concrete under compression were calculated from infinitesimal area, dA of shown in figure 2-6.

$$dN_c = f_c(y)dA \rightarrow N_c = \iint f_c\,(y)dA \dots\dots\dots\dots\dots\dots 2.6$$

$$dM_{xc} = -yf_c(y)dA \rightarrow M_{xc} = -\iint yf_c\,(y)dA \dots\dots\dots 2.7$$

$$dM_{yc} = xf_c(y)dA \rightarrow M_{yc} = \iint xf_c\,(y)dA \dots\dots\dots\dots 2.8$$

Resultant stresses of reinforcement were calculated as:

$$N_s = \sum_{J=1}^{N} A_{sj}\, f_{sj} \ldots\ldots\ldots\ldots\ldots\ldots\ldots\ldots\ldots\ldots\ldots\ldots\ldots\ldots 2.9$$

$$M_{xs} = \sum_{J=1}^{N} y_{sj} A_{sj}\, f_{sj} \ldots\ldots\ldots\ldots\ldots\ldots\ldots\ldots\ldots\ldots\ldots\ldots\ldots\ldots 2.10$$

$$M_{ys} = \sum_{J=1}^{N} x_{sj} A_{sj}\, f_{sj} \ldots\ldots\ldots\ldots\ldots\ldots\ldots\ldots\ldots\ldots\ldots\ldots\ldots\ldots 2.11$$

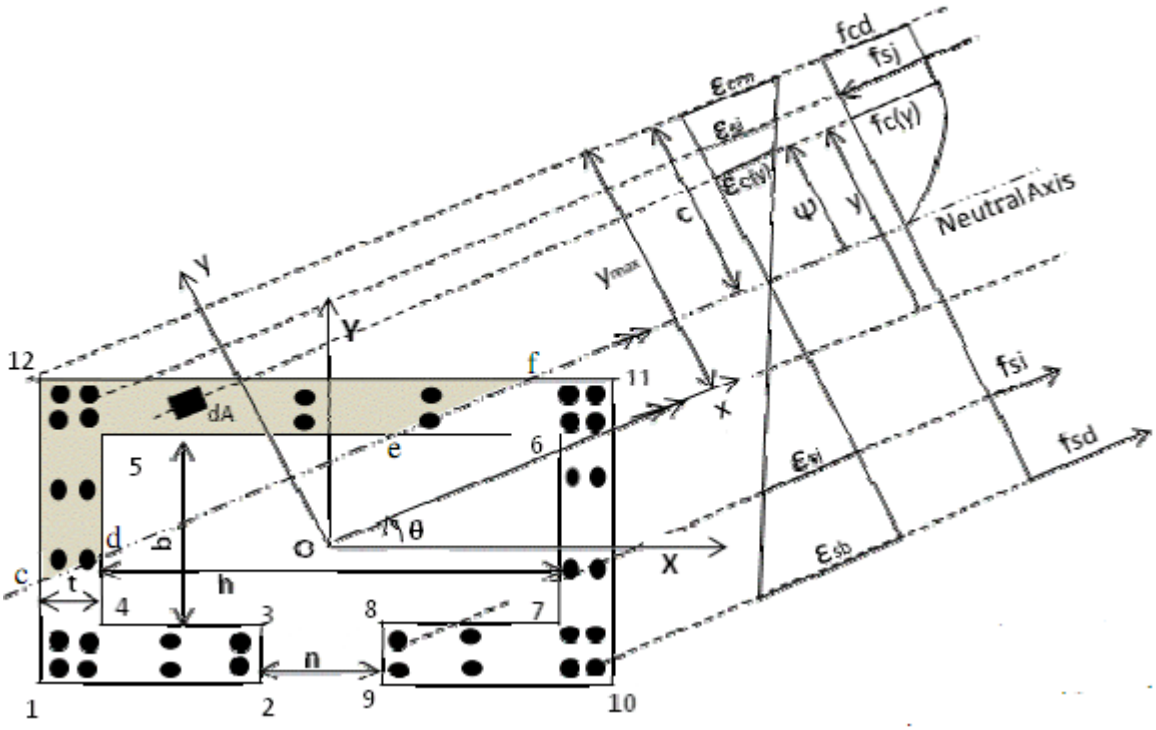

Figure 2-6. Cross section and stress-strain relation of channel section core wall at rotated neutral axis *(Asnakew Abebe, 2009)*

Total stress resultants about the global axes (X and Y) were calculated by resolving stresses in local coordinate system to global coordinate system.

$$p_n = N_C + N_S \ldots\ldots\ldots\ldots\ldots\ldots\ldots\ldots\ldots\ldots\ldots\ldots\ldots\ldots\ldots 2.12$$

$$M_{Xn} = (M_{xc} + M_{xs})\sin(\theta) + (M_{yc} + M_{ys})\cos(\theta) \ldots\ldots 2.13$$

$$M_{Yn} = (M_{xc} + M_{xs})\cos(\theta) + (M_{yc} + M_{ys})\sin(\theta) \ldots\ldots 2.14$$

A_{sj}-is the area of reinforcement bar j.

f_{sj}- is the stress on reinforcement bar j.

M_{xc} and M_{yc} are moment stress resultants of concrete about the local centroidal axis.

$M_{xs}$and M_{ys} are moment stress resultants of steel about the local centroidal axis.

M_{xn} and M_{yn} are moment capacities of the considered section about the centroidal global axes.

ε_{cu} -the limiting compressive strain of concrete

ε_{yd}-the yield strain of reinforcement steel

ε_b -strain value of the least compressed steel.

$\varepsilon_c(y)$- the strain at 'y' distance from the x-axis

y_{max}- the perpendicular distance between the local x-axis and the most compressed fiber.

c - the perpendicular distance between the neutral axis (NA) and the most compressed fiber. After equations were written visual fortran-90 was used to develop computer program.

(Jyoti S.Tekavde & S.S.Angalekar, 2016) Investigated the buckling behavior of rectangular reinforced concrete shear wall subjected to axial load by modeling using ANSYS finite element software. They have modelled a wall of 1450mm thickness and 4500mm height which has slenderness ratio (height/width) of 19.56. While modelling they use different steel ratio for constant slenderness ratio and they used different thickness (230mm and 300mm) keeping other parameters constant. Finally after they observed the load deformation behavior of their sample, they have concluded both thickness and steel ratio have influence on the buckling behavior of the rectangular reinforced concrete shear wall subjected to axial load.

(K.Beyer & R.Constantin, 2012) Investigated global as well as local behavior of U-shaped wall under bi-directional loading. To achieve their investigation they had compared their detailed finite element results to test results done by (Beyer et al., 2008a). The test unit

they considered during their investigation was wall of thickness 150mm whish's detailing and elevation is shown in Figure 2-7.

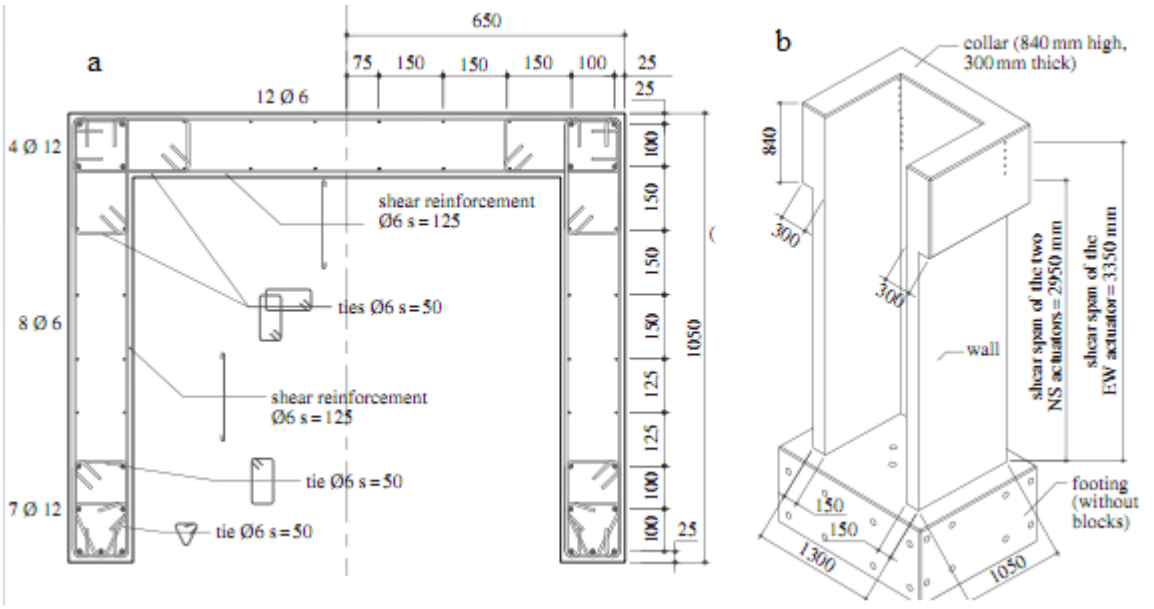

Figure 2-7. (a) Wall cross section (b) elevation *(K.Beyer & R.Constantin, 2012)*

The test unit was subjected different reverse cycle loading pattern parallel to the web, parallel to flange and diagonal direction. The pattern was repeated at different displacement ductility (μ) levels.

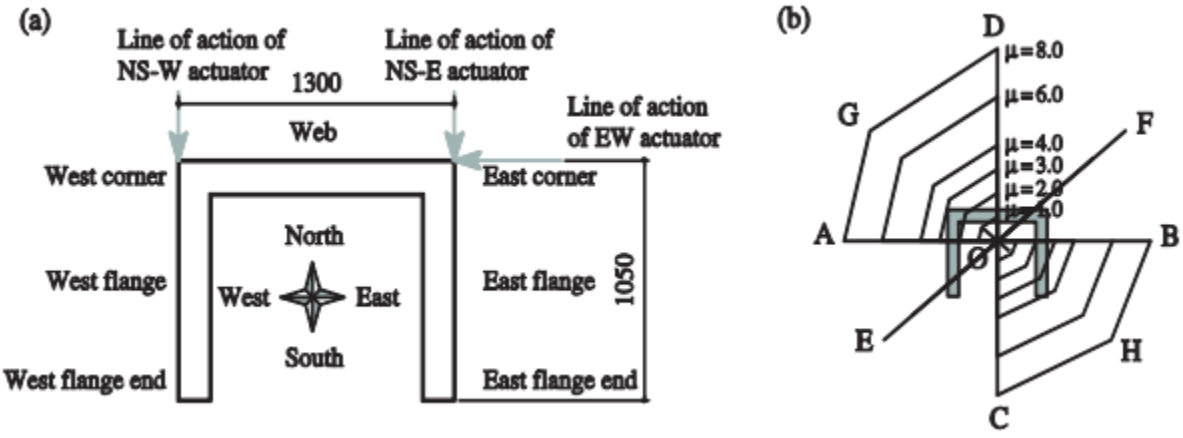

Figure 2-8. (a) Labelling of different wall sections and line of action of the actuators (b) bidirectional displacement loading history *(K.Beyer & R.Constantin, 2012)*,(all dimension in mm).

During the entire test, the axial force was maintained constant and the rotation of the top of the wall (the wall collar) was restrained by imposing equal displacements at the level of

the NS-W and the NS-E actuators. The numerical analyses have been performed using the nonlinear finite element analysis software VecTor4.The test unit was modelled using multi-layered rectangular shell elements. A number of eight concrete layers of equal thickness were used to model the thickness of the wall by constraining all degrees of freedom of its base. Input materials were from test results of reinforcement bar and cylindrical concrete strength. Perfect bond was assumed between concrete and reinforcement. Rotation was constrained at the top of the wall. Loading patterns were taken to be similar with that of the test. Globally, the force capacity and hysteresis shape of the test results and numerical modeling were found to be matched for those loading patterns parallel to web and flange. But for the diagonal loading pattern numerical results over estimates 25% of the test results. Locally, the strain measured from test result inside face of the wall over equal vertical distance 200mm from base of the wall was found to be matched with the strain at 170mm distance from base of the numerical modelling.

(AHMER, DOOKIE, & CHO., 2013) Investigated the reverse cyclic behavior of I-shaped composite steel-concrete shear walls (CSCSW) through nonlinear numerical studies. Equation (2.16) was adopted to calculate compressive behavior of concrete.

$$\sigma_c = \frac{f_c' \gamma \left(\frac{\varepsilon_c}{\varepsilon_c'}\right)}{\gamma - 1 \left(\frac{\varepsilon_c}{\varepsilon_c'}\right)^{\gamma}} \dots\dots\dots\dots\dots\dots\dots\dots\dots\dots\dots\dots\dots 2.16$$

Where σ_c is the compressive strength of concrete,ε_c is compressive strain of concrete,f_c' is cylinder compressive strength of concrete,$(\varepsilon_c' = 0.002)$ is strain corresponding to f_c' and γ is given by

$$\gamma = \left(\frac{f_c'}{32.4}\right)^3 + 1.5 \dots\dots\dots\dots\dots\dots\dots\dots\dots\dots\dots 2.17$$

Initially concrete behaves linearly up to the tensile stress of concrete and then material propagates towards the strain softening mechanism of the cracked concrete. In modelling steel, to account progressive hardening and softening effects, the steel was assumed to have bilinear kinematic hardening. In modelling concrete and steel plates by using ABAQUS software, 8-node solid element (C3D8R) was used and fixed all degrees of

freedom at the bottom. Illustrative test specimen which was modeled in finite element is shown in Figure 2-9.

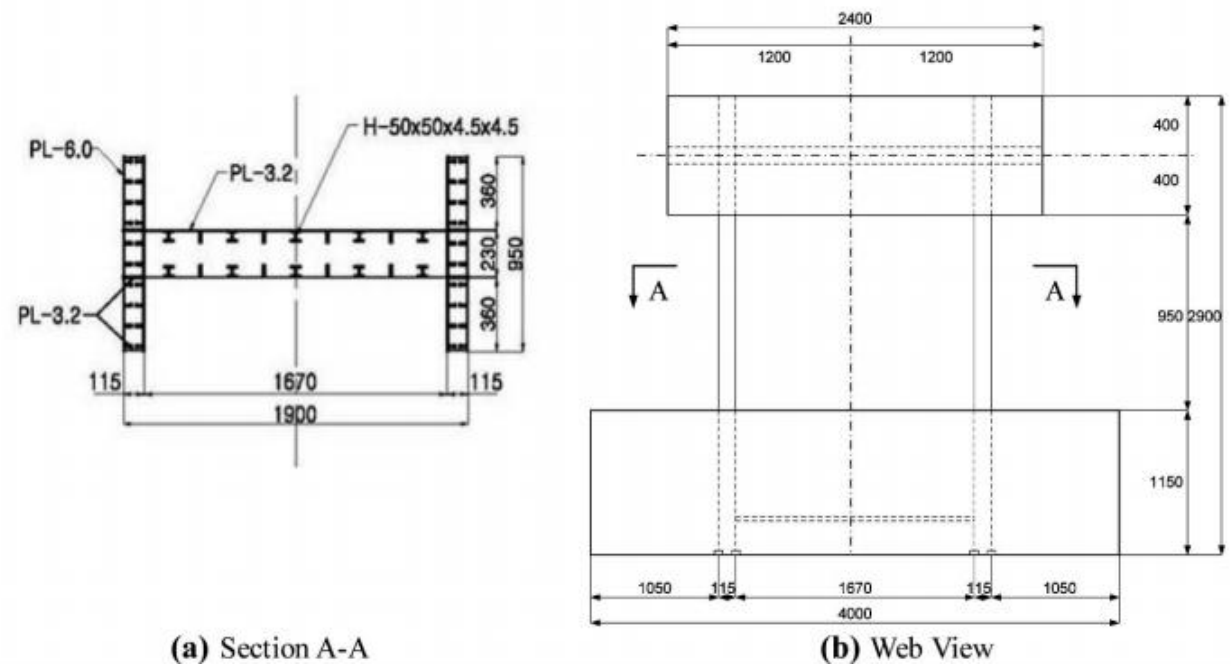

Figure 2-9. Geometric and Components detail of test specimen composite steel concrete shear wall (CSCSW-1), *(AHMER, DOOKIE, & CHO., 2013)*

Four identical I-shaped composite steel-concrete shear wall (CSCSW) specimens subjected to reverse cyclic loading were tested. Each specimen consists of a hybrid web and two flanges at its ends, supported by 1150 mm thick base slab. Horizontal displacement controlled loading to the shear walls was applied through 800 mm thick concrete slab over the top, acting as a boundary condition. Both base and top slabs have the plan dimensions of 4000 mm x 1500 mm and 2400 mm x 1500 mm, respectively. Moreover, steel plates were embedded in the flanges to strengthen the concrete. All the experimental models were geometrically symmetrical; besides, thickness of concrete was kept same in all test specimens. The only geometric variable was the steel thickness provided in the flanges of specimens CSCSW-1, 2 and 3 whereas web steel thickness was changed in the specimen CSCSW-4 as an expectance to notice the effect. The type of reversed cyclic lateral displacement was considered as another variable because ultimate and failure values were supposed to be different based on deformation capacities of the

test models. The standard strength tests were performed to grasp practical deformation behaviors of both steel and concrete. In conducting test, lateral load was applied at a quasi-static rate in displacement controlled cycles considering cracking, yielding and ultimate state as the major states. Linear transducers and strain gauges were placed in the middle top of the web to monitor the in- plane horizontal displacement and sequence of the yielding process.

Table 2-1. Thickness of structural component and material strength used in CSCSW test and FE modelling

specimen	Steel thickness(mm)		Concrete thickness(mm)		Steel yield strength(Mpa)	Steel tensile strength(Mpa)	Concrete cylinder compressive strength(Mpa)
	flange	web	flange	web			
CSCSW1	6	3.2	115	230	298.2	442.6	53.7
CSCSW2	4.5	3.2	115	230	323.9	479.3	48.9
CSCSW3	3.2	3.2	115	230	305.6	379.3	48.1
CSCSW4	3.2	6	115	230	305.6	379.3	44.1

Even though almost similar load-displacement curves were found from all specimens of their finite element modelling, increasing web thickness of steel much contributes to the load bearing capacity of the shear wall i.e. CSCSW4 was found to have larger load bearing capacity.

For validation CSCSW1 was considered. Finite element and test results were found to be agreed as shown in Figure 2-10.

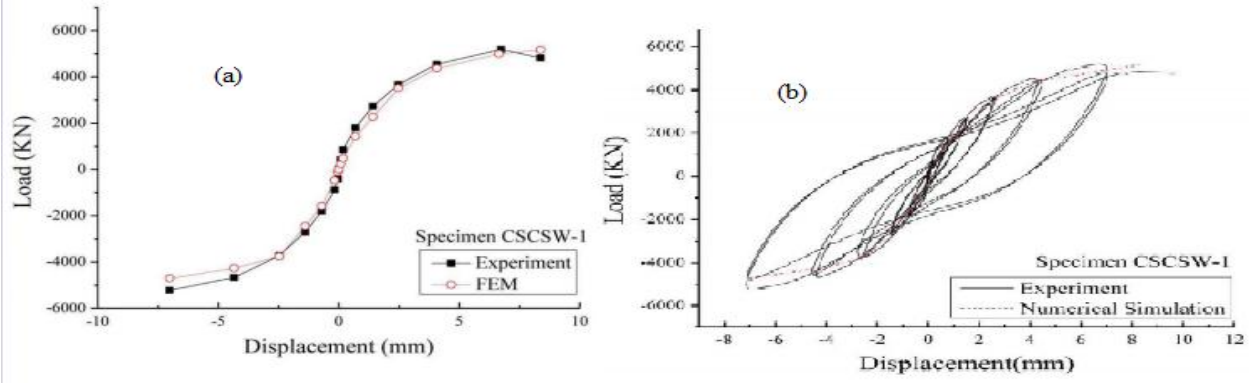

Figure 2-10. (a) Comparison between Experimental and Numerical envelope curves (b) Comparison between Experimental and Numerical hysteretic response in terms of skeleton curve.

Orakcal and Wallace (2006) present the most comprehensive study available on the ability of current modelling approaches to capture the cyclic response of relatively slender reinforced concrete walls for combined bending and axial load (W.WALLACE, 2007). An MVLE (Multiple vertical line element) model was employed in their study for walls subjected to reversed, cyclic, uni-axial loading. Multiple-vertical-line-element-model (MVLEM) was formulated to idealize a generic wall member as multiple vertical line elements with infinitely rigid beams at top and bottom floor levels. The MVLEM element command is used to simulate two dimensional flexure dominated reinforced concrete behavior. A single model element incorporates six global degrees of freedom, three of each located at the center of rigid top and bottom beams as illustrated in Figure 2-11. The axial/flexure response of the MVLEM is simulated by a series of uniaxial elements connected to the rigid beams at the top and bottom (e.g. floor) levels, whereas the shear response is described by the shear spring located at the height ch from the bottom of the wall element as shown in Figure 2-11. Outside element model with axial stiffness k_1 and km of the boundary column and interior elements with axial stiffness $k_2 \ldots k_{m-1}$ represent globally the axial and flexural stiffness values of the central panel. The horizontal spring with stiffness k_H and hysteretic behavior described by the oriented hysteresis model, simulated the nonlinear response of the wall element. The relative rotation between top and bottom faces of the wall element occurs about the point located on the central axis of the element at height ch. Rotation and resulting transverse displacement are calculated

based on the wall curvature, derived from section and material properties, corresponding to the bending moment at height ch of each element. A value of c=0.4 was recommended by vulcano et.al (1988) based on comparison of the model response with experimental results.

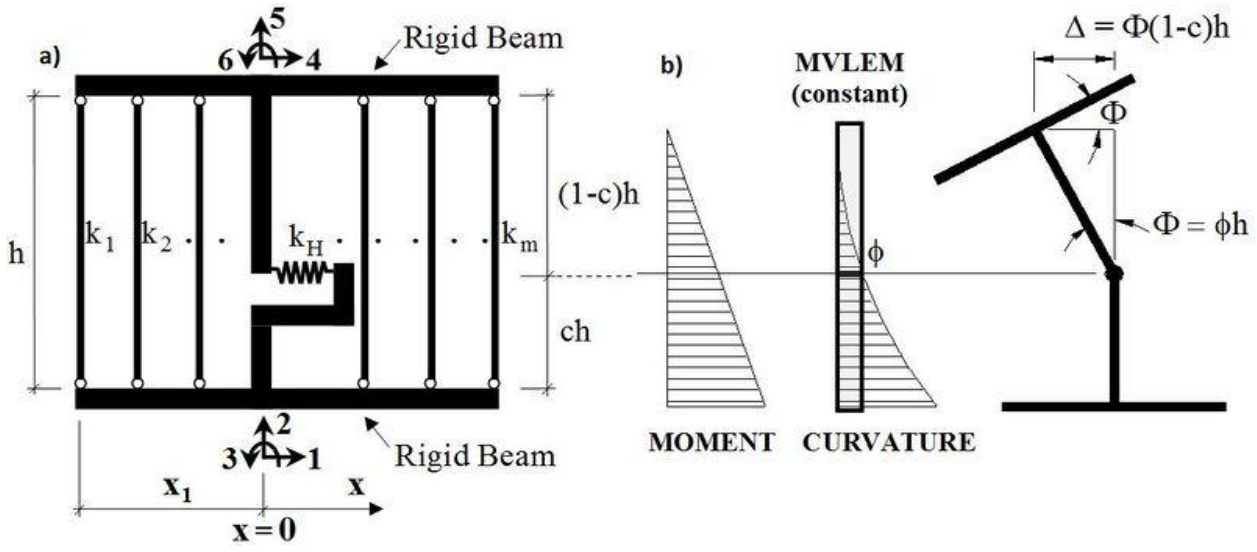

Figure 2-11. (a) MVLEM element (b) MVLEM rotation and displacement (vulcano et.al 1988)

ϕ-in the figure above represents curvature and Φ represents rotation where$\phi = \frac{M}{EI}$.

Some of the results of their study are shown in Figure 2-13 for a test of a 12-foot tall wall with a 4 foot by 48-inch cross-section subjected to constant axial load and reversed cyclic lateral displacements at the top of the wall.

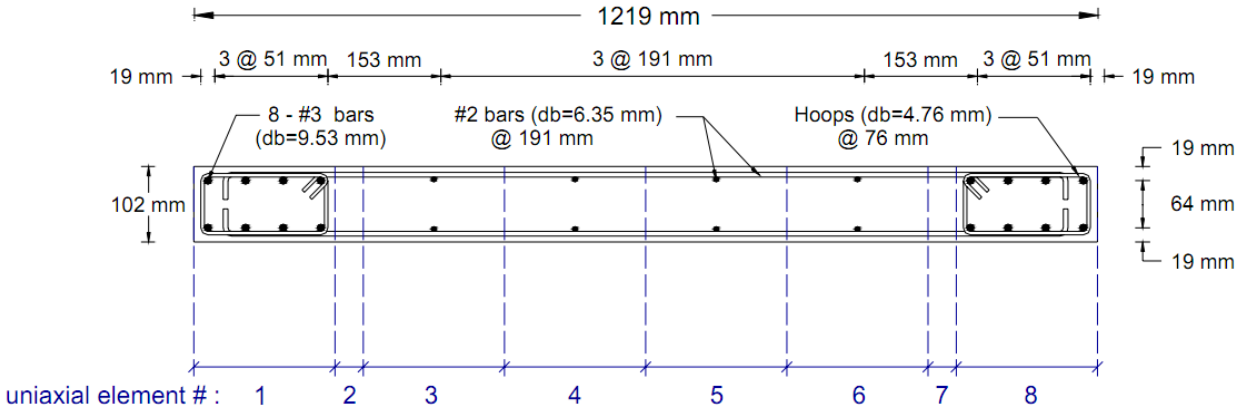

Figure 2-12. Orackal and Wallace model details

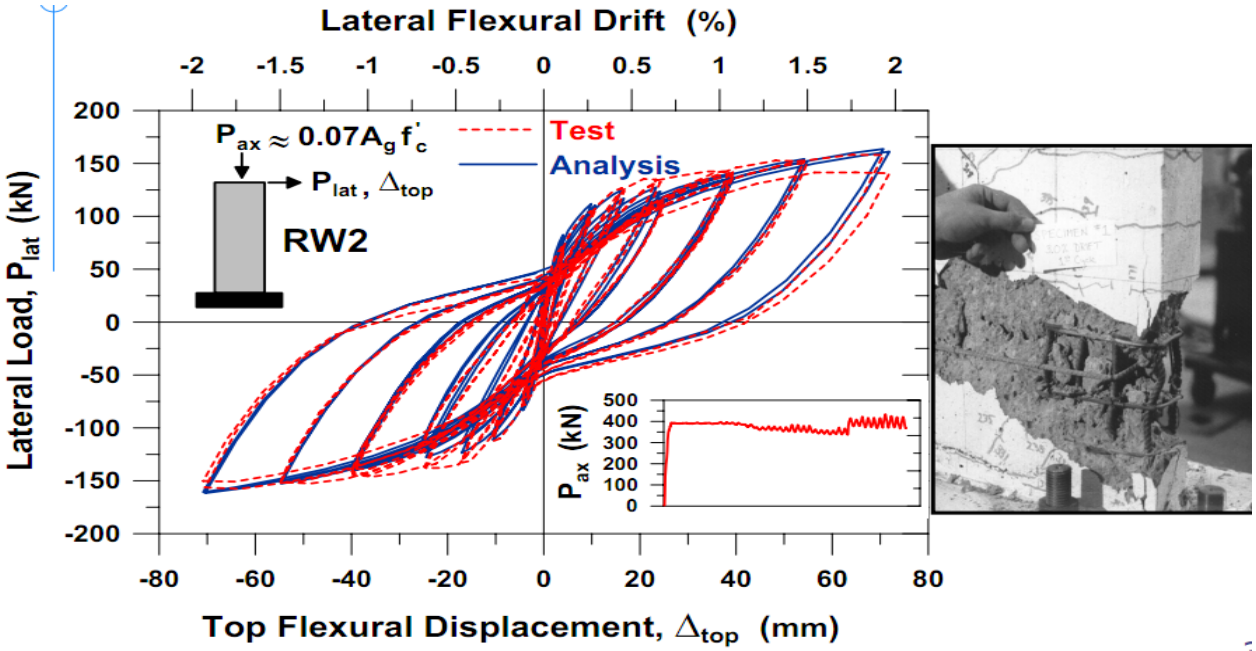

Figure 2-13. Results of Orackal and Wallace model

(Sosa, et al., 2017) Investigated the behavior of slender rectangular reinforced concrete shear wall of 4.2 m height on the applied load and length of 1.5m parallel to the direction of the applied load whose detailing is shown in Figure 2-14.

Figure 2-14. Specimen detailing of *(Sosa, et al., 2017).*

The wall was subjected to a cyclic in-plane lateral load and it is intended to use experimental results to make a fibre model using SeismoStruct. The proposed analytical model considers the shear wall as an inelastic frame force-based element, with nonlinear behavior of its materials, using constitutive models: bilinear steel model; Menegotto-Pinto steel model; Dodd-Restrepo steel model; and Mander et al. nonlinear concrete model .Finally the model establishes the best constitutive material combination that converges better with the experimental results. At the end of their test they have observed a huge horizontal crack at the base of the wall with yielding of reinforcing bar and spalling of

unconfined concrete which is the demonstration of flexural failure. In this study after using the three constitutive rebar constitutive models mentioned above with similar concrete model, Menegotto-Pinto steel model was found to fit well with experiments.

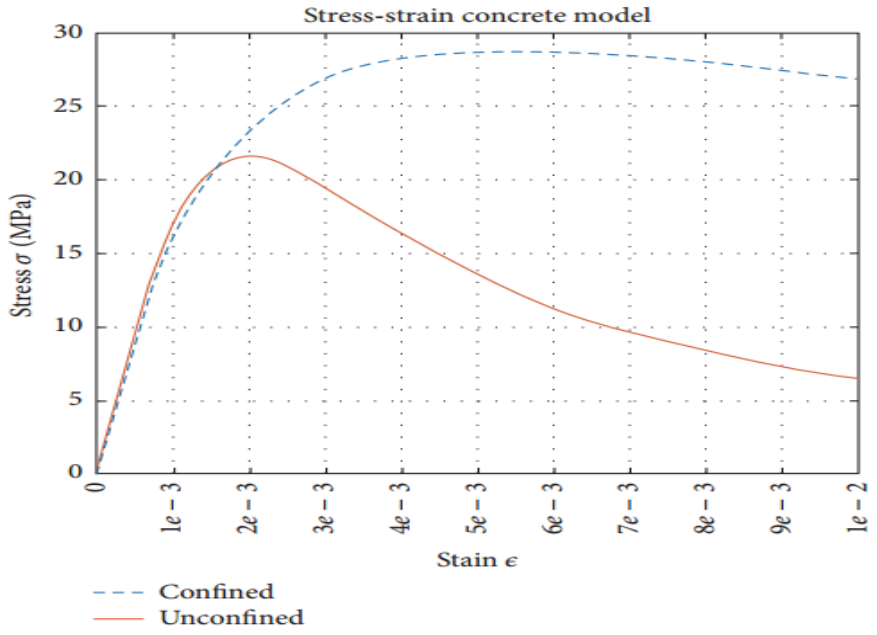

Figure 2-15. Concrete constitutive model used by *(Sosa, et al., 2017)*

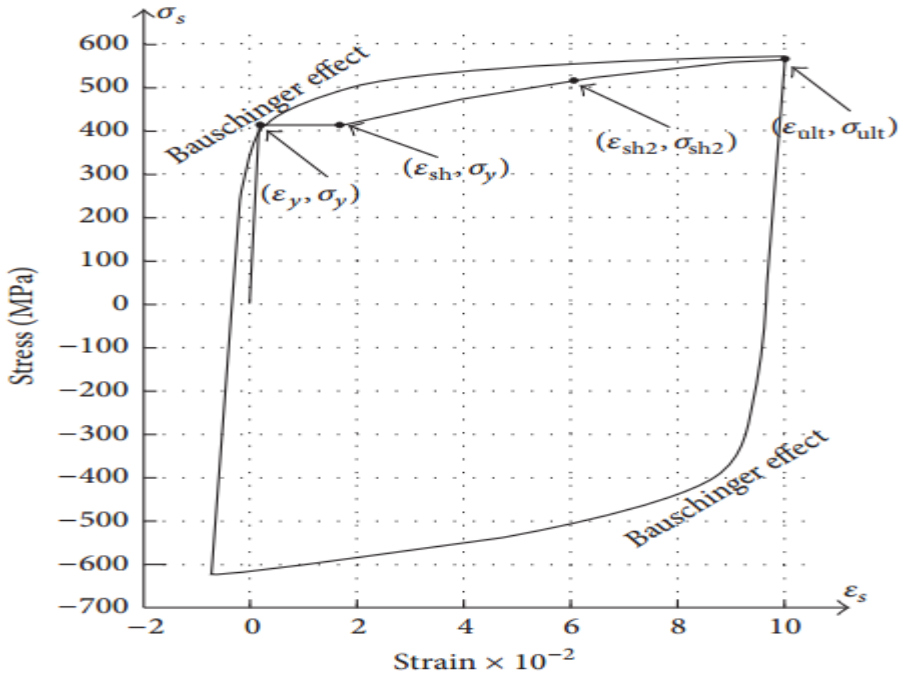

Figure 2-16. Dodd-restrepo steel model used by *(Sosa, et al., 2017)*

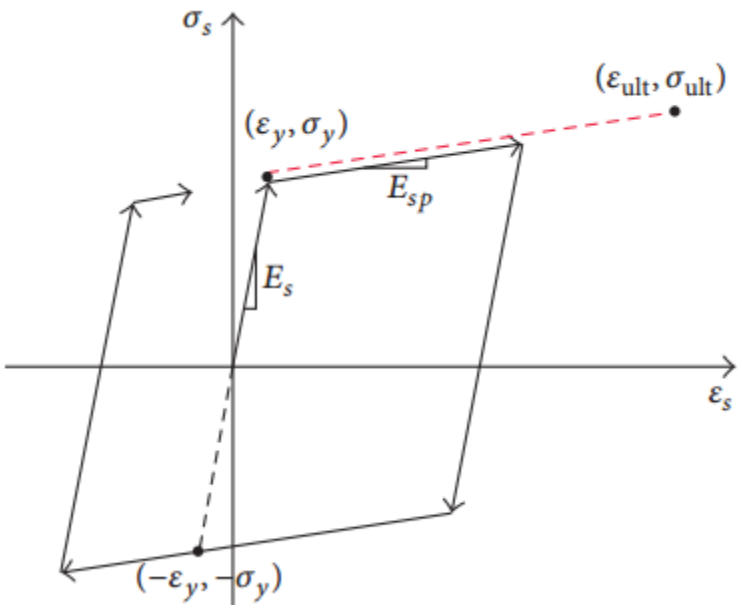

Figure 2-17. Analytical bilinear steel model used by *(Sosa, et al., 2017)*

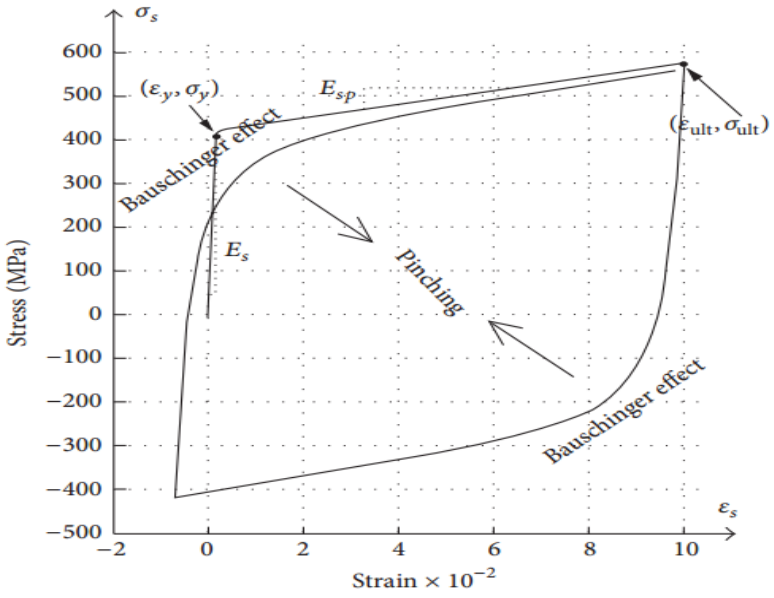

Figure 2-18. Meneggoto-pinto steel model used by *(Sosa, et al., 2017)*

(Ashraf, Mohie, & Janet, 2014) Studied the behavior of simply supported reinforced concrete deep beams with and without openings as well as the effect of reinforcement distribution on the overall capacity of the beam to compare it with Egyptian code guide lines. The damaged plasticity model in ABAQUS which uses the concept of isotropic damaged elasticity in combination with isotropic tensile and compressive plasticity to

represent the inelastic behavior of concrete was used for analysis. An 8 node solid element with one point integration was used to create the concrete beam mesh. An embedded truss reinforcement a 2 node linear 3D truss element was used to model steel rebar. To insure the reality of their study, they modeled and analyzed a deep beam shown in Figure 2-19 (a) whish's force-displacement curve was plotted by Hong et al. experimentally .After they modelled the beam with similar concrete and steel material property of the test specimen, the same beam dimension and the same reinforcement detailing they found well agreed force-displacement curve as shown in Figure 2-19 (b) which validates concrete damage plasticity model for reinforced concrete section.

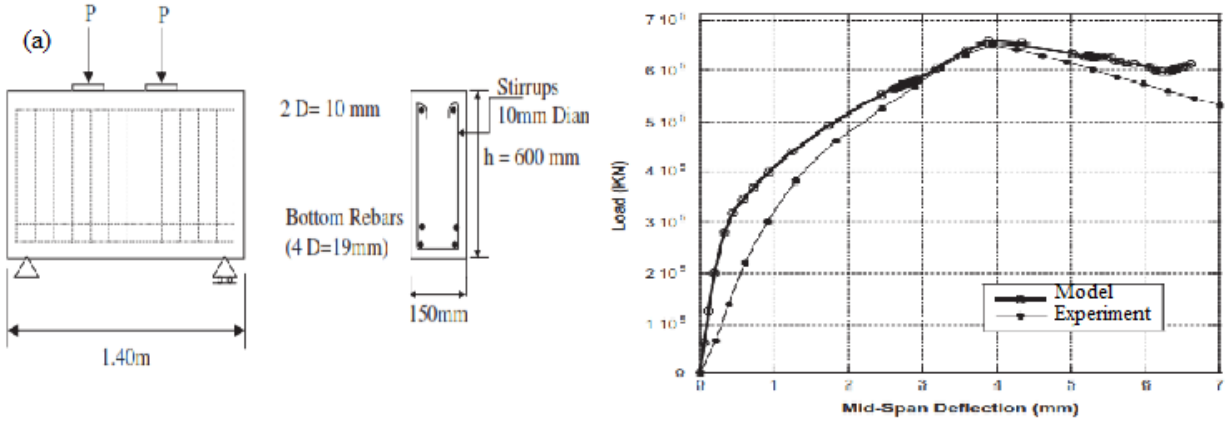

Figure 2-19. (a) dimension and detailing of tested and modeled beam (b) force-displacement curves of test result and analysis result *(Ashraf, Mohie, & Janet, 2014).*

(M.M. Islam, et al., 2015) Attempted to construct the P-M Interaction Diagram for short square column made of steel fiber reinforced concrete (SFRC) experimentally and via finite element (FE) approach. This study was conducted to provide real experimental data as well as FE analysis on P-M Interaction Diagram of square RC columns for predicting the axial load as well as bending moment capacity. In this paper a numerical model was introduced for SFRC as well as PC specimens with varying eccentricities and a good correlation had been obtained between FE model and experimental results. Thus the FE models of SFRC and plain RC columns are validated by experimental results.

Experimentally, special types of specimens are casted to apply eccentric loading and tested in a 1000 kN digital universal testing machine (UTM) to get the actual axial and bending behavior of square RC columns.

In finite element analysis a reasonable modeling of concrete on a FE platform using suitable element type, adequate mesh size, appropriate boundary conditions, realistic loading environment and proper time stepping were used to represent the actual situation of test condition and thus can help to estimate the capacity from FE models.

An eight node solid element, SOLID65 was used to model the concrete and also SFRC. The solid has eight node with three degrees of freedom at each node-translational in the nodal x, y, and z directions. The element is capable of plastic deformation, cracking in three orthogonal directions, and crushing. The element is also applicable for reinforced composites such as fiberglass as well as SFRC (ANSYS 11). The 3-D spar element, LINK8 was used to model the steel reinforcement which is a uniaxial tension-compression element with three degrees of freedom at each node: translations in the nodal x, y, and z directions and material properties like Plasticity, creep, swelling, stress stiffening, and large deflection capabilities were included.

Material properties for PC and SFRC such as (i) elastic modulus, (ii) density, (iii) Poisson's ratio, (iv) multilinear elastic stress-strain behavior, (v) ultimate uniaxial tensile strength were applied together with Newton Raphson approach to obtain the simplest nonlinear solution.

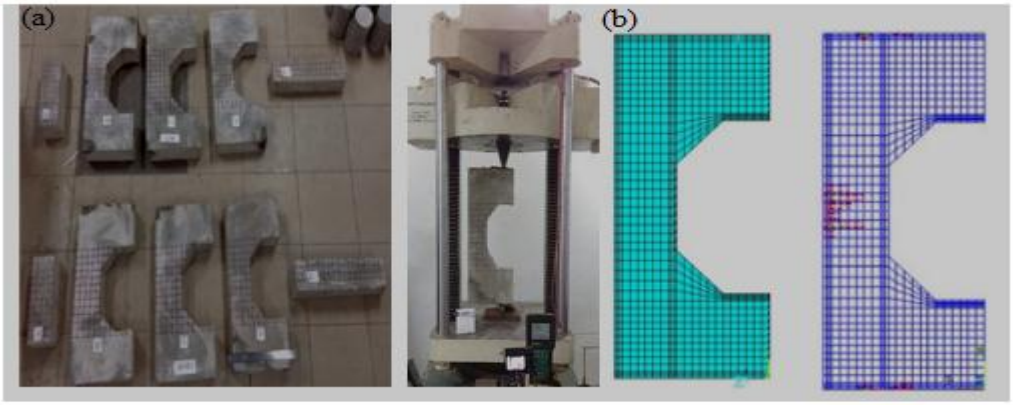

Figure 2-20. (a) Test specimens (b) Finite element models *(M.M. Islam, et al., 2015).*

From this research it is concluded as construction of P-M interaction diagram is possible by finite element analysis. Plain concrete was found to have less axial load capacity when compared to ACI 318-14 due to absence of tie reinforcements while that of steel fiber reinforced member has almost equal axial load capacity with that of ACI 318-14.

Steel fiber reinforced concrete column has enhanced capacity as well as ductility when compared to that of plain concrete column

(Yunus Dere & Mehmet Alpaslan Koroglu, 2017) Studied nonlinear finite element modeling of plain and reinforced concrete. Several parameters affecting the modeling of reinforced concrete were discussed. Commercial ABAQUS software package along with the concrete damaged plasticity model was suggested to be used for the modeling of reinforced concrete structural members. Compressive and tensile uniaxial stress-strain relationship curves for concrete material to be effectively used in ABAQUS were suggested.

In this study, the unconfined stress-strain relationship model for concrete which was first proposed by Popovics and later modified by Thoronfeldt et al was adapted. According to this model, the relation between compressive strain (ε_c)and stress (f_c) is given by

$$\frac{f_c}{f_c'} = \frac{n\left(\frac{\varepsilon_c}{\varepsilon_{co}}\right)}{(n-1)+\left(\frac{\varepsilon_c}{\varepsilon_{co}}\right)^n} \ldots\ldots\ldots\ldots\ldots\ldots\ldots\ldots\ldots\ldots\ldots 2.18$$

Where f_c' and ε_{co} are the compressive strength and strain corresponding to the maximum stress, respectively. 'n' is defined as

$$n = 0.4x10^{-3} f_c'(psi) + 1 \ldots\ldots\ldots\ldots\ldots\ldots\ldots\ldots 2.19$$

Tensile stress strain (σ-ε) relationship was assumed to be linear up to the uniaxial tensile strength and then determined using the exponential function.

$$\sigma = f_t \left(\frac{\varepsilon_t}{\varepsilon}\right)^{(0.7+1000\varepsilon)} \ldots\ldots\ldots\ldots\ldots\ldots\ldots\ldots\ldots 2.20$$

$$\varepsilon_t = \frac{f_t}{E_c} \ldots\ldots\ldots\ldots\ldots\ldots\ldots\ldots\ldots\ldots\ldots\ldots 2.21$$

Here, Ec is obtained as the slope of the initial tangent of compressive stress-strain curve.
From this study it is observed that realistic simulations of reinforced concrete structural systems became possible through analyses of 3D nonlinear FE models.
From the observed force – displacement curves concrete damage plasticity model was found to well approach to test specimen of simple cube element.

2.4. Finite element method

Any continuous object has infinite degrees of freedom so that it is difficult to solve the problem in this format. To make calculations at only limited (fine) number of points and to interpolate the results for entire domain, finite element method is appropriate. This is done by reducing the degrees of freedom from infinite to finite with the help of discretization i.e., meshing (nodes and elements).An element is one dimensional if one of the dimension is very large when compared to the rest of the two like beam element, two dimensional if two of the dimensions are very large when compared to the third one like thin shell, plate, membrane, plain stress, plain strain etc., three dimensional if all three dimensions are comparable like solid element. Software cannot make calculations unless geometry is not completely defined via meshing.

2.5. Concrete constitutive model relations

There are three main concrete constitutive models available in ABAQUS. Each can be used for modeling concrete at low confining pressures in all types of elements.

1. Smeared Crack Concrete Model – This model is intended for applications in which the concrete is subjected to essentially monotonic straining (noncyclic straining). In this model, linear elastic behavior is used to define elastic properties and smeared cracking is used to describe the reversible part of the material's response after cracking failure. The model consists of an isotropically hardening yield surface that is active when the stress is dominantly compressive and an independent crack detection surface that determines if a point fails by cracking. The model is dominated by the cracking and post-cracking anisotropic behavior and at each integration point, constitutive calculations are performed independently and the stress and stiffness are affected by the presence of cracking.

The uniaxial behavior of the model can be seen in the Figure 2-21 below. Because the model assumes primarily monotonic straining and little or no unloading, the unload/reload response is elastic.

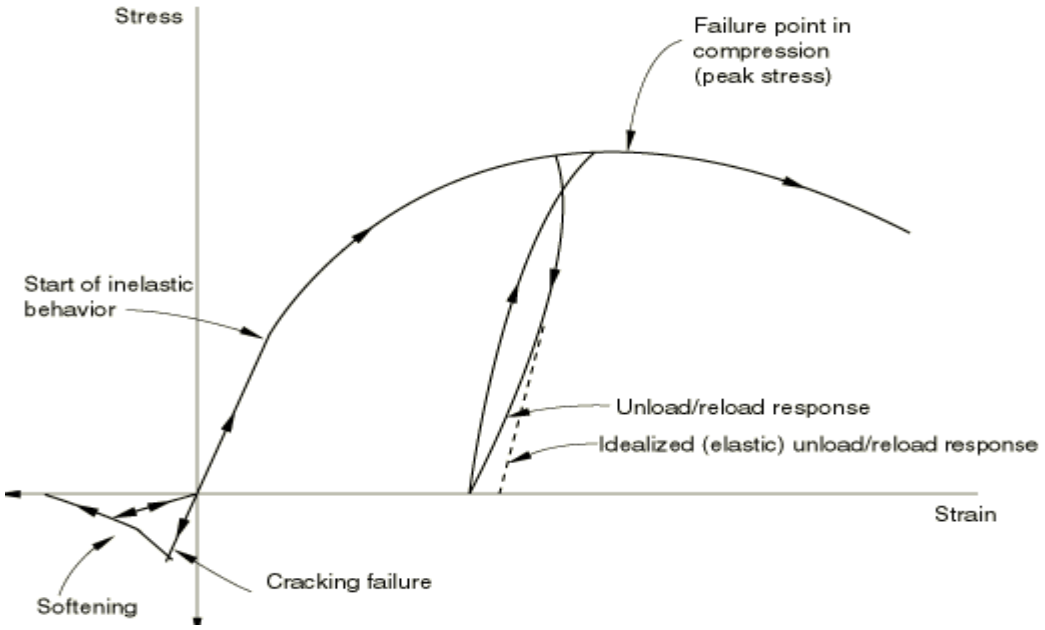

Figure 2-21. Uniaxial concrete behavior *(Dassault systemes simulia crop., 2013)*

Tension stiffening is accounted for by specifying a post-failure stress-strain relation or by applying a fracture energy cracking criterion. With the fracture energy criterion, the behavior is specified by a stress-displacement response which requires the definition of a characteristic crack length.

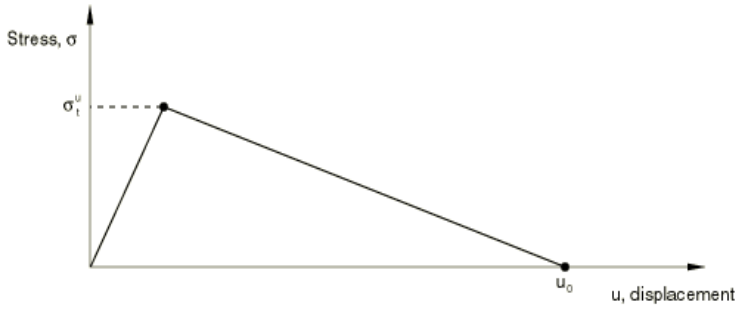

Figure 2-22. Fracture energy cracking model of concrete *(Dassault systemes simulia crop., 2013)*

2. Brittle Cracking Model – This model is available only in ABAQUS/Explicit and is intended for applications in which the concrete behavior is dominated by tensile cracking and compressive failure is not important. A brittle failure criterion can be defined, in which the material point is considered to have failed once the number of cracks at that point reach a user specified value. The associated element is then removed.

3. Concrete Damaged Plasticity Model – This model takes into consideration the degradation of the elastic stiffness induced by plastic straining both in tension and compression. It also accounts for stiffness recovery effects under cyclic loading. The compressive stress-strain relation can be seen in the Figure 2-23. The compressive behavior is elastic until initial yield and then is characterized by stress hardening followed by strain softening after the ultimate point.

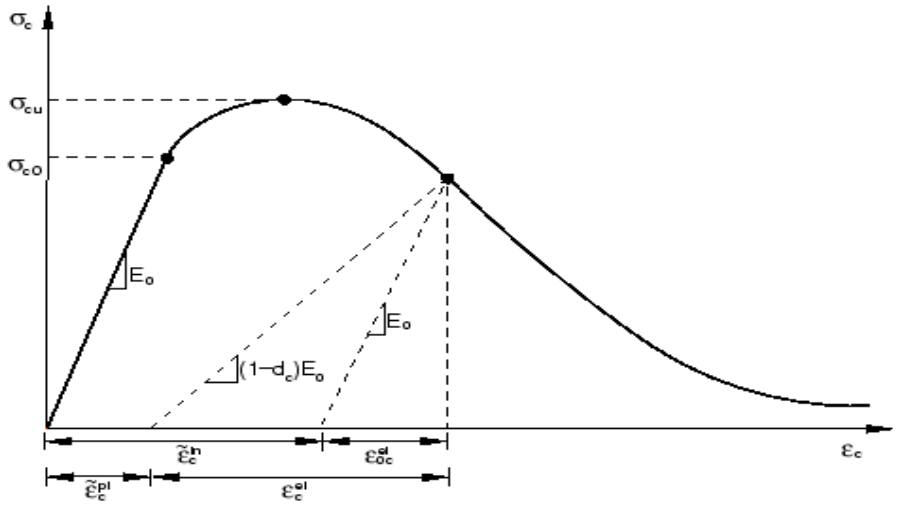

Figure 2-23. Damage Plasticity uniaxial concrete compressive behavior *(Dassault systemes simulia crop., 2013)*

$$\widetilde{\varepsilon_c^{pl}} = \widetilde{\varepsilon_c^{in}} - \frac{d_c}{1-d_c}\frac{\sigma_c}{E_o} \quad \ldots\ldots\ldots\ldots\ldots\ldots\ldots\ldots\ldots\ldots\ldots 2.22$$

Inelastic strain (ε_c^{in}) is the difference between the total strain calculated from the non-linear stress strain curve and the elastic strain of concrete.

$$\widetilde{\varepsilon_c^{in}} = \varepsilon_c - \varepsilon_{oc}^{el} \quad \ldots\ldots\ldots\ldots\ldots\ldots\ldots\ldots\ldots\ldots\ldots 2.23$$

$$\varepsilon_{oc}^{el} = \frac{\sigma_c}{E_O} \quad \ldots\ldots\ldots\ldots\ldots\ldots\ldots\ldots\ldots\ldots\ldots\ldots\ldots 2.24$$

$$\varepsilon_c^{el} = \frac{\sigma_c}{E_O}\left(1 + \frac{d_c}{1-d_c}\right) \quad \ldots\ldots\ldots\ldots\ldots\ldots\ldots\ldots\ldots\ldots 2.25$$

$$d_c = 1 - \frac{\sigma_c}{\sigma_{max}} \quad \ldots\ldots\ldots\ldots\ldots\ldots\ldots\ldots\ldots\ldots 2.26$$

$$d_t = 1 - \frac{\sigma_t}{\sigma_{tmax}} \quad \ldots\ldots\ldots\ldots\ldots\ldots\ldots\ldots\ldots\ldots 2.27$$

After the onset of micro cracking (failure stress) the response is softened, inducing strain localizations in the concrete structure. Like the previous two models, post-cracking behavior can be accounted for by specifying a post stress-strain relation or by applying a fracture energy criterion. In both the tensile and compressive stress strain curves, the unloading response is characterized by a weakening of the material and a degradation of the elastic stiffness. These phenomena are defined by particular damage parameters.

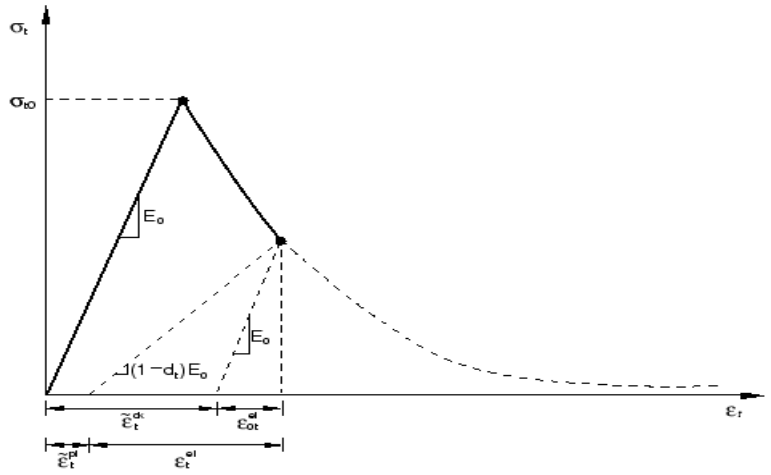

Figure 2-24. Damage plasticity tension response of concrete *(Dassault systemes simulia crop., 2013)*

The damage variables (dc and dt) can take values from zero, representing the undamaged material, to one, which represents total loss of strength. To avoid potential numerical problem ABAQUS enforces a lower limit on tensile stress of concrete equal to one hundredth of initial tensile failure stress ($\sigma_t = \frac{\sigma_{to}}{100}$) (Dassault systemes simulia crop., 2013).

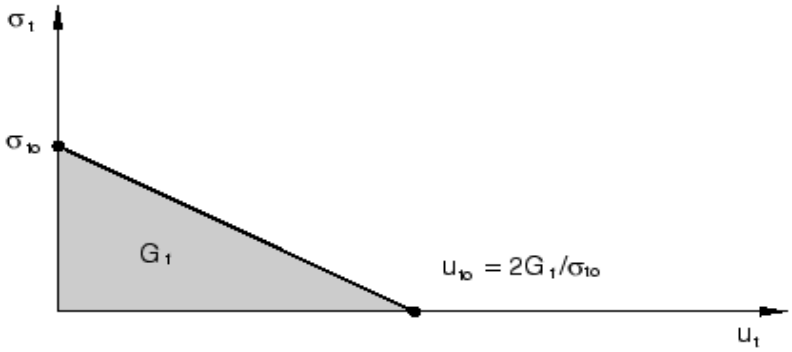

Figure 2-25. Post failure stress-fracture energy curve *(Dassault systemes simulia crop., 2013)*

CHAPTER THREE

3. METHODOLOGY

3.1. General

In this thesis uniform thickness cross-section is assumed throughout the height of the bearing wall being considered. In finite element modelling, the maximum compressive strain in the concrete, the maximum tensile and compressive strain in the reinforcement bars are taken from the Ethiopian Building Code Standard EBCS EN 1992-1-1:2013. Finite element modelling will account slender walls to develop design aid for such bearing walls.

There are two common methods of compression and biaxial bending moment's interaction chart presentation. For constant axial load P combination of M_x and M_y are plotted as load contour. Axial load P and resultant moment M are also plotted for constant inclination angle and for various neutral axis depth on the radial plane passing through Pn axis. The second method will be adopted in in developing of P-M interaction chart for this thesis.

3.2. Stress-strain relation for non-linear structural analysis

The relation between stress (σ_c) and strain (ε_c) of plain concrete shown in Figure 3-1 for short term uniaxial loading is described by the equation:

$$\frac{\sigma_c}{f_{cm}} = \frac{\mathrm{k}\eta - \eta^2}{1 + ((\mathrm{k}-2)\eta} \quad \ldots\ldots 3.1$$

$$\eta = \frac{\varepsilon_c}{\varepsilon_{c1}} \quad \ldots\ldots 3.2$$

$$k = \frac{1.05E_{cm}|\varepsilon_{c1}|}{f_{cm}} \quad \ldots\ldots 3.3$$

$$f_{cm} = (f_{ck} + 8)(MPa) \quad \ldots\ldots 3.4$$

$$E_{cm} = 22\left(\frac{f_{cm}}{10}\right)^{0.3}(GPa) \quad \ldots\ldots 3.5$$

For tensile properties of concrete, the cracking stress (maximum tensile stress) is calculated as:

$$f_{ctm} = (2.12\ln\left(1 + \left(\frac{f_{cm}}{10}\right)\right)(MPa) \geq \frac{C50}{60} \quad \ldots\ldots 3.6$$

$$f_{ctm} = 0.3(f_{ck})^{\frac{2}{3}}(MPa) < C50 \quad \ldots\ldots 3.7$$

Where σ_c (MPa)– compressive stress of concrete, f_{cm} (MPa)– mean compressive strength of concrete, f_{ck} (MPa) - cylindrical characteristic compressive strength of concrete, E_{cm} (GPa)– elastic modulus of concrete, f_{ctm} (MPa)– tensile strength of concrete, ε_c – compressive strain of concrete and ε_{c1} -strain at pick compressive stress of concrete.

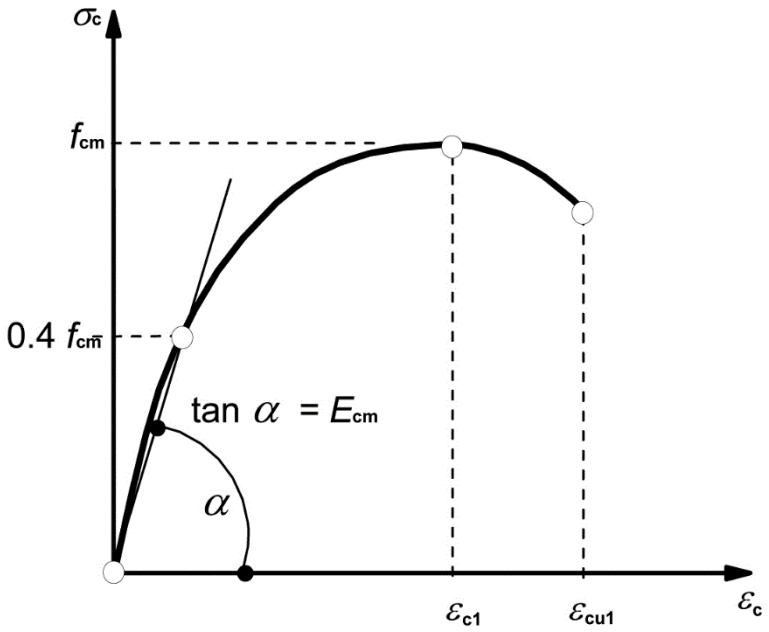

Figure 3-1. Schematic representative of the stress-strain relation of structural analysis (the use 0.4fcm for the definition of Ecm is approximate) *(EBCS EN 1992-1-1:2013)*

3.2.1. Concrete input data for finite element modelling in ABAQUS

It is assumed that the uniaxial stress-strain curves can be converted into stress versus plastic-strain curves. This conversion is performed automatically by ABAQUS from the user-provided stress versus inelastic strain relationship (Dassault systemes simulia crop., 2013). ABAQUS automatically converts the inelastic strain values to plastic strain values using the relationship:

$$\varepsilon_c^{pl} = \varepsilon_c^{in} - \frac{d_c}{1-d_c}\frac{\sigma_c}{E_o} \quad \ldots\ldots\ldots\ldots\ldots\ldots\ldots\ldots\ldots\ldots 3.8$$

Inelastic strain (ε_c^{in}) is the difference between the total strain calculated from the non-linear stress strain curve and the elastic strain of concrete.

$$\varepsilon_c^{in} = \varepsilon_c - \varepsilon_{oc}^{el} \quad \ldots\ldots\ldots\ldots\ldots\ldots\ldots\ldots\ldots\ldots\ldots 3.9$$

$$\varepsilon_{oc}^{el} = \frac{\sigma_c}{E_O} \ldots\ldots\ldots\ldots\ldots\ldots\ldots\ldots\ldots\ldots\ldots\ldots\ldots\ldots 3.10$$

The post-failure behavior is simulated with tension stiffening by applying a fracture energy cracking criterion. Fracture energy is the amount of energy necessary to create one unit area of crack. To determine the stress-crack opening curve for tension, a linear crack opening curve as described by (ACI Committee 446 on fracture mechanics, 1992) which is also described in ABAQUS manual is used.

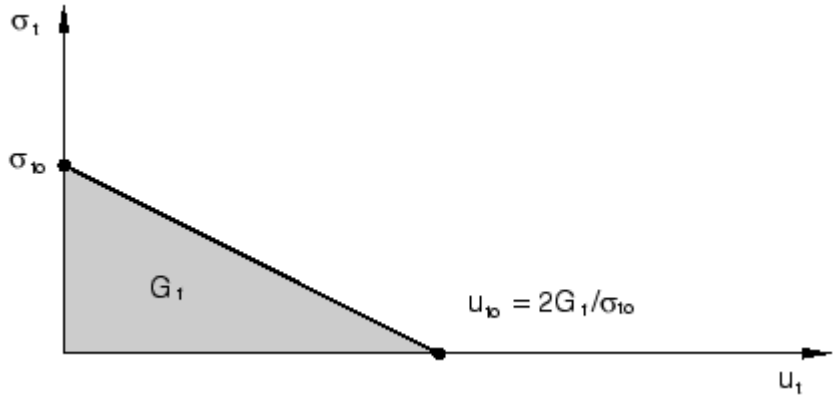

Figure 3-2. Post failure stress-fracture energy curve *(Dassault systemes simulia crop., 2013)*

In Figure 3-2, σ_{to} is tensile strength of concrete and G_F fracture energy and u_t is cracking displacement. As described by (Rozalija Kozul & David Darwin, 1997), both increasing the amount of aggregate and the size of aggregate yields lesser fracture energy.

Table 3-1. Fracture energy test results as described by *(Rozalija Kozul & David Darwin, 1997).*

Group*	Gf (1) (N/m)	Gf (2) (N/m)	Gf (3) (N/m)	Gf (avg) (N/m)	Test Age (days)	Group*	Gf (1) (in/lb)	Gf (2) (in/lb)	Gf (3) (in/lb)	Gf (avg) (in/lb)
HB-19h.1	136	137	187	**154**	137	**HB-19h.1**	0.78	0.78	1.07	**0.88**
HB-19h.2	215	140	152	**169**	116	**HB-19h.2**	1.23	0.80	0.87	**0.97**
HB-12h.1	148	164	151	**154**	164	**HB-12h.1**	0.84	0.94	0.86	**0.88**
HB-12h.2	169	194	151	**172**	149	**HB-12h.2**	0.97	1.11	0.86	**0.98**
HB-12h.3	173	206	155	**178**	119	**HB-12h.3**	0.99	1.18	0.89	**1.02**
HB-12l.1	167	x	x	**167**	160	**HB-12l.1**	0.95	x	x	**0.95**
HB-12l.2	158	203	127	**163**	117	**HB-12l.2**	0.90	1.16	0.73	**0.93**
HL-12h.1	x	x	x	**x**	148	**HL-12h.1**	x	x	x	**x**
HL-12h.2	69	63	59	**64**	111	**HL-12h.2**	0.39	0.36	0.34	**0.36**
HL-12l	68	69	59	**65**	94	**HL-12l**	0.39	0.39	0.34	**0.37**
NB-19h	230	220	227	**226**	5	**NB-19h**	1.31	1.26	1.30	**1.29**
NB-12h	198	164	193	**185**	5	**NB-12h**	1.13	0.94	1.10	**1.06**
NB-12l	177	184	177	**183**	5	**NB-12l**	1.01	1.05	1.01	**1.05**
NL-12h	70	67	60	**66**	5	**NL-12h**	0.40	0.38	0.35	**0.37**
NL-12l	53	48	66	**56**	5	**NL-12l**	0.31	0.27	0.38	**0.32**

*Concrete Strength	Aggregate Type	Aggregate Size	Aggregate Content
H = high	B = basalt	12 = 12 mm (1/2 in.)	h = high
N =normal	L = limestone	19 = 19 mm (3/4 in.)	l = low

However as (CEB-FIP, 1993), tensile fracture energy of concrete is defined as a function of concrete compressive strength and expressed as the equation:

$$G_F = G_{fo}\left(\frac{f_{cm}}{10}\right)^{0.7} \quad \ldots\ldots\ldots\ldots\ldots\ldots\ldots\ldots\ldots\ldots\ldots 3.6$$

Where G_{fo} is the coefficient related to the maximum aggregate size as shown in Table 3-2.

Table 3-2. Aggregate sized based fracture energy coefficients (Rots, 1988)

Maximum aggregate size d_{max} (mm)	Coefficient G_{fo} (J/m²)
8	25
16	30
32	58

As cited by (Damigo J.Carreira & Kuanh-Han Chu, 1986), (Velbo and Ghali, 1977) used bilinear and trilinear piece wise stress-strain relationship for concrete in tension. Their independent variables are modulus of rapture (f_r) and modulus of elasticity(E_C), where (f_r) is $(0.62\sqrt{f_c'})$ in Mpa and where f_c' is compressive strength of concrete. In the two bilinear relationships, the ascending branch is a straight line with a slope of (E_C) up to (f_r).In one case the descending branch has a slope of $(\frac{-100}{E_C})$ which is almost a vertical drop to zero stress. In the other bilinear case, the descending branch has $(-\frac{E_C}{5})$ to zero stress.

In the trilinear relationship, the ascending branch has a slope of $(0.75E_C)$ and reaches at pick at$(0.9f_r)$. It then changes to slope of $(-\frac{E_C}{2})$ until$(0.45f_r)$; from there it changes to $(-\frac{E_C}{20})$ until it reaches zero stress.

Damage, d_t and d_c, can be specified in tabular form. (If damage is not specified, the model behaves as a plasticity model; consequently,$\varepsilon_c^{pl} = \varepsilon_c^{in}\ and\ \varepsilon_t^{in} = \varepsilon_t^{pl}$). In ABAQUS the damage variables are treated as non-decreasing material point quantities. The choice of the damage properties is important since, generally, excessive damage may have a critical effect on the rate of convergence. It is recommended to avoid using values of the damage variables above 0.99, which corresponds to a 99% reduction of the stiffness.

$$d_c = 1 - \frac{\sigma_c}{\sigma_{max}} \quad \ldots\ldots\ldots\ldots\ldots\ldots\ldots\ldots\ldots\ldots 3.7$$

$$d_t = 1 - \frac{\sigma_t}{\sigma_{tmax}} \quad \ldots\ldots\ldots\ldots\ldots\ldots\ldots\ldots\ldots\ldots 3.8$$

The default flow potential eccentricity which is also used in this research is $\epsilon = 0.1$.

$\frac{\sigma_{bo}}{\sigma_{co}}$ is the ratio of initial equibiaxial compressive yield stress to initial uniaxial compressive yield stress (the default value is 1.16).

K_c is the ratio of the second stress invariant on the tensile meridian. $0.5 < kc < 1$ (The default value is $\frac{2}{3}$).

In finite element analysis when using finer meshes and negative slope in the material relation (stress-strain or stress-displacement) for larger models, convergence problems are common. To solve this problems using normalization viscosity to such extent it can not affect the result is proposed by previous researchers.

(Y F Gao & A F Bower, 2004) Found that convergence problems which occur in finite element simulations of crack nucleation on a cohesive interface can be avoided by including a small viscous term in the constitutive equations for the interface. Including this term provides a mechanism for dissipating strain energy during unstable debonding and therefore ensures a quasi-static equilibrium path exists connecting the state of the solid before and after the instability. But in ABAQUS standard the default value is zero. The proposed viscosity value by (Y F Gao & A F Bower, 2004) is 0.00125.

(Szczecina Michal & WinnickiAndrzej, 2015) Performed numerical simulations concerning uniaxial and biaxial compression and uniaxial tension of a sample concrete specimen and then the results were compared with test results. In this research dilation angle of 5^{o} and viscosity of 0.0001 were recommended to be used in concrete damage plasticity model. Dilation angle and viscosity parameter recommended by (Szczecina Michal & WinnickiAndrzej, 2015) is also used in this thesis.

3.2.2. Reinforcing steel

The rebar elements are used with standard metal plasticity models that define the behavior of the reinforcement material as described in (EBCS EN 1992-1-1:2013) .

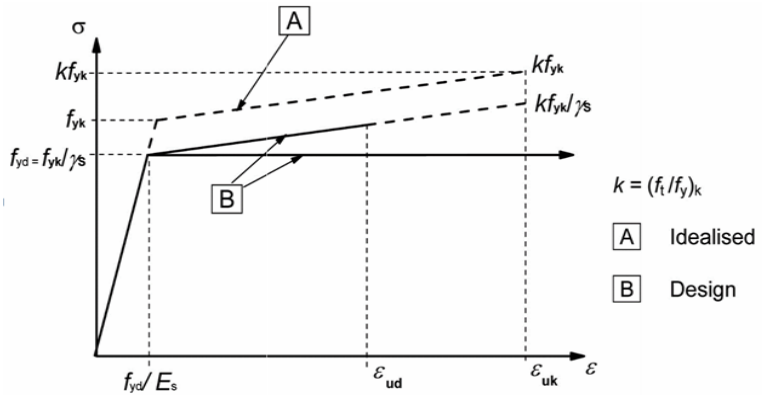

Figure 3-3. Idealized (nominal) and design stress-strain diagram for reinforcing steel (for tension and compression), *(EBCS EN 1992-1-1:2013)*.

ABAQUS assumes the stress-strain data to be true stress and true strain (Dassault systemes simulia crop., 2013). The conversion from nominal stress and strain to true stress and strain is by the equations below:

$$\sigma_{true} = \sigma_T = \sigma_{nominal}(1 + \varepsilon_{nominal}) \dots\dots..3.9$$

$$\varepsilon_{true} = \varepsilon_T = ln(1 + \varepsilon_{nominal}) \dots\dots\dots\dots...3.10$$

$$where, \varepsilon_{nominal} = \frac{f_y}{E}$$

True plastic strain can be calculated as:

$$\varepsilon_T^p = \varepsilon_T - l_n\left(1 + \frac{\sigma_T}{E}\right) \dots\dots\dots\dots.\dots\dots\dots\dots 3.11$$

Where $f_y \; and \; E$ are yield strength and modulus of elasticity of reinforcement steel.

ABAQUS finite element commercial software packages is used for modeling and nonlinear analysis of reinforced concrete walls. Loads are applied at different location of eccentricities to determine capacity of the section to draw P-M interaction chart for a given core wall.

In modelling of material, concrete damage plasticity model is used for concrete with C3D8R (Continuum, 3-D, 8-Node, Reduced integration) element. Two node linear 3D truss element (T3D2) is used to model reinforcement steel.

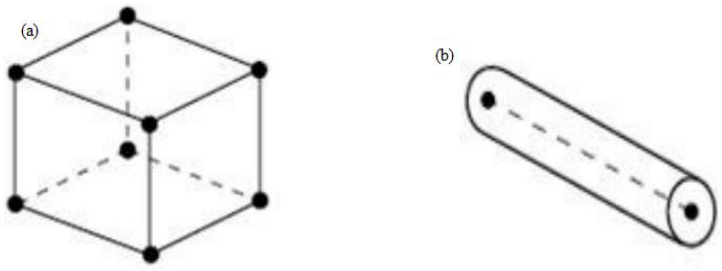

Figure 3-4. (a) C3D8 element (b) T3D2 element

C3D8 (Hexahedral) element is used for homogenous element or layers of different material for analysis. They also used to model linear and complex non-linear mechanical analysis and has good convergence rate than triangle and tetrahedral meshes. 3-D truss element

(T3D2) is three dimension truss elements having two degrees of freedom. Truss elements are used in two and three dimensions to model slender, line like structure that support loading only along the center line of the element. No moment or force perpendicular to the center line is supported.

3.3. Reinforcement provision of walls as per EBCS EN 1992-1-1:2013

3.3.1. Vertical reinforcements

(1) The area of the vertical reinforcement should lie between $A_{s,vmin}$ and $A_{s,vmax}$ Where the recommended value of $A_{s,vmin}$ and $A_{s,vmax}$ respectively are $0.002A_c$ and $0.04A_c$.

(2) Where the minimum area of reinforcement, $A_{s,vmin}$, controls in design, half of this area should be located at each face.

(3) The distance between two adjacent vertical bars shall not exceed 3 times the wall thickness or 400 mm whichever is the lesser.

3.3.2. Horizontal reinforcements

(1) Horizontal reinforcement running parallel to the faces of the wall (and to the free edges) should be provided at each surface. It should not be less than $A_{s,hmin}$ Where the recommended value of $A_{s,hmin}$ is either 25% of the vertical reinforcement or 0.001 Ac, whichever is greater.

(2) The spacing between two adjacent horizontal bars should not be greater than 400 mm.

3.3.3. Transverse reinforcements

(1) In any part of a wall where the total area of the vertical reinforcement in the two faces exceeds $0.02\ A_c$, transverse reinforcement in the form of links should be provided in maximum spacing of

-20 times the minimum diameter of longitudinal bars

-lesser dimension of the wall

-400mm

3.4. Slenderness criterion for isolated members

3.4.1. Slenderness criterion for isolated member according to EBCS EN 1992-1-1-2013

Second order effects may be ignored if the slenderness λ is below a certain value λ_{lim} which's recommended value is expressed in equation:

$$\lambda_{lim} = \frac{20.A.B.C}{\sqrt{n}} \ldots\ldots\ldots\ldots\ldots\ldots\ldots\ldots\ldots\ldots 3.12$$

Where:

$A = \frac{1}{1+0.2\varphi_{ef}}$ (if φ_{ef} is not used A=0.7 may be used)

$B = \sqrt{1+2\omega}$ (if $\omega\ is\ not\ known\ \ B = 1.1\ may\ be\ used$)

$C = 1.7 - r_m$ (if r_m is not known C=0.7 may be used)

φ_{ef} is effective creep ratio expressed as:

$$\varphi_{ef} = \varphi(_{\infty,10}).\frac{M_{0Eqp}}{M_{0Ed}} \ldots\ldots\ldots\ldots\ldots\ldots\ldots\ldots 3.13$$

Where:

$\varphi(_{\infty,10})$ is the final creep coefficient according to (EBCS EN 1992-1-1:2013).

M_{0Eqp} is the first order bending moment in quasi permanent load combinations(SLS)

M_{0Ed} is the first order bending moment in design load combination(ULS)

$\omega = A_s f_{yd}/A_C f_{cd}$ Mechanical reinforcement ratio

A_s is the total area of longitudinal reinforcement

A_C is the area of concrete cross section

$n = \frac{N_{Ed}}{A_c f_{cd}}$ Relative normal force

$r_m = \frac{M_{01}}{M_{02}}$ Moment ratio, $M_{01}\ and\ M_{02}$ are the first order end moments,$|M_{02}| \geq |M_{01}|$

The slenderness ratio is defined as follows

$$\lambda = \frac{l_0}{i} \dots\dots\dots\dots\dots\dots\dots\dots\dots\dots\dots\dots\dots\dots\dots\dots 3.14$$

Where l_0 is the effective length and i is the radius of gyration of uncracked concrete section. The values of l_0 is the function of unsupported length of the member (l) and the end boundary conditions as described in Figure 3-5.

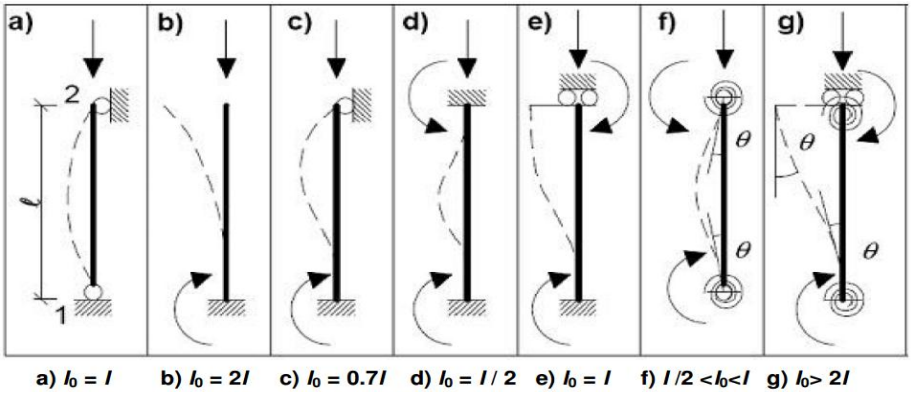

Figure 3-5. Examples of different buckling modes and corresponding effective lengths for isolated members *(EBCS EN 1992-1-1:2013)*

3.4.2. Slenderness criterion for isolated member according to ACI code section 10.10.1.

ACI code section 10.10.1 allows slenderness effect to ignored in case of columns in sway frame if

$$\frac{kl_u}{r} \leq 22 \dots\dots\dots\dots\dots\dots\dots\dots\dots\dots\dots\dots\dots\dots\dots 3.15$$

And non-sway frame if:

$$\frac{kl_u}{r} \leq 34 - 12\frac{M_1}{M_2} \leq 40 \dots\dots\dots\dots\dots\dots\dots 3.16$$

Where k refers the effective length factor is 1 for pin ended column which is used in this thesis, l_u is unsupported height (ACI 10.10.1) and r is the radius of gyration taken as 0.3h for rectangular section and 0.25h for circular section (ACI code section 10.10.1.2).For other shapes, the value for r can be calculated from the area and moment of inertia of the cross section by definition $r = \sqrt{\frac{I}{A}}$, the sign of M_1 and M_2 are given in Figure 3-6.

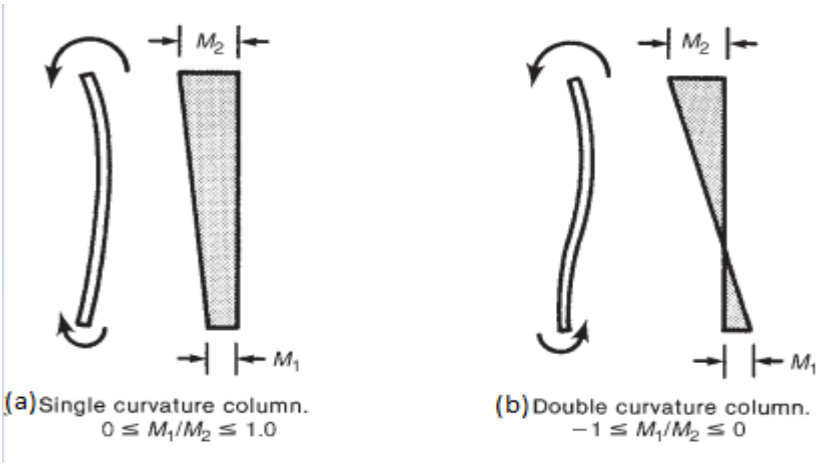

Figure 3-6. Direction of moments due to eccentrically loaded columns *(JAMES K.WIGHT & GAMES G.MACGREGOR, 2012)*

An eccentrically loaded slender column deflects laterally by an amount δ as shown in Figure 3-7. For equilibrium the internal moment at mid height is

$$M_C = p(e + \delta) \dots\dots\dots\dots\dots\dots\dots\dots\dots\dots\dots\dots 3.17$$

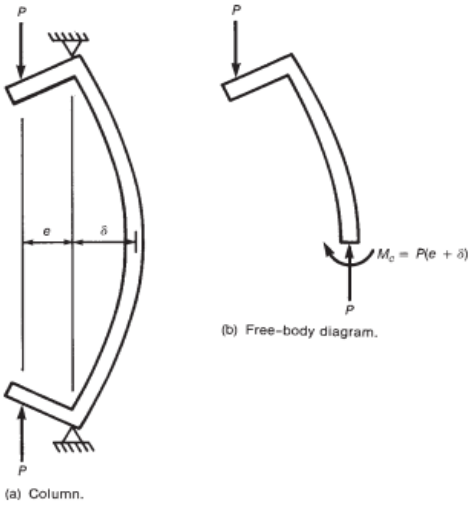

Figure 3-7. Forces in deflected column *(JAMES K.WIGHT & GAMES G.MACGREGOR, 2012).*

Slenderness limit calculation in both ACI code and EBCS EN 1992-1-1-2013-EBCS 2 is a function of effective length of the member, radius of gyration and first order end moment ratio. Additionally in EBCS EN 1992-1-1-2013-EBCS 2 it is a function of mechanical reinforcement ratio (ω) which is impossible to fix and design value of axial force (N_{ed}) which is the result extracted from the analysis. Due to this reason ACI code slenderness

classification of isolated member is used to model and analyze slenderer reinforcement walls.

3.5. Boundary conditions and Constraints

For displacement controlled loading, boundary conditions are defined in ABAQUS as six degrees of freedom at each node for three dimensional analysis.

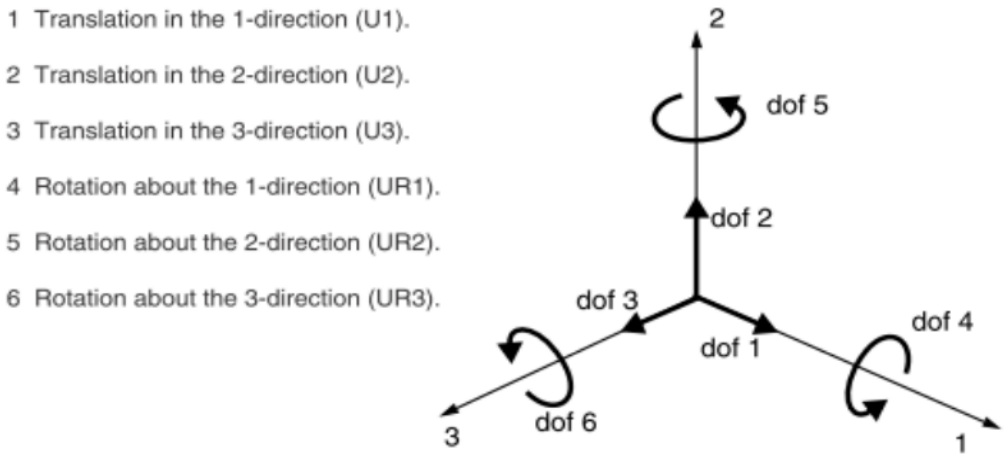

Figure 3-8. Boundary conditions notation in ABAQUS

A rigid body constraint is used between end nodes of the member and the reference node to simplify the size of the model so that convergence problem is reduced. A rigid body constraints allows to constrain the motion of selected parts and points so that the relative position of points in the body remain constant throughout the analysis, prohibiting deformation. A rigid body will, therefore have three free translational and three free rotational option; these motion can be prescribed by applying boundary condition to rigid body. A rigid body can consists of three dimensional bodies, groups of points or combination of bodies and points. The point can be connected to other deformable bodies. Points that are part of a rigid body can be defined as either tie node or pin nodes. A tie node transits both translational and rotational degrees of freedom to anybody to which it is attached. A pin node transmits only translational degrees of freedom to anybody.

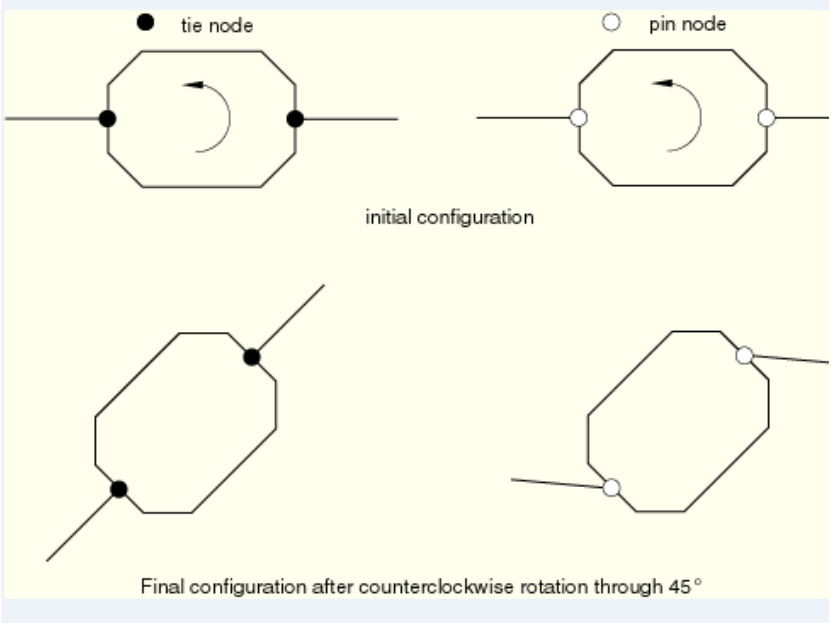

Figure 3-9. Behavior of rigid body constraints *(Dassault systemes simulia crop., 2013)*

From the expressed material stress-strain relations, yield stress versus inelastic strain for concrete compressive property, tensile yield stress versus cracking displacement for concrete tensile property, damage parameter versus inelastic strain for concrete compressive damage, damage parameter versus cracking displacement for concrete tensile damage and yield stress versus plastic strain for property of reinforcement steel are used for modeling as described in appendix B. In modeling reinforced concrete walls, $f_{ck} = 25\ Mpa$ for concrete and $f_y = 420\ Mpa$ for reinforcement bar are used.

CHAPTER FOUR

4. VALIDATION

4.1. Definition of validation

Model verification and validation is an enabling methodology for the development of computational models that can be used to make engineering predictions with quantified confidence. Quantifying the confidence and predictive accuracy of model calculations provides the decision-maker with the information necessary for making high-consequence decisions. The development of guidelines and procedures for conducting a model verification and validation program are currently being defined by a broad spectrum of researchers.

Model verification and validation are the primary processes for quantifying and building credibility in numerical models. Verification is the process of determining that a model implementation accurately represents the developer's conceptual description of the model and its solution. Validation is the process of determining the degree to which a model is an accurate representation of the real world from the perspective of the intended uses of the model. Both verification and validation are processes that accumulate evidence of a model's correctness or accuracy for a specific scenario; thus, verification and validation cannot prove that a model is correct and accurate for all possible scenarios, but, rather, it can provide evidence that the model is sufficiently accurate for its intended use.

In model verification and validation, the end product is a predictive model based on fundamental physics of the problem being solved. In all applications of practical interest, the calculations involved in obtaining solutions with the model require a computer code, like finite element analysis. Therefore, engineers seeking to develop credible predictive models critically need model verification and validation guidelines and procedures.

The expected outcome of the model verification and validation process is the quantified level of agreement between experimental data and model prediction, as well as the predictive accuracy of the model.

4.2. Validation one

When a symmetrical column is subjected to concentric axial load, longitudinal strains develop across the section, since concrete and steel are bonded together strain in concrete is similar to strain in steel. As described in (JAMES K.WIGHT & GAMES G.MACGREGOR, 2012) the axial load capacity of tied column for well-defined yield strength is calculated as equation (4.1).

$$P_O = k_3 f_c'(A_g - A_{st}) + f_y A_s \ldots\ldots\ldots\ldots\ldots\ldots\ldots\ldots 4.1$$

Where $k_3 = 0.85$ as described in (ACI committee 318, 2011),$P_{c=}k_3 f_c'(A_g - A_{st})$ is the load carried by concrete and $P_{s=}f_y A_{st}$ is the load carried by steel.p_s

A 2200mm length L-shaped wall which is 600x600mm with thickness of 150 mm shown in Figure 4-1 is modelled modeled by ABAQUS software and concentrically loaded to compare its capacity with that of (JAMES K.WIGHT & GAMES G.MACGREGOR, 2012) equation results for different steel ratios. Mean compressive strength of concrete is used for analysis as it is specified by (EBCS EN 1992-1-1:2013) for nonlinear analysis.

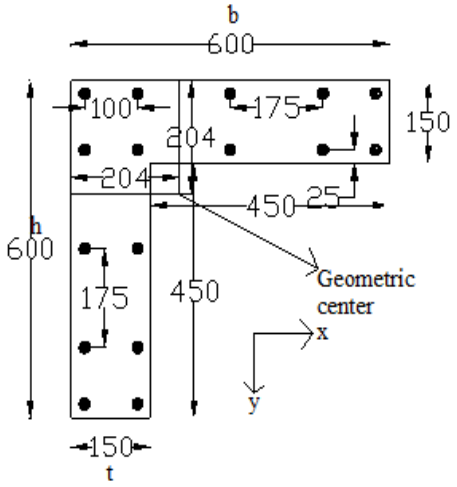

Figure 4-1.L-shaped wall detailing used for validation and to develop P-M interaction charts,(all dimensions in mm).

Transverse reinforcements are provided at spacing of 200mm with the addition of corner stirrups at spacing of 150mm. The column has cross sectional area of $157500mm^2$ and corresponding moment of inertia of $4.77924x10^9 mm^4$ about both orthogonal axes. The radius of gyration the section is then,$r = \sqrt{\frac{I}{A}} = 174.2mm$ and the corresponding

Slenderness ratio as per (JAMES K.WIGHT & GAMES G.MACGREGOR, 2012) is $\frac{kl_u}{r} = 12.63$ for pin-pin end case and $\frac{kl_u}{r} = 6.315$ for fixed-fixed case. Once modeling and analyzing this wall with element size of 30 mm and material properties as in appendix B, the results from finite element analysis and result from the equation is compared.

Table 4-1.Axial load capacity of short L-shaped wall from equation.

ρ	K3	Ag (mm^2)	As (mm^2)	Fcm (MPa)	Fy (MPa)	Ps=(Asxfy) (N)	Factored Pc=(k3xfcmx(Ag-As)) (N)	Po=(Ps+Pc) (N)
0.032	0.85	157500.00	5026.55	33.00	420.88	2115579.77	4276880.27	6392460.04
0.020	0.85	157500.00	3217.00	33.00	420.88	1353974.42	4327638.15	5681612.57
0.012	0.85	157500.00	1809.56	33.00	420.88	761609.56	4367116.84	5128726.40
0.008	0.85	157500.00	1256.64	33.00	420.88	528895.99	4382626.25	4911522.24

Table 4-2: Axial load capacity of short L-shaped wall from analysis for pin-pin end case

ρ	K3	As (mm2)	Fy (MPa)	Ps=(Asxfy) (N)	Po gross from analysis(N)	Pc gross=(Po gross from analysis-Ps)(N)	Pc Factored=(Pc grossxk3) (N)	Po factored=(Ps+Pc factored)(N)
0.032	0.85	5026.55	420.88	2115579.77	7078966.00	4963386.23	4218878.30	6334458.07
0.020	0.85	3217.00	420.88	1353974.42	6478113.50	5124139.08	4355518.22	5709492.64
0.012	0.85	1809.56	420.88	761609.56	6002849.00	5241239.44	4455053.53	5216663.08
0.008	0.85	1256.64	420.88	528895.99	5814024.00	5285128.01	4492358.80	5021254.80

Table 4-3. Axial load capacity of short L-shaped wall from analysis for fixed-fixed end case.

ρ	K3	As(mm^2)	Fy(MPa)	Ps=(Asxfy) (N)	Po gross from analysis(N)	Pc gross=(Po gross from analysis-Ps) (N)	Pc Factored=(Pc grossxk3) (N)	Po factored=(Pc factored+Ps) (N)
0.032	0.85	5026.55	420.88	2115579.77	7164606.00	5049026.23	4291672.30	6407252.07
0.020	0.85	3217.00	420.88	1353974.42	6542167.00	5188192.58	4409963.69	5763938.11
0.012	0.85	1809.56	420.88	761609.56	6041148.00	5279538.44	4487607.68	5249217.23
0.008	0.85	1256.64	420.88	528895.99	5831975.00	5303079.01	4507617.15	5036513.15

Table 4-4. Comparison of axial load capacity from equation and analysis.

Po factored JAMES K.WIGHT & JAMES G.MACGREGOR(N)	Po factored from analysis by ABAQUS pin-pin end case(N)	Po factored from analysis ABAQUS fixed-fixed end case(N)	Po factored JAMES K.WIGHT & JAMES G.MACGREGOR/Po factored from analysis by ABAQUS pin-pin ended case (%)	Po factored JAMES K.WIGHT & JAMES G.MACGREGOR/Po factored from analysis by ABAQUS fxed-fixed ended case (%)
6392460.041	6334458.065	6407252.065	100.916	99.769
5681612.569	5709492.638	5763938.113	99.512	98.572
5128726.400	5216663.084	5249217.234	98.314	97.705
4911522.242	5021254.799	5036513.149	97.815	97.518
			average=99.139	average=98.391

From comparison of axial load capacity of L-shaped wall from equation and analysis, we can conclude as it is possible to use finite element analysis to determine axial load capacities of desired walls by those parameter used in this model.

4.3. Validation two

(Hany A.Kottb,Nasser F.El-Shafey, & Akram A. Torkey, 2015) Studied the behavior of high strength concrete columns under eccentric loads at Cairo University research center to observe the effect of eccentricity of axial load, column slender ness ratio, longitudinal steel ratio and diameter of stirrups. The study was carried on by conducting a test of different specimens with different parameters including different reinforcement details. A test was carried by AMSELLER compression machine with 5000 KN capacity at Cairo University concrete research laboratory. The concrete strains in both tension and compression sides were measured by 200mm demec gauges, the demec gauges were placed at column mid height, lower and upper quarter of column height in both tension and compression sides. Prior to casting of column two electrical strain gauges having 10mm length were attached to both longitudinal and transverse steel at mid height and were connected to data logger indicator to observe strain of steel directly. Lateral deformation of column due to applied load were measured using three LVDT (linear variable differential transformer) of 0.001 mm accuracy placed ,at column mid height and both of column `quarter in tension side. Among the specimens tested by (Hany A. Kottb et al.,

2015) three columns having detailing shown in figure 4.2 are used to validate ABAQUS software result so that the reliability of simulation will be insured.

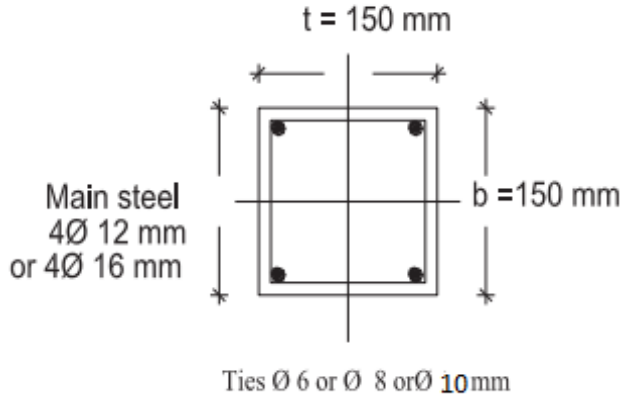

Figure 4-2. Cross section and reinforcement detailing of column used for validation *(Hany A.Kottb et al., 2015)*

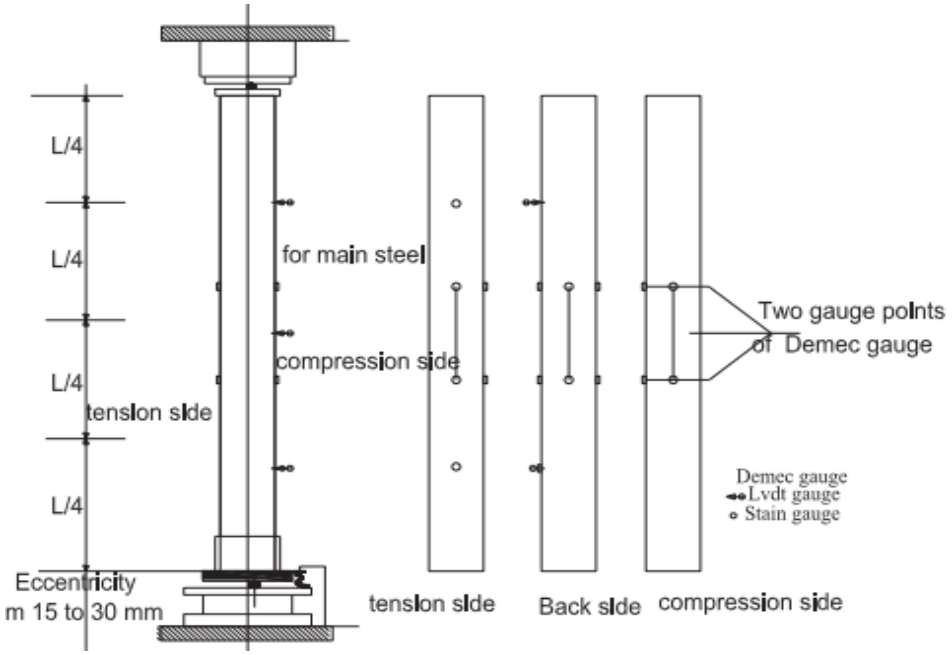

Figure 4-3. Column setup, demec points and details *(Hany A.Kottb et al., 2015.*

Finally test result were compared with nonlinear finite element program ANSYS 11 software results and the results of the experiment was found to agree with that that of ANSYS 11 software results. All the specimens tested were pin ended column having 15 mm concrete cover. Stirrups were at spacing of 60mm for all columns considered. For this

study, Axial load capacity of three columns' test results are compared with ABAQUS finite element analysis result. Details of tested specimens with their designation in (Hany A.Kottb et al., 2015) are listed in Tables 4-5 and Table 4-6 to model to model them for finite element analysis.

Table 4-5. Description of columns used for validation

Column	L(mm)	bxw(mm)	Concrete Cover(mm)	Eccentricity(mm)	Stirrup spacing(mm)	End condition
S8-St8	1500	150x150	15	15	60	Pin-pin
S9-St10	1500	150x150	15	15	60	Pin-pin
S1-R	1500	150x150	15	15	60	Pin-pin

Table 4-6. Material properties of column used for validation.

Column	Concrete(f_{cu}) Mpa	Diameter of stirrup (mm)	Diameter of Longitudinal bar (mm)
S8-St8	65	Φ8 (fy=290 MPa)	Φ12 (fy=580 MPa)
S9-St10	65	Φ10 (fy=650 MPa)	Φ12 (fy=580 MPa)
S1-R	65	Φ6 (fy=290 MPa)	Φ12 (fy=580 MPa)

In (Hany A.Kottb et al.,2015) study, test result were compared with nonlinear finite element program ANSYS 11software results and the results of the experiment was found to agree with that that of ANSYS 11 software results. But for this thesis, the load vs mid height displacement are compared with that of (Hany A.Kottb et al., 2015) test results after modelling and analyzing the above listed columns by ABAQUS software. For validation element mesh size of 20mm and other material properties as mentioned in appendix B are used. Maximum load capacity of all three models are illustrated in Table 4-7. As described by (Hany A.Kottb et al., 2015) all of the three columns were governed by compression failure. As observed from finite element analysis, failure mode specifically at maximum axial load condition are found to be compression failure to all of the three columns which insures the agreement of finite element result and test results.

Table 4-7. Comparison of maximum axial load capacities of columns used for validation.

Column	Max load from Experiment(KN)	Max load from analysis (KN)	$P_{Experiment}/P_{analysis}$ (%)	Average of $P_{Experiment}/P_{analysis}$ (%)
S8-St8	1067	1201.26	88.8	91.98
S9-St10	1262	1212.66	104.1	
S1-R	970	1168.17	83.04	

Comparison of axial load versus mid height displacement relationship of columns tested by (Hany A.Kottb et al.,2015) and finite element analysis results measured from the compression side are compared and found to be agreed well.

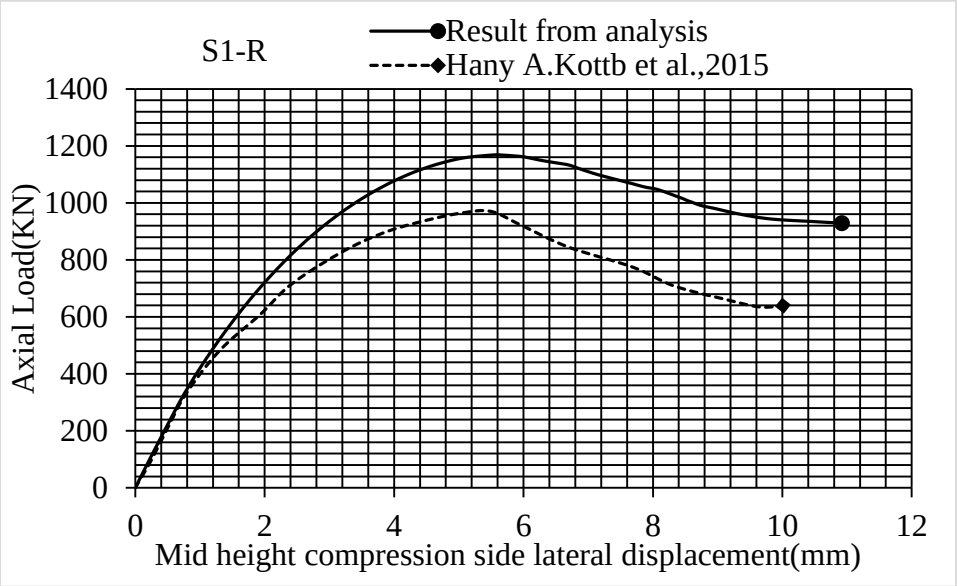

Figure 4-4. Axial load and mid height displacement relation comparison of (Hany A.Kottb et al., 2015) test result and analysis result for column S1-R.

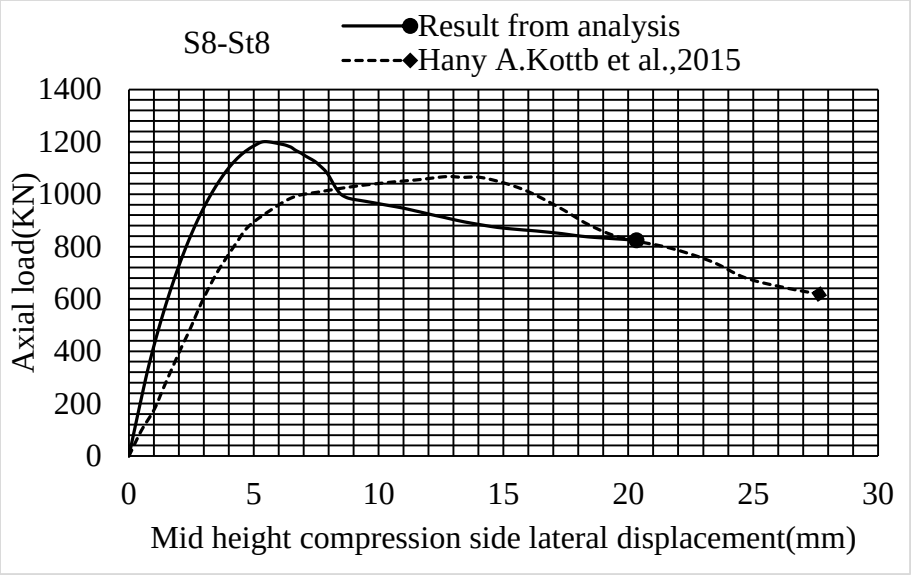

Figure 4-5. Axial load and mid height displacement relation comparison of (Hany A.Kottb et al., 2015) test result and analysis result for column S8-St8.

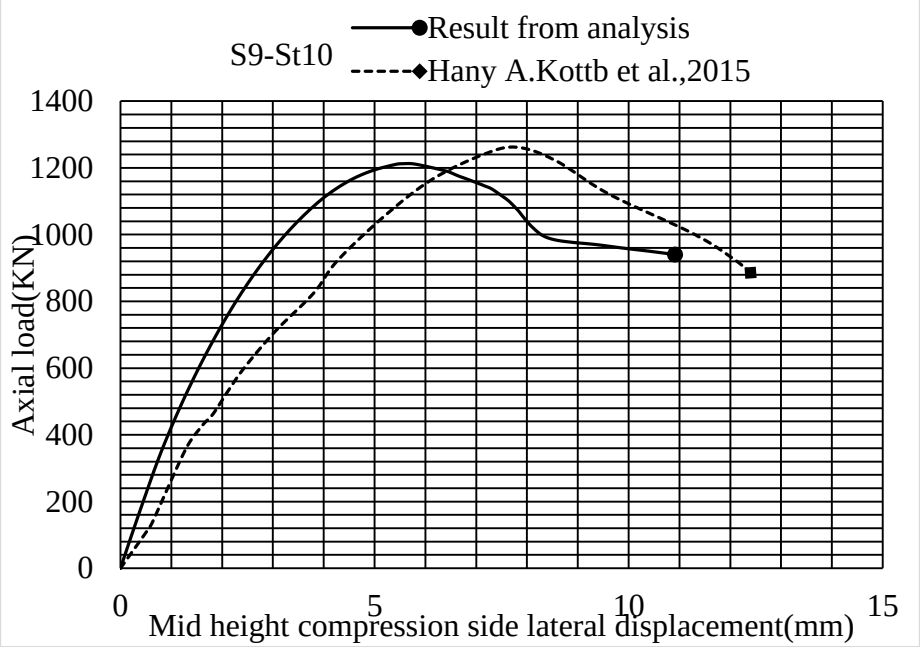

Figure 4-6. Axial load and mid height displacement relation comparison of (Hany A.Kottb et al., 2015) test result and analysis result for column S9-St10.

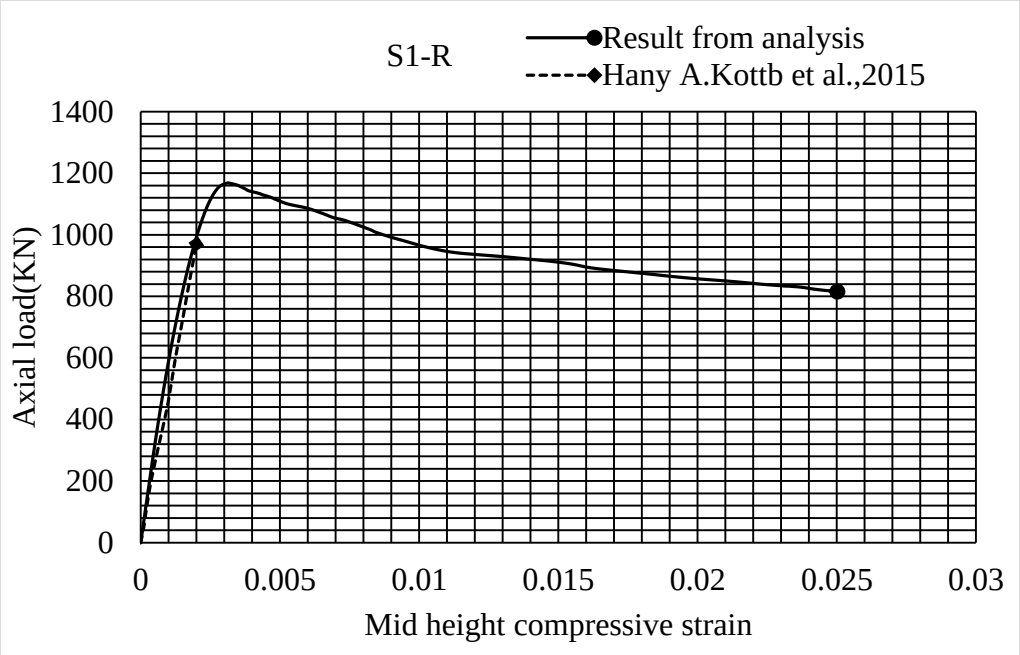

Figure 4-7. Axial load and mid height compressive strain relation comparison of (Hany A.Kottb et al., 2015) test result and analysis result for column S1-R.

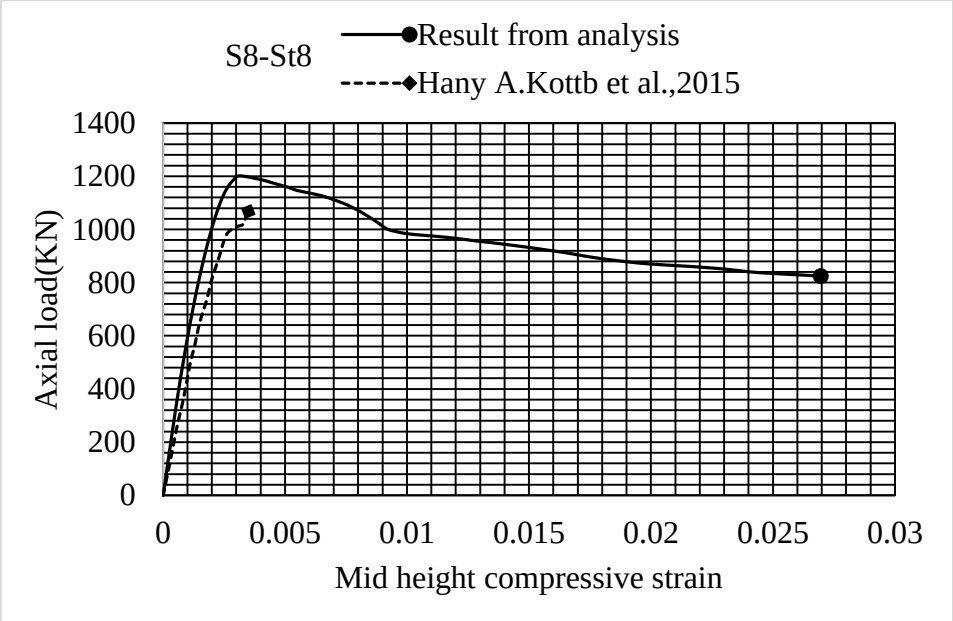

Figure 4-8. Axial load and mid height compressive strain relation comparison of (Hany A.Kottb et al., 2015) test result and analysis result for column S8-St8

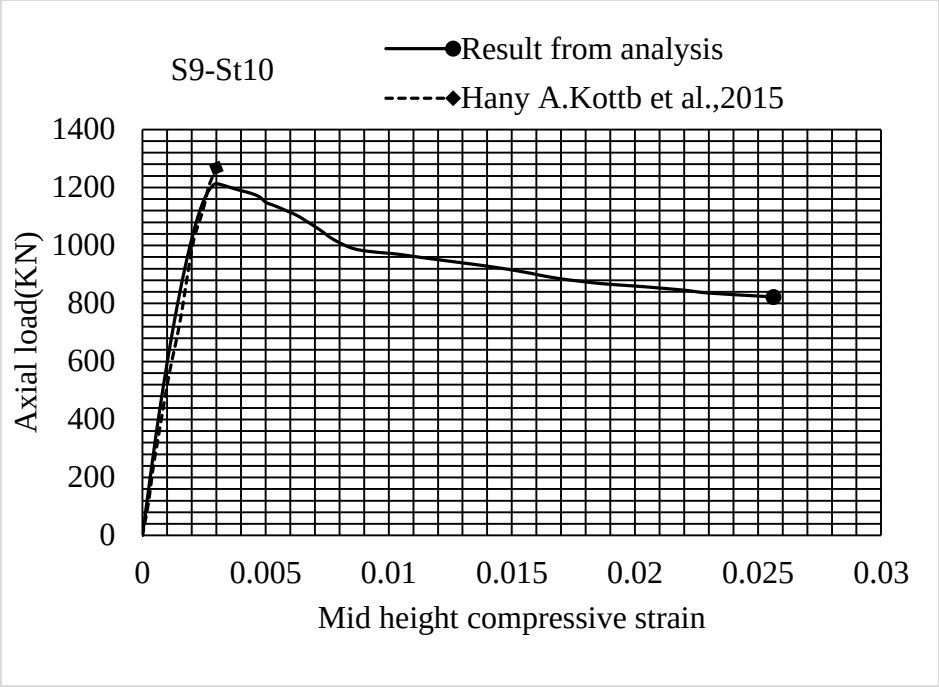

Figure 4-9. Axial load and mid height compressive strain relation comparison of (Hany A. Kottb et al., 2015) test result and analysis result for column S9-St10.

From the load versus mid height displacement relation and load-mid height compression strain relation it is observed that test results and finite element results are approached well.

CHAPTER FIVE

5. RESULT AND DISCUSSION

In this thesis pin ended L-shaped walls with different slenderness ratio (12.63, 22, 33.33) and scaled down C-shaped wall of slenderness ratio (23) are modelled and P-M interaction diagrams are plotted using displacement controlled loading condition for concentric and eccentric load cases. Behavior of such walls observed during the failure modes are discussed. The L-shaped walls are analyzed in different reinforcement steel ratios. Maximum load capacity at each loading condition is extracted from the analysis then moment is calculated from maximum load and eccentricities including mid height deflection during the analysis at maximum load level to account slenderness effect. As end condition is taken to be pin ended, the effective length factor is taken to be 1.

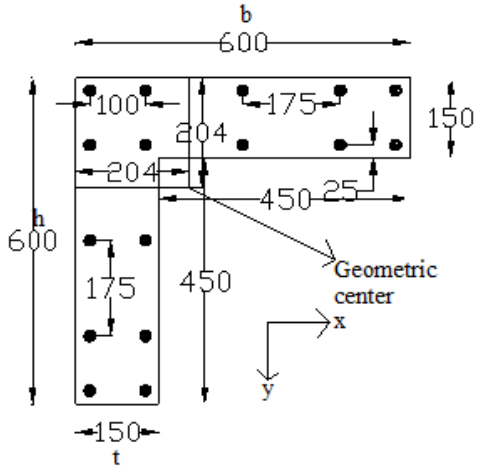

Figure 5-1. Considered cross section and detailing of L-shaped reinforced concrete wall for analysis (all dimensions in mm).

Table 5-1. Considered walls for plotting P-M interaction diagram.

Wall number	Type of wall	Unsupported length(mm)	$\frac{kl_u}{r}$	Column classification
1	L-shaped	2200	12.63	short
2	L-shaped	3800	22	Intermediate
3	L-shaped	5800	33.33	slender
4	C-shaped	4000	23	slender

5.1. Load-mid height lateral displacement curve variation

To develop P-M interaction diagram walls are loaded from zero eccentricity (concentric load) up to large eccentricity (flexural failure).The increment of eccentricity continues up to the point at which the axial load capacity of the walls becomes very small. As concrete is much influence the failure mode at small eccentricities the load mid height displacement curve drops with steeper slopes after pick load to show that failure is accidental. For larger eccentricities as both the steel and concrete influences the failure mode the load displacement curve becomes gentler after pick load to show the contribution of steel up to yield stress which increases ductility after failure. An illustration of load displacement curve for biaxial loads of the wall with slenderness ratio of 22 and steel ratio of 0.032 at different eccentricities is shown in the figure 5-2.

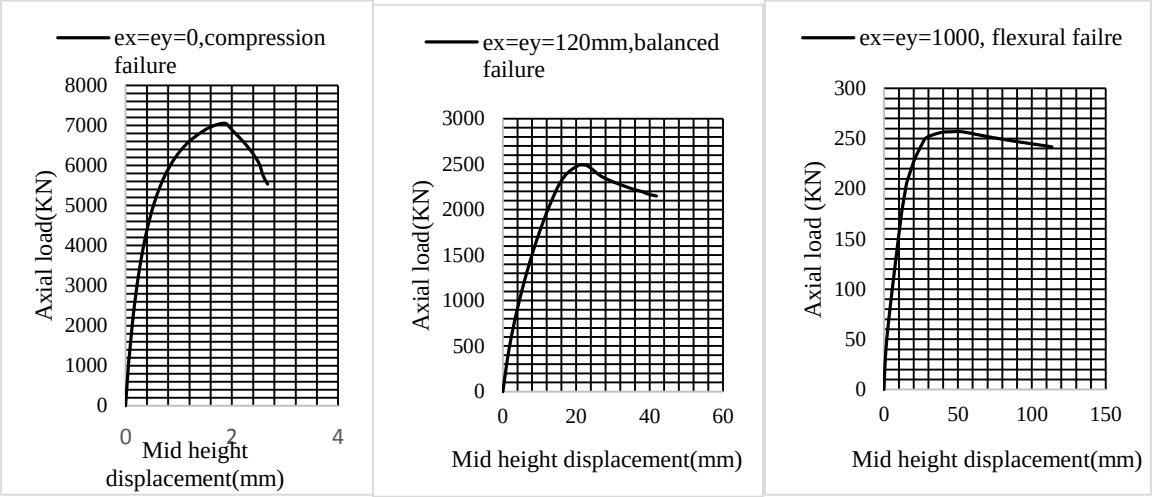

Figure 5-2Variation of load –mid height displacement with eccentricities for L-shaped wall with klu/r=22 and ρ=0.032

5.2. Variation of axial stress distribution with variation of eccentricities

For concentric loads (ex=ey=0), damages of concrete occurs around the support while for those of concentric loads, damage of concrete occurs at the mid height of the considered wall as shown in Figure 5-3.At more compressively damaged regions both concrete and longitudinal bars are subjected to compressive strain while the stirrup is subjected to tensile strain. Damages of concrete are expressed in %.

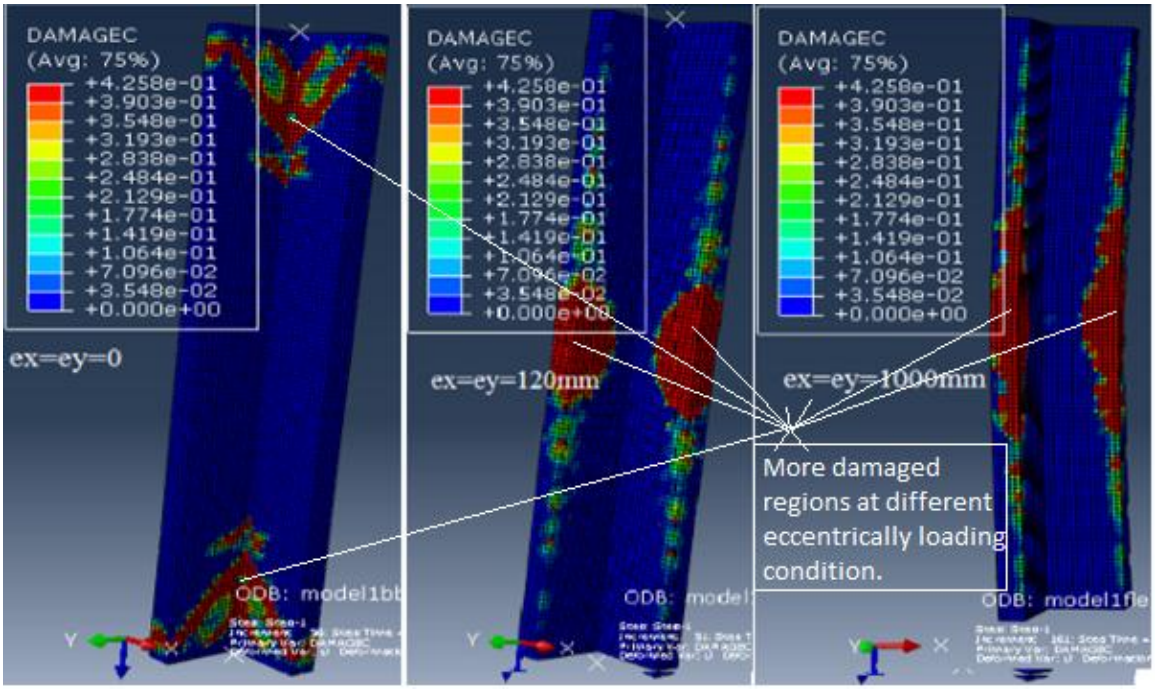

Figure 5-3.Variation of concrete compression damage location with location of axial load for wall with klu/r=22 and ρ=0.032.

As practically known when a specimen is axially in compression, it is in tension laterally and when it is in tension longitudilly, it is in compression laterally. This phenomena is well illustrated in appendix C-4 from analysis results using ABAQUS software.

For concentric loads both concrete and steel (longitudinal bar and stirrup) are much stressed near to the support at which more damages of concrete is illustrated as Figure 5-3. The stress of reinforcement bars when half part of the member is considered is illustrated in Figure 5-4.

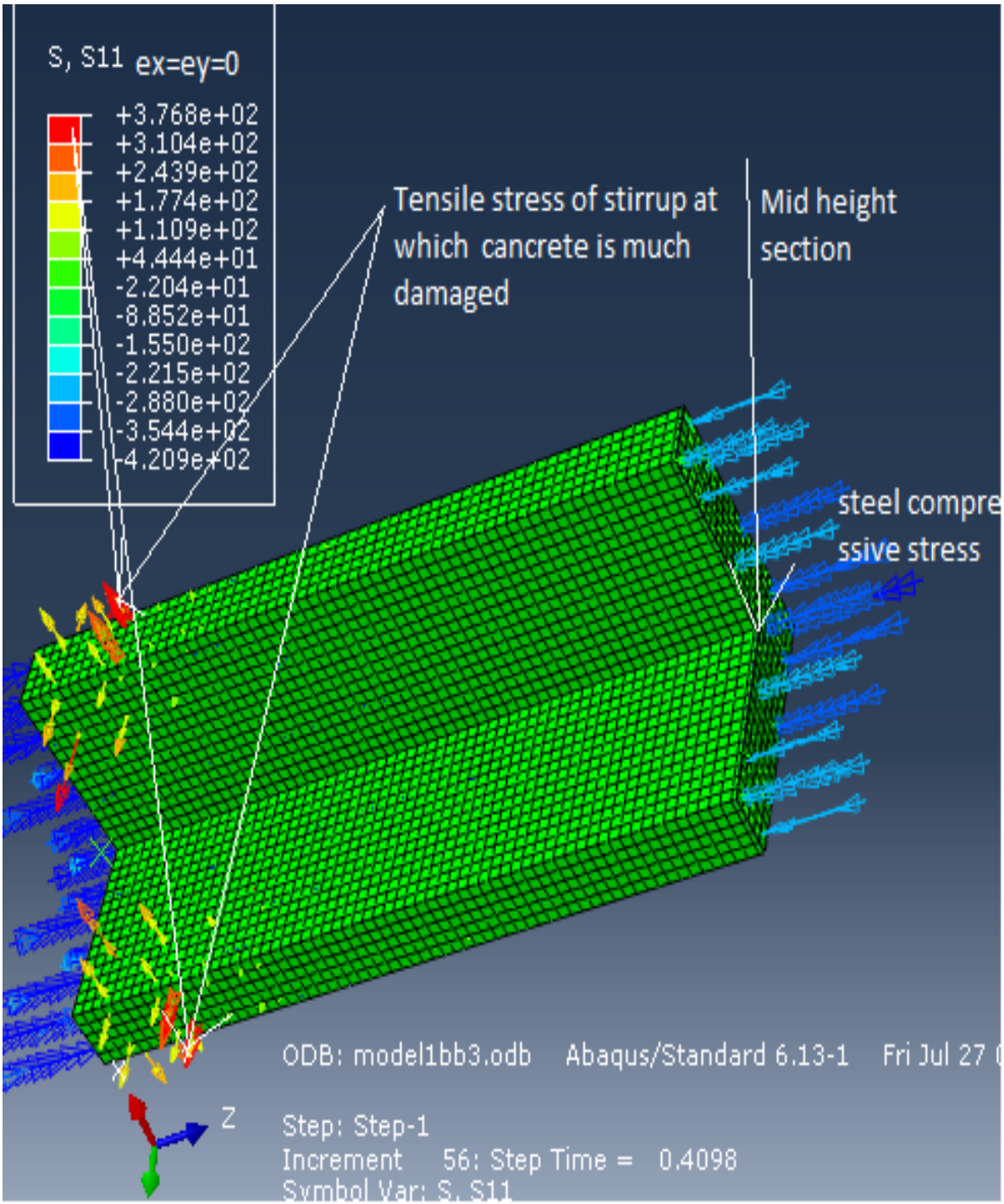

Figure 5-4. Reinforcement steel stress distribution for concentric loads of L-shaped wall taken below mid height section for wall with klu/r=22 and ρ=0.032.

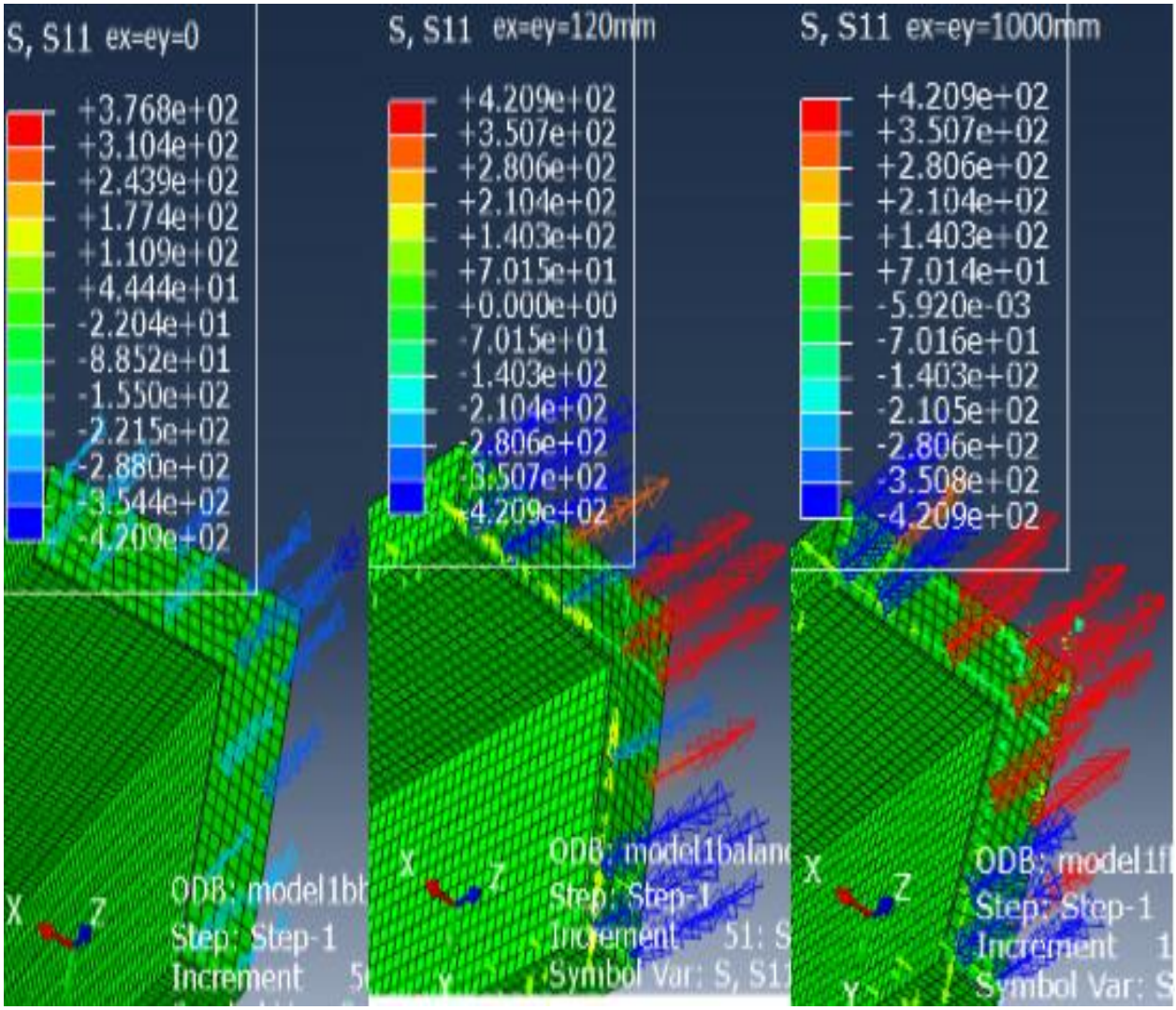

Figure 5-5. Variation of axial stress distribution with eccentricities of reinforcement steel at mid height of wall for wall with klu/r=22 and ρ=0.032.

For concentric loads mid height section is subjected for compressive stress like that of longitudinal bars as shown in Figure 5-6.

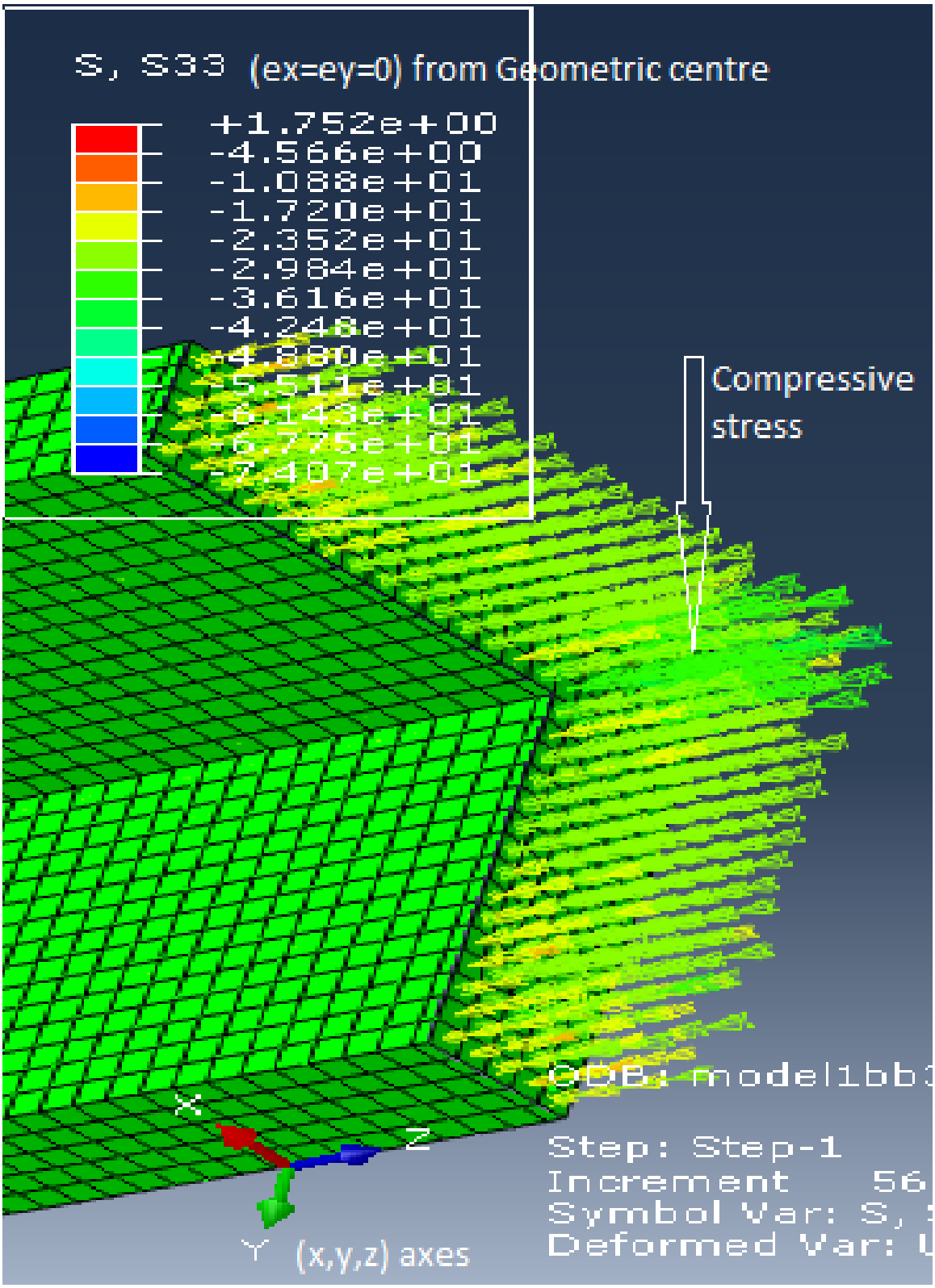

Figure 5-6. Concrete stress distribution for concentric load of considered wall at the mid height for wall with klu/r=22 and ρ=0.032.

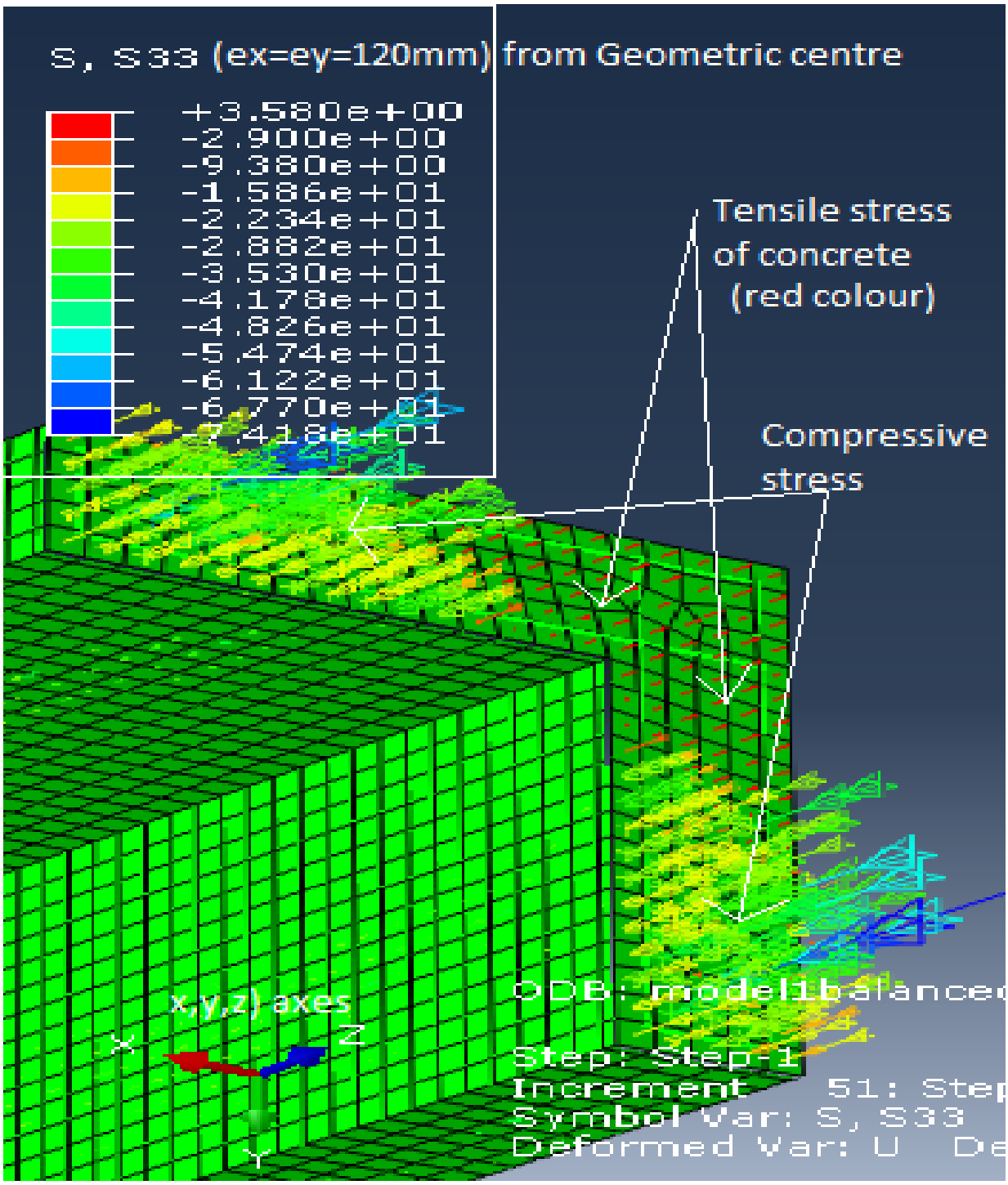

.Figure 5-7.Concrete stress distribution for eccentric load of considered wall at balanced failure at the mid height of the wall with klu/r=22 and ρ=0.032.

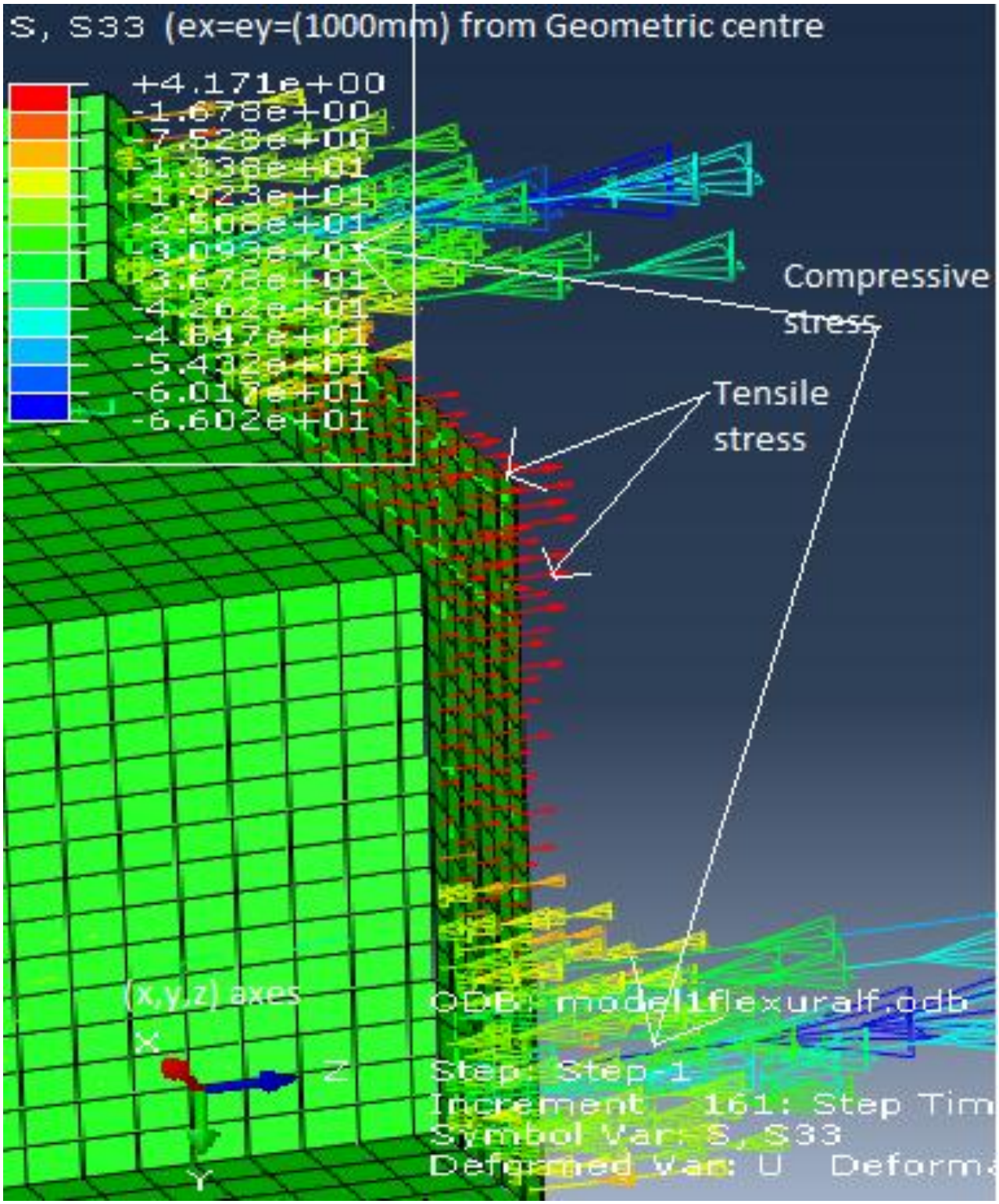

Figure 5-8. Concrete stress distribution for eccentric load of considered wall at flexural failure at the mid height of the wall with klu/r=22 and ρ=0.032.

The concrete compression damage for concentric load condition occurs near the support while this damage occurs around the mid height for eccentric load condition.

5.3. Effect of slenderness ratio on the P-M interaction diagram

As the column becomes slender, because of the increase of maximum moment at mid height due to the increase of mid height deflections, the axial load capacity is reduced. This reduction in axial load capacity results from what are referred to as slenderness effect (JAMES K.WIGHT & GAMES G.MACGREGOR, 2012).From this thesis, effect of slender ness ratio is found to lesser for short walls which approaches the dictated theory by (JAMES K.WIGHT & GAMES G.MACGREGOR, 2012).

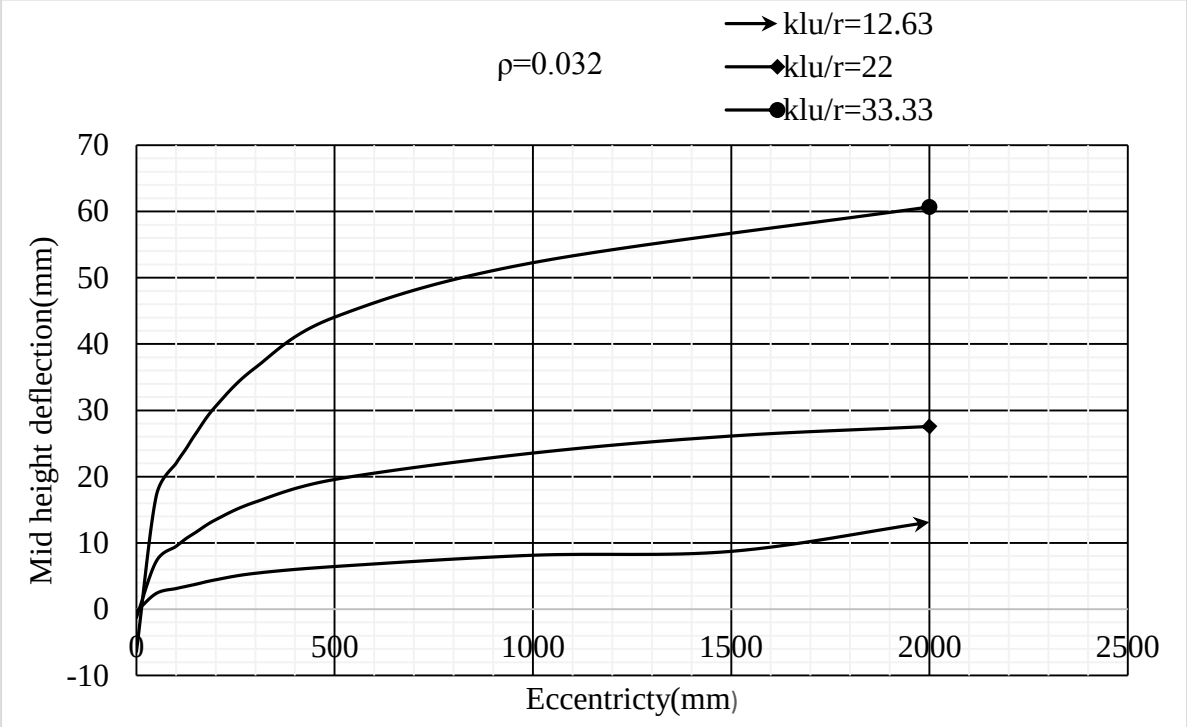

Figure 5-9.Increment of mid height deflection at maximum axial load level of L-shaped wall loaded uniaxialy with variation of slenderness ration for equal eccentricities.

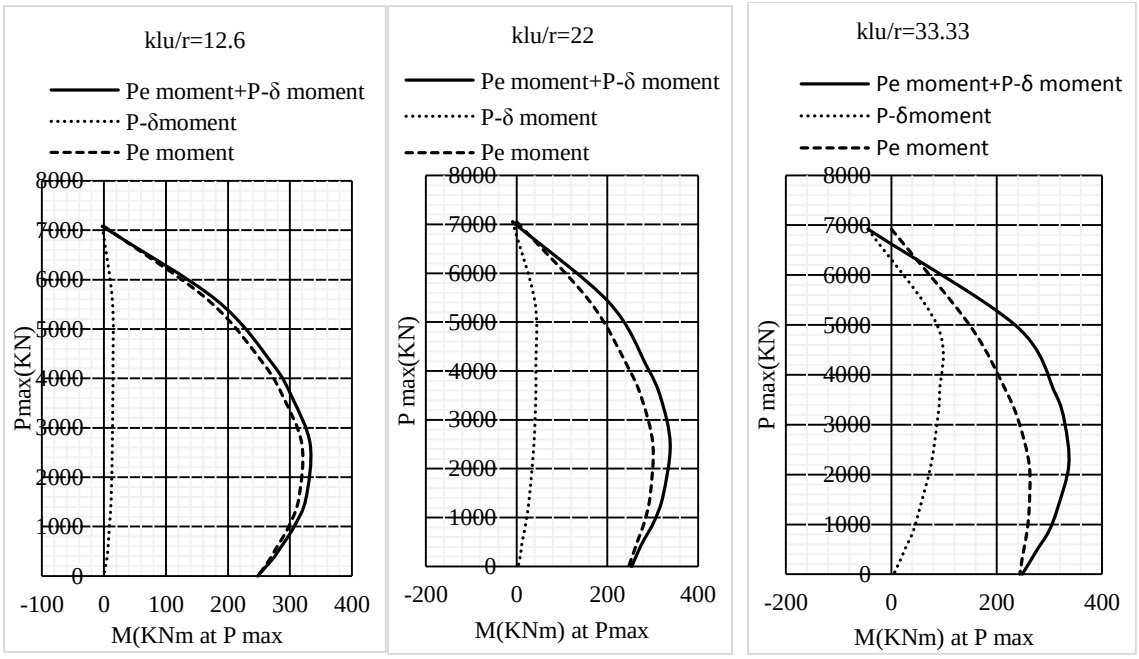

Figure 5-10. Illustration of P-δ moment and Pe moment contribution to total moment on P-M interaction diagram keeping all parameters constant for L-shaped wall loaded biaxialy at 45°.

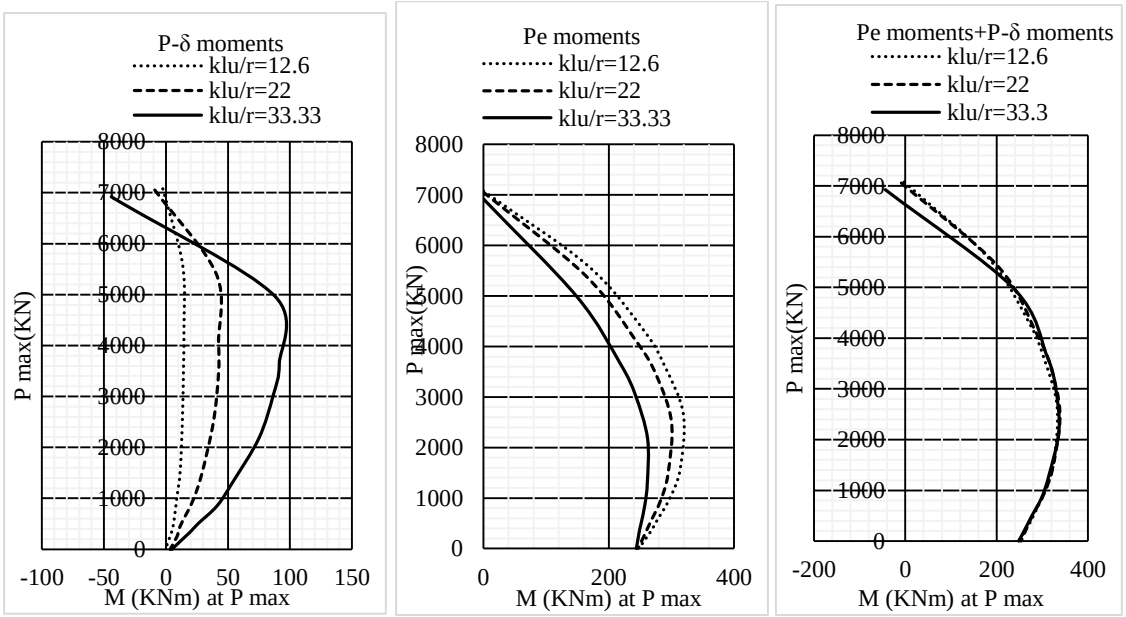

Figure 5-11. Illustration of Pe moment and P-δ moment independently for different slenderness ratio keeping all parameters constant for L-shaped wall loaded biaxialy 45°.

Detailed P-M interaction diagrams are well illustrated in appendix A.Walls are investgated by loading them both in uniaxial eccentricities and by axial eccentricities at an angle of 45 degree from both x and y axes. Steel ratios are varried with the limmit specified by (EBCS

EN 1992-1-1:2013) .Once the maximum axial load carrying capacity of walls at different eccentricities are extractted from soft ware analysis, then moments are calaculated from axial load and eccentricities including second order effect.For the case of channel section core walls,to model and analyse standarad sections there is convergence problems of resonable element size so that the model is scaled down by a factor of 1/3.In this thesis investigation of C-shaped wall is limmited to scaled down model.

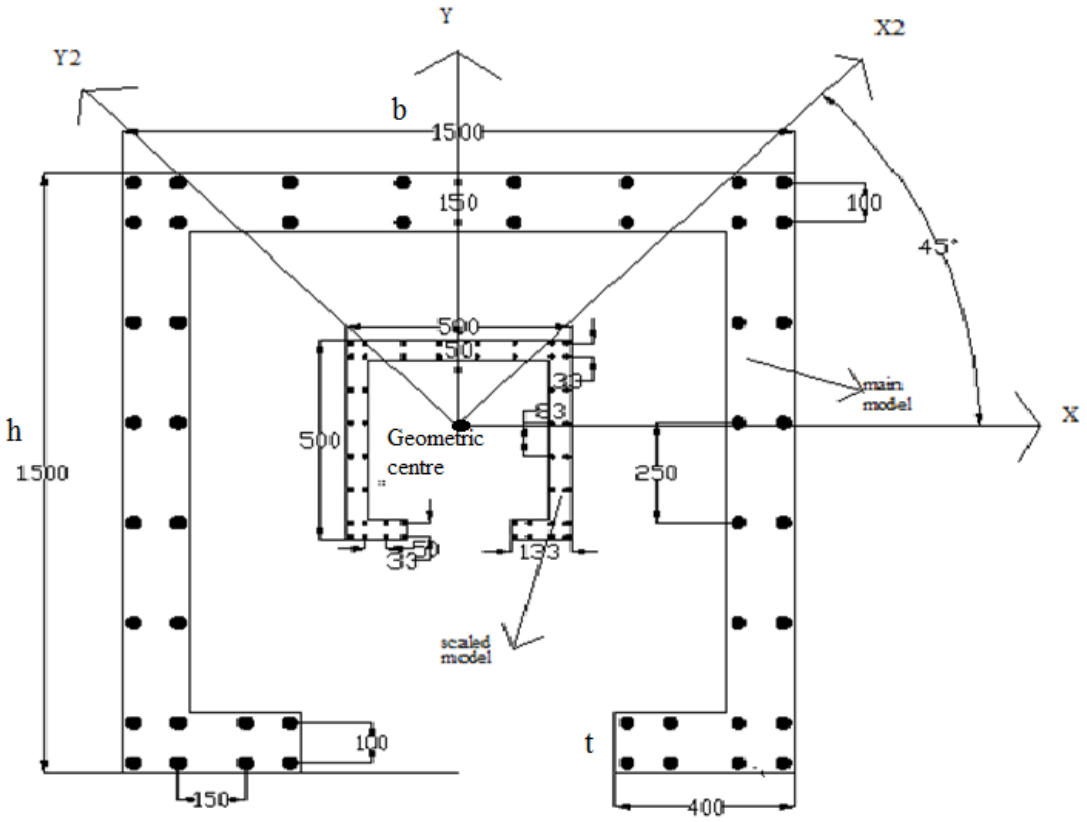

Figure 5-12. Stanadard and scaled down channel shaped core wall considered for finite element analysis (all dimension in mm)

The scaled down model with length of 4000m has cross sectional area of 78333 mm^2 and corresponding moment of inertia of $I_x = 2.394x10^9 mm^4$ and $I_y = 3.022x10^9 mm^4$ about both x and y axes. The radius of gyration of the section is then $r_x = \sqrt{\frac{I_x}{A}} = 174.82\ mm$ and the corresponding slenderness ratio for pip-pin ended case is $\frac{kl_u}{r} = 23$ for pin-pin end case.

Axial stress variation with variation of eccentricity of channel shaped reinforced concrete wall for only steel ratio of 0.03 is illustrated in appendix C.

CHAPTER SIX

6. CONCLUSION AND RECOMMENDATION

6.1. Conclusion

From the investigation of this thesis, the following points are observed

- Axial load versus mid height lateral displacement curve becomes smoother as the eccentricity increases throughout the curve (before ultimate load and after ultimate load) but much significant after point of failure load.
- From the stress distribution of mid height cross-section, concrete material is effectively used for concentric loading condition, while longitudinal reinforcement is effectively used at lager eccentricities.
- Concrete compression damage of considered walls is around the support for concentric loads and propagates towards the mid height compression side for eccentric loads.
- Lateral mid height deflection of walls for both biaxial and uniaxial load cases increase as the slenderness ratio of the wall increases keeping the eccentricity and other parameters constant.
- In P-M interaction diagram P-δ moment (moment due to mid height deflection of braced walls) contributes much in slender column when compared to that of short column for both uniaxial and biaxial load cases.

6.2. Recommendation

As specific cross-section and one material property (unique concrete and steel grades) for only axial load with pin ended boundary condition is investigated in this thesis, one is recommended to have investigation on the following cases.

- Analysis of reinforced concrete walls for other concrete and steel grades or other cross-sections as is tiresome to study effects of many parameters by a single research.
- Formulation of an equation to scale up or scale down axial load carrying capacity of reinforcement concrete wall from a sample by having a look at effect parameters used in modelling of reinforced concrete walls.
- Analysis of reinforced concrete walls incorporating lateral load to the analysis and then investigating axial force-moment-shear (P-M-V) interaction relation.

References

A.W.Irwin. (1984). *Design of shear wall buildings.* London.

ACI committee 318. (2011). *Building code requirments for structural concrete (ACI 318M-11) an ACI standard and comentary.* U.S.A.

ACI Committee 446 on fracture mechanics. (1992). Fracture mechanics of concrete structures. Colorado,USA.

AHMER, A., DOOKIE, K., & CHO., S. G. (2013). Modelling of non linear cyclic load behavior of I-shaped composite still concrete shear walls of nulear power plants. *Nuclear Engineering and Technology*.

Ashraf, R. M., Mohie, S. S., & Janet, M. S. (2014). Prediction of the behavior of reinfored concrete deep beams with openings using finite element method. *Alexandria Engineering Journal*.

Asnakew Abebe. (2009). Development of design aid for selected single channel flanged reinforced concrete core walls. Addis Ababa, Ethiopia.

Damigo J.Carreira & Kuanh-Han Chu. (1986). Stress-strain relationship for reinforced concrete in tension. *ACI Journal*.

Dassault systemes simulia crop. (2013). *Abaqus 6.13-1 manual.* providence,RI,USA.

EBCS EN 1992-1-1:2013, *EBCS-2 Design of concrete structures.Etiopian Building Codes of Standard prepared by Ministry of Urban Development and Construction,* Addis Ababa, Ethiopa.

EBCS2. (1995). *EBCS-2,Structural use of concrete.Etiopian Building Codes of Standard prepared by Ministry of Works and Urban Development,*Addis Ababa,Ethiopia.

EBCS-8. (1995). *Design of structures for earth quake resistance.Etiopian Building Codes of Standard prepared by Ministry of Works and Urban Development,*Addis Ababa,Ethiopia.

EC-2. (1985). *Manual for the design of rienforced concrete building structures.*

Fragomeni, S., Doh, J.-H., & Lee, D. (2012). Behavior of axially loaded concrete wall panels with openings:An experimental study. *Advances in structural engineering*.

Hany A.Kottb,Nasser F.El-Shafey, & Akram A. Torkey. (2015). Behavior of high strength columns under eccentric loads. *Housing and Building National Research Center*.Giza,Egypt.

JAMES K.WIGHT & GAMES G.MACGREGOR. (2012). *Reinforced concrete mechanics and design.* USA: Pearson education,Inc.,Upper Saddle River,New Jercy 07458.

Jyoti S.Tekavde & S.S.Angalekar. (2016). Non linear buckling analysis of reinforced concrete wall by using different parameter. *Intrenational jouranal of Engineering Science and Research Technology*.

K.Beyer & R.Constantin. (2012). Modelling of Reinforced Concrete Core Walls Under Biadirectional Loading.

Kibrealem Mebrahtu. (2005). *Development of computer program and preparation of design aids for commonly used sections of RC shear wall systems.* Addis Ababa.

M.M. Islam, A., Dhar, F., Patowary, J., Asif, S., Rahman, S., Das, S., . . . A, S. (2015). Experimental investigation and finite element analysis on P-M interaction diagram of RC square column made of steel fiber reinforced concrete(SFRC). Dhaka,Bangladesh.

Mario M.Attard. (1994). Buckling of reinforced concrete walls. Sydney, Australia.

Melaku Mohammed. (2009). *A computer program for generating design chart of L-shaped short columns on the basis of EBCS-2 1995.* Addis Ababa.

Rozalija Kozul & David Darwin. (1997). *Effects of aggregate type,size and content on concrete strength and fructure energy.* Lwrence,Kansas.

S.S.Ray. (1995). *Reinforced concrete analysis and design.* London WC1N 2BL,: Blackwell science Ltd.

Sabetahd, R., Reza Bagerzadeh Karimi, M., & Sadeg bagerzadeh, M. (2012). Seismic behavior of reinforced concrete thin shear walls under various axial load ratios. *International Journal of Civil and Environmental Engineering*.

Sosa, D. E., Arévalo, D., David, M., Correa, B., Albuja, D., Gómez, & Christian. (2017). Experimental and analytical study of slender reinforced concrete shear wall under in-plane cyclic lateral load. *Mathematical problem in engineering*, 14.

Szczecina Michal & WinnickiAndrzej. (2015). Calibration of the CDP model parameters in ABAQUS. *Advance in Structural Engineering and Mechanics.* Incheon.Korea.

T.PAULAY*. (1972). Some aspects of shear wall design. *Bulletin of N.Z.society for Eart quake Engineering*.

T.POULAY&R.PARK. (1974). *Reinforced concrete structures.* Christchurch,New Zealand.

Thakkar, B. K. (2012). Analysis of shear wall under compression and bending. *Current Trends in Technology and Science*.

The Inistitution of Structural Engineers. (2000). *Manual for design of reinforced concrete building structures to EC2.*

Velbo and Ghali. (1977). Moment curvature relation of reinforced concrete slabs. *American society of civil Engineers.*

W.WALLACE, J. (2007). *Modelling issues for tall reinforced concrete core wall buildings.* Retrieved from www.interscience.wiley.com

Y F Gao & A F Bower. (2004). A simple technique for avoiding convergence problems in finite element simulations of crack nucleation and growth on cohesive interfaces. *Modelling and simulation in material Science and Engineering*.

Yunus Dere & Mehmet Alpaslan Koroglu. (2017). Nonlinear FE Modelling of Reinforced Concrete. *International Journal of Structural and Civil Engineering Research*.

Appendix

Appendix A:P-M interaction diagrams of L-shaped walls for different cases

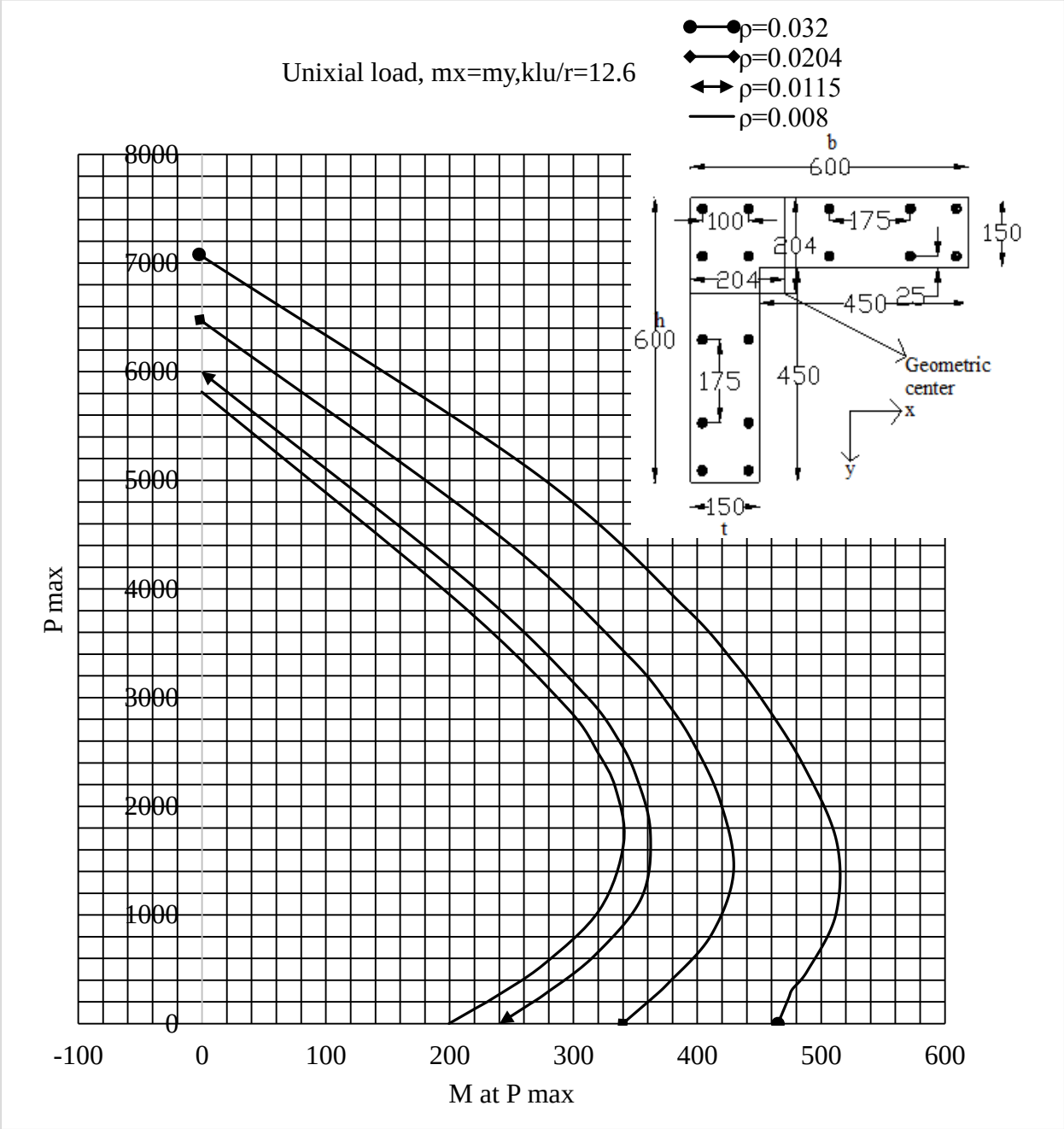

Figure A-1. P-M interaction diagrams of L-shaped wall of klu/r=12.6 loaded uniaxially.Dimensions in mm

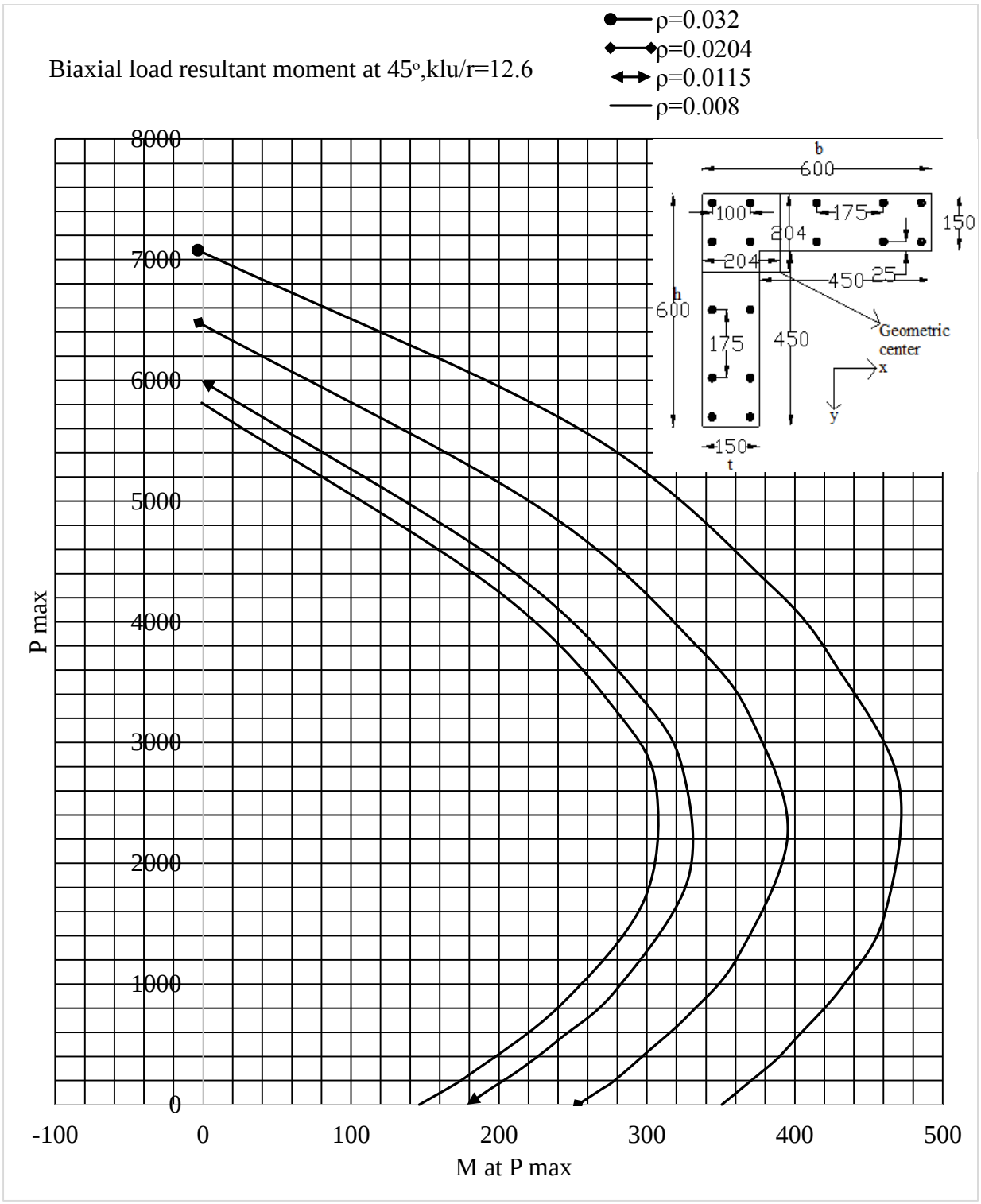

Figure A-2. P-M interaction diagrams of L-shaped wall using resultant moment for klu/r=12.6 loaded biaxially at 45°. Dimensions in mm.

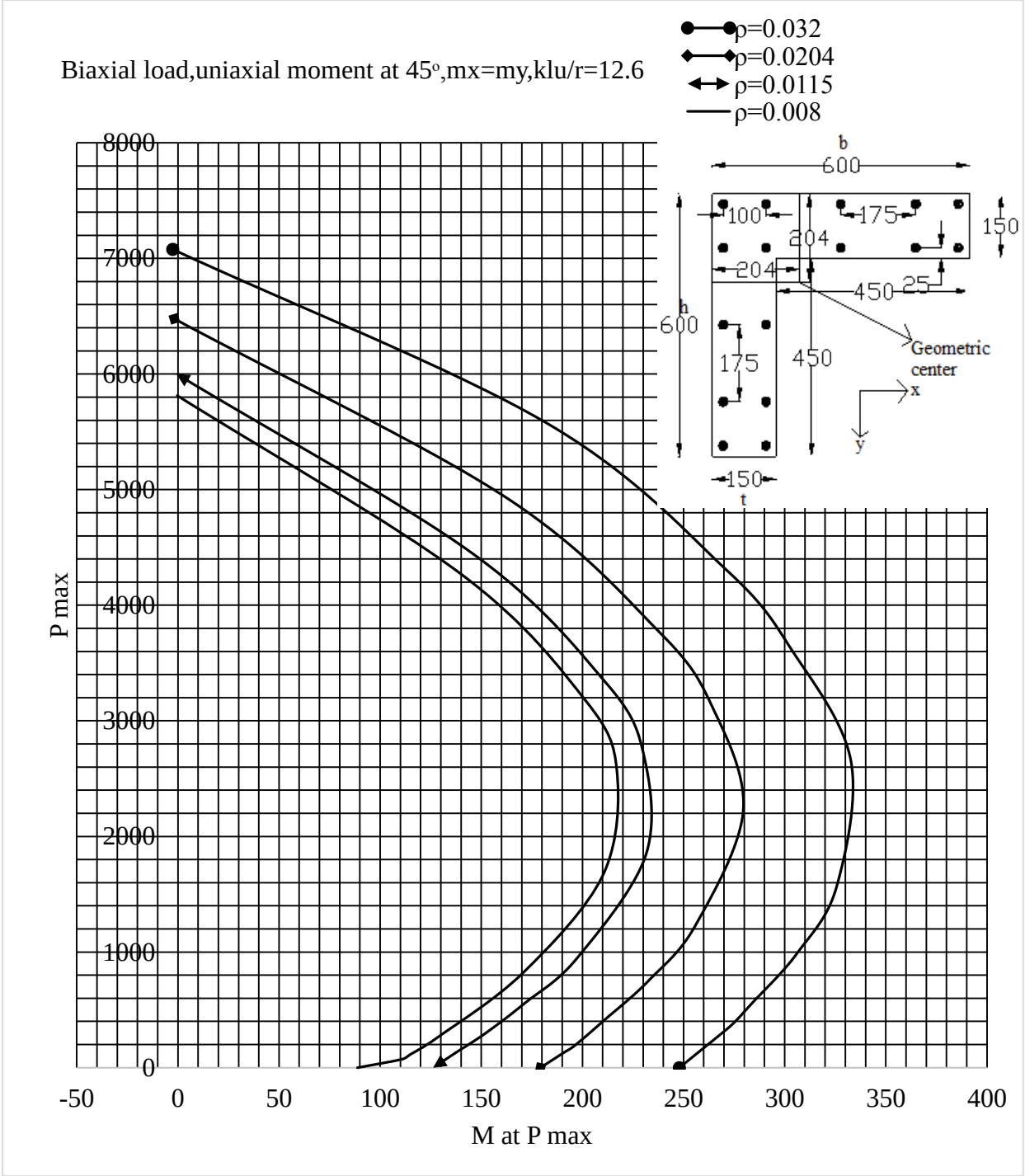

Figure A-3. P-M interaction diagrams of L-shaped wall using uniaxial moment for klu/r=12.6 loaded biaxially at 45°. Dimensions in mm.

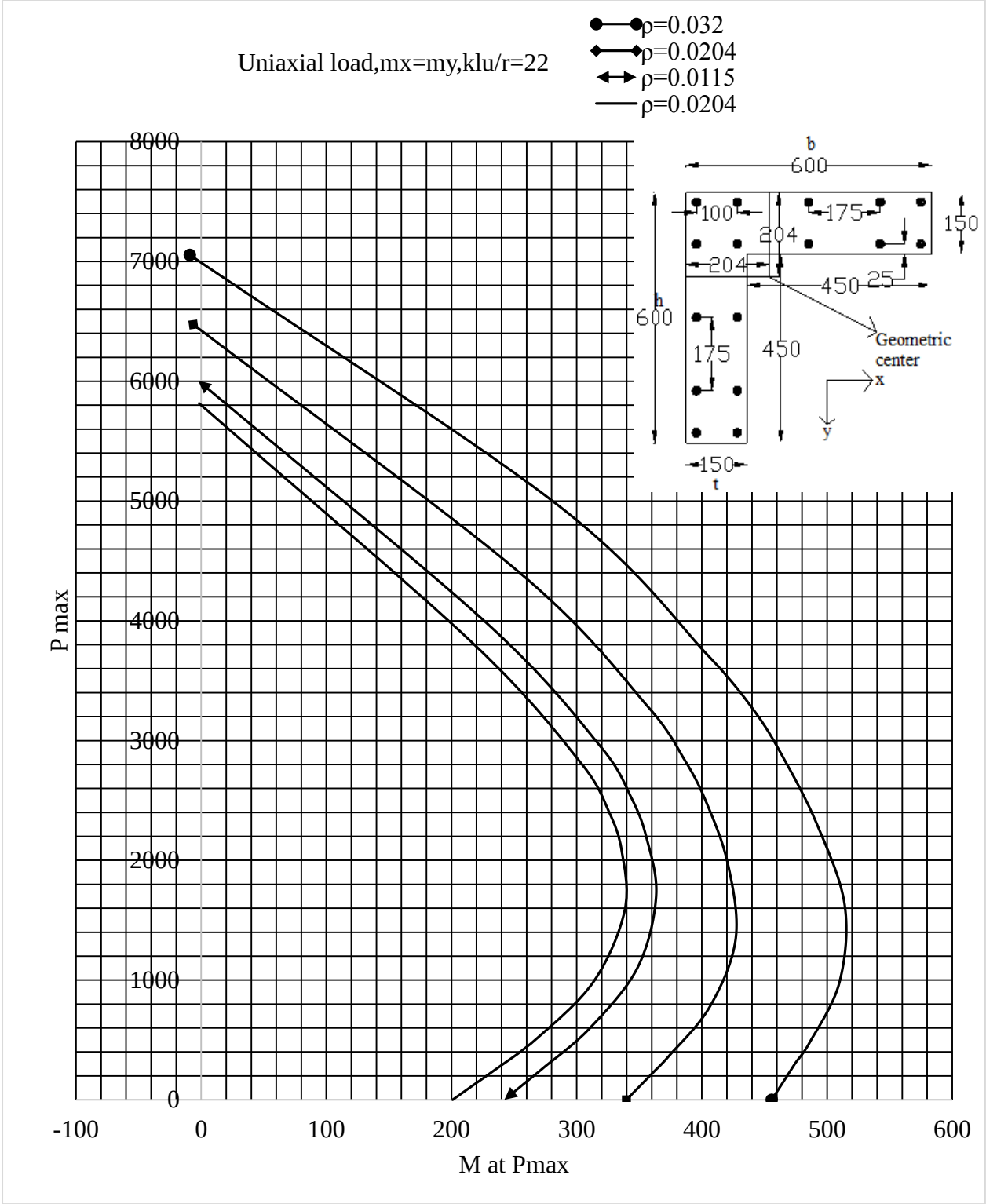

Figure A-4. P-M interaction diagrams of L-shaped wall of klu/r=22 loaded uniaxially. Dimensions in mm.

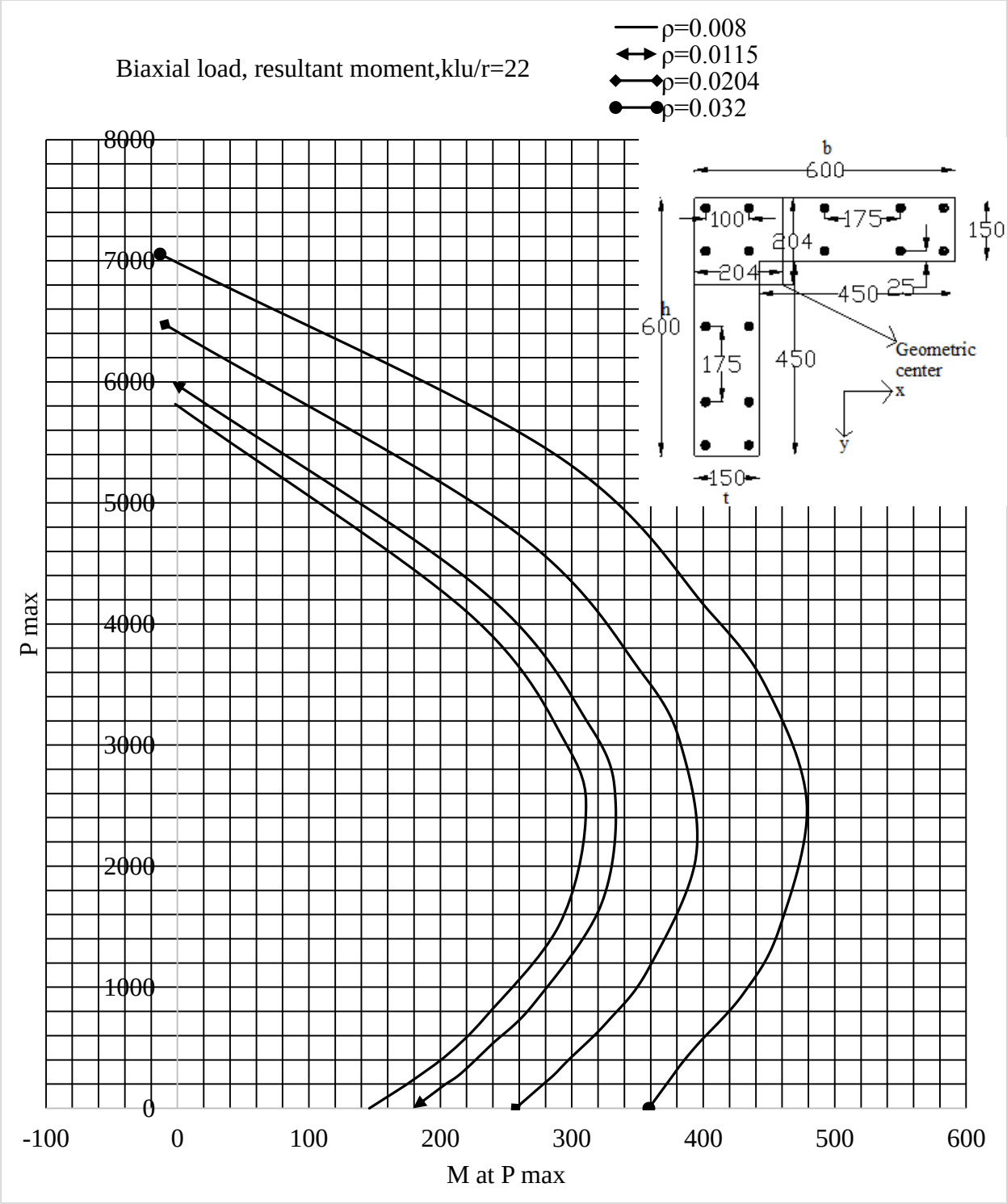

Figure A-5. P-M interaction diagrams of L-shaped wall using resultant moment for klu/r=22 loaded biaxially at 45°. Dimensions in mm.

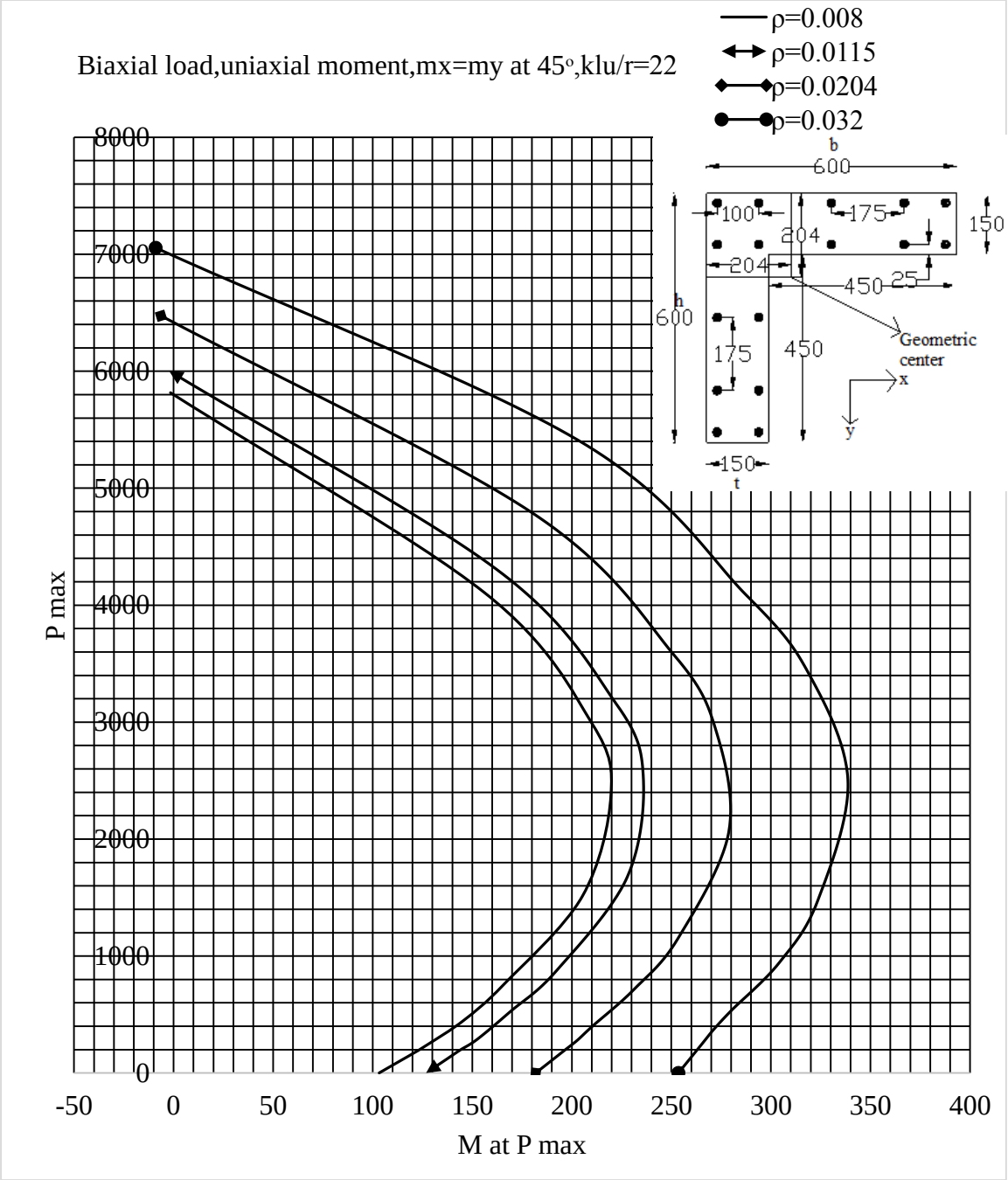

Figure A-6. P-M interaction diagrams of L-shaped wall using uniaxial moment for klu/r=22 loaded biaxially at 45°. Dimensions in mm.

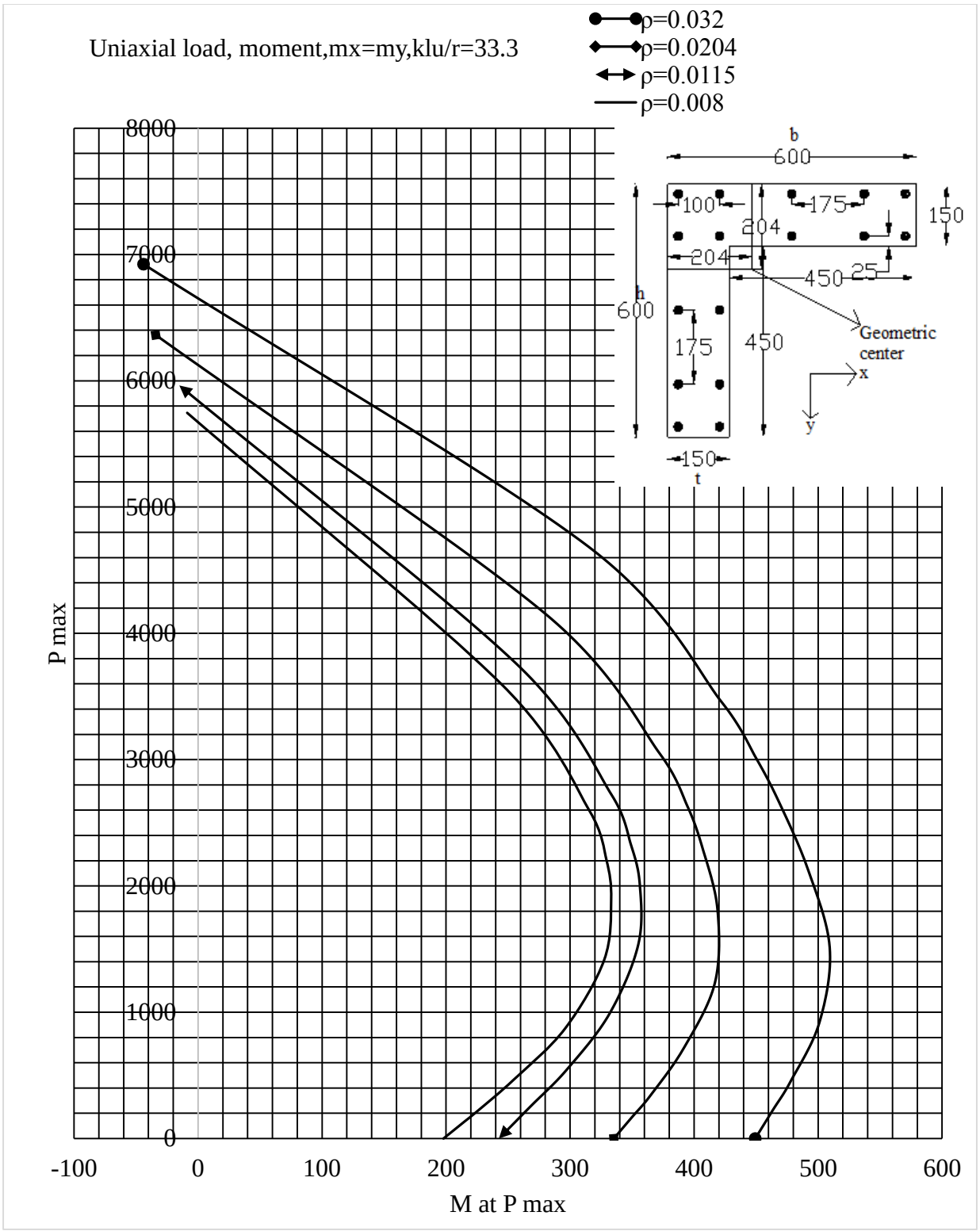

Figure A-7. P-M interaction diagrams of L-shaped wall of klu/r=33.33 loaded uniaxially. Dimensions in mm.

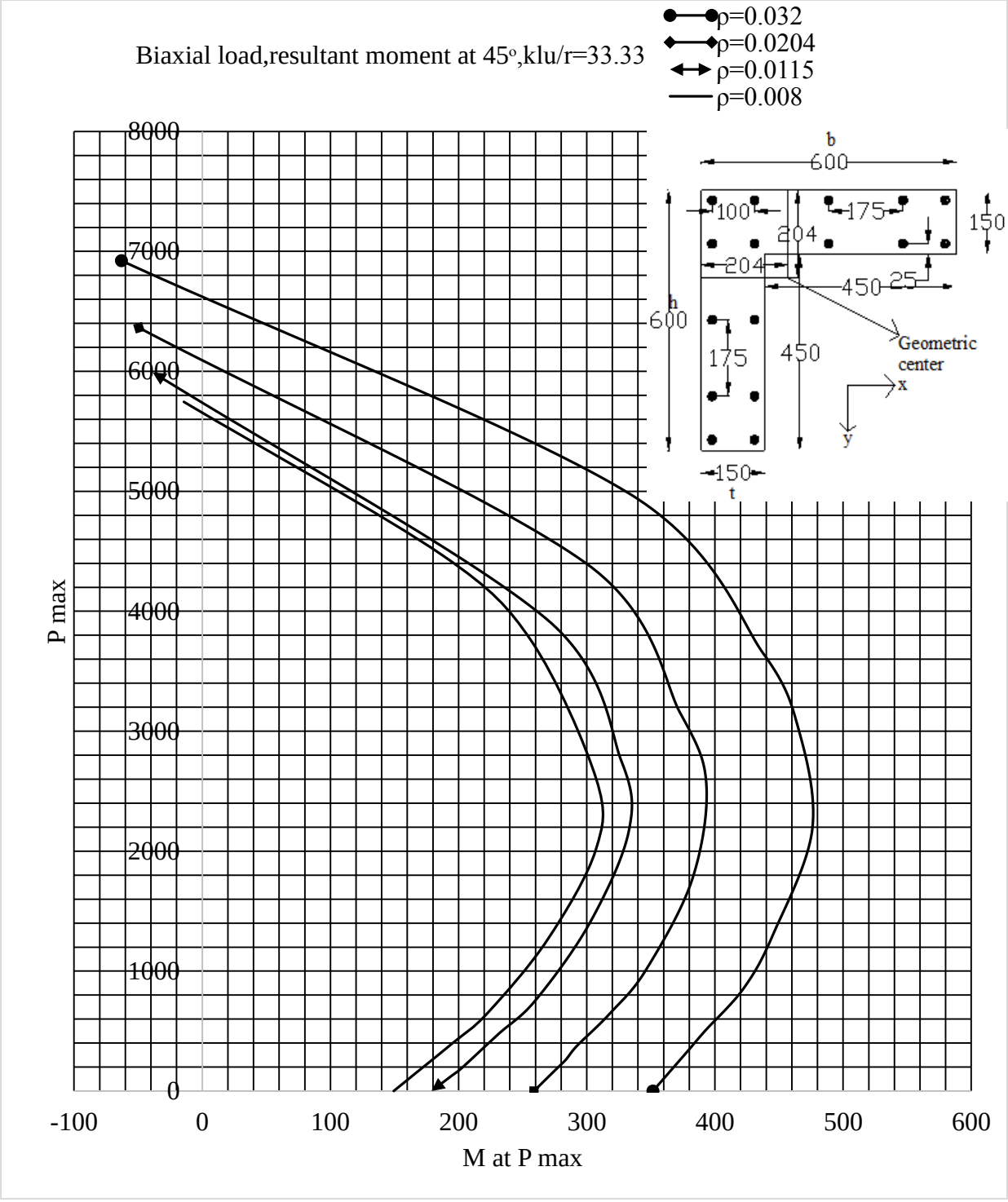

Figure A-8. P-M interaction diagrams of L-shaped wall using resultant moment for klu/r=33.33 loaded biaxially at 45°. Dimensions in mm.

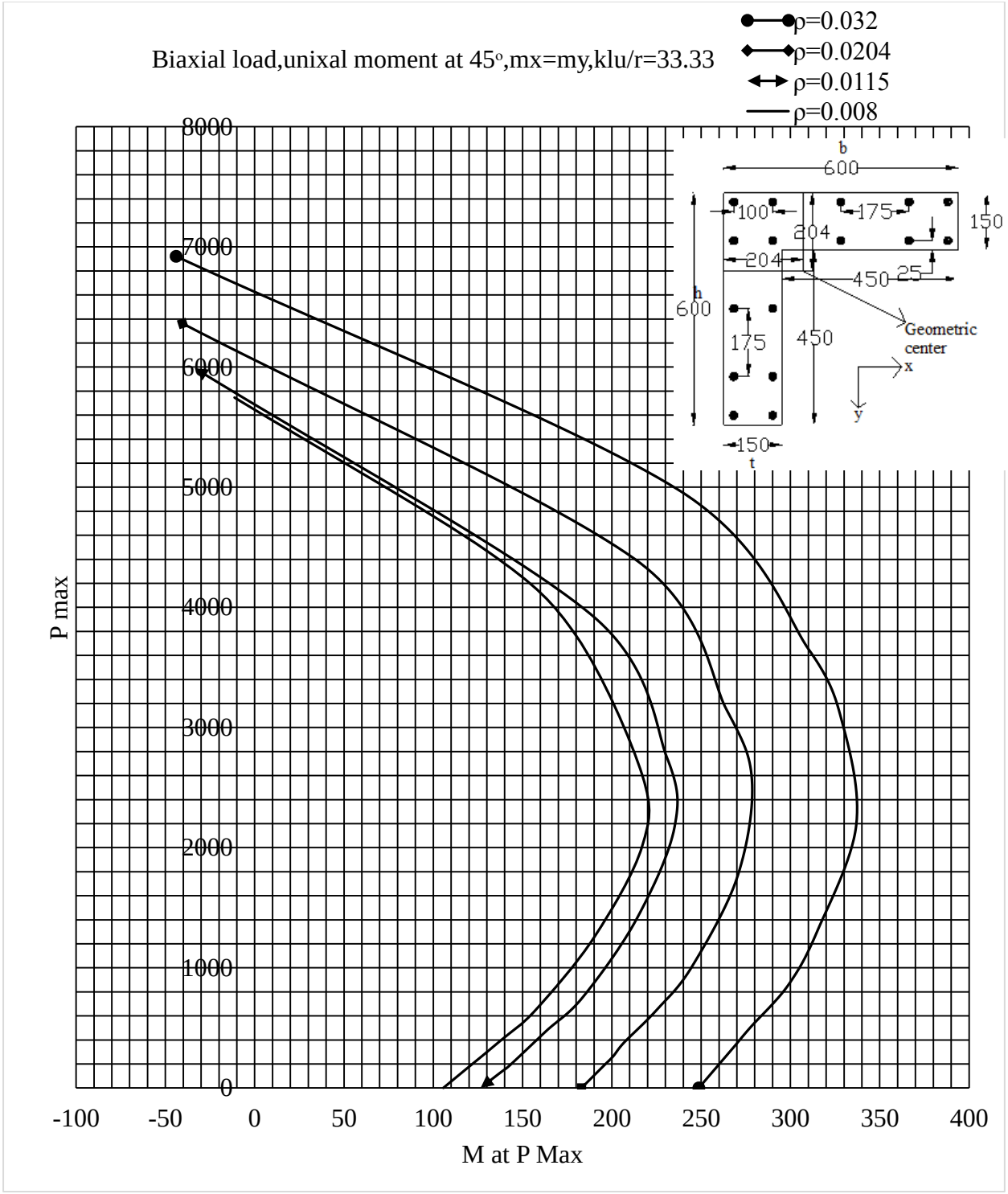

Figure A-9. P-M interaction diagrams of L-shaped wall using uniaxial moment for klu/r=33.33 loaded biaxially at 45°. Dimensions in mm.

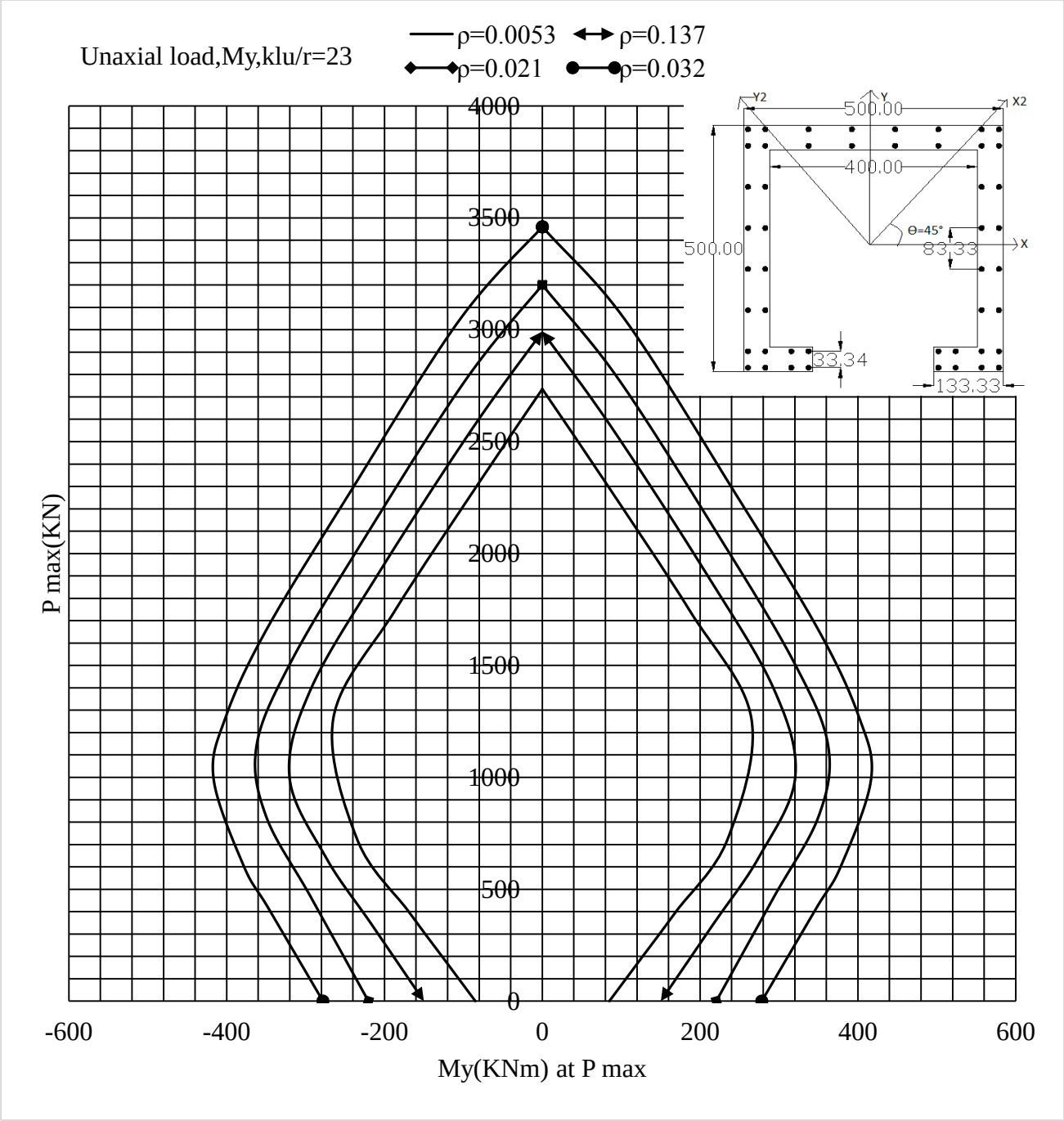

Figure A-10. P-M interaction diagrams of scaled down channel-shaped wall of klu/r=23 eccentrically loaded only in the X-direction. Dimensions in mm.

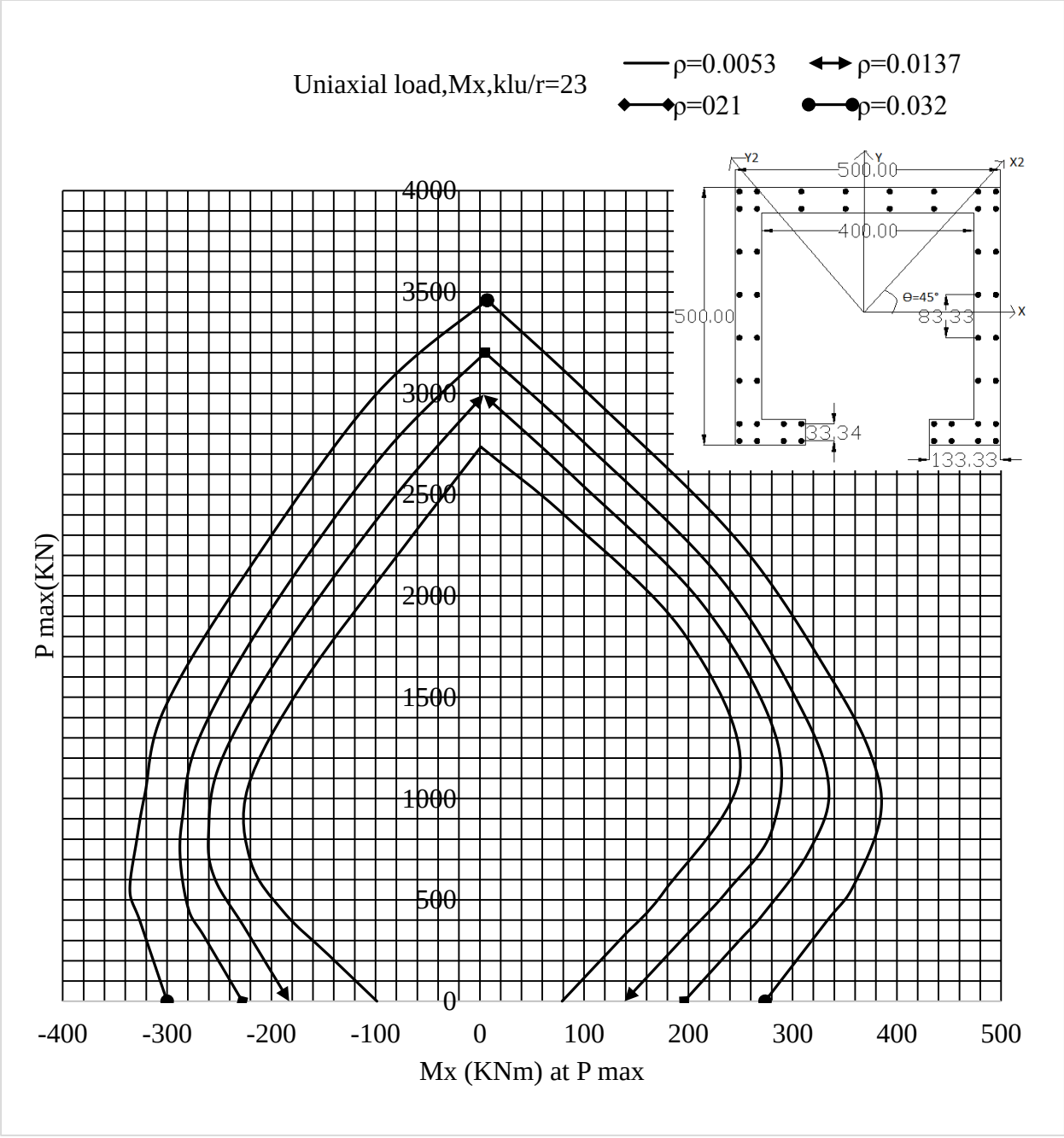

Figure A-11. P-M interaction diagrams of scaled down Channel-shaped wall of klu/r=23 eccentrically loaded only in the Y-direction. Dimensions in mm.

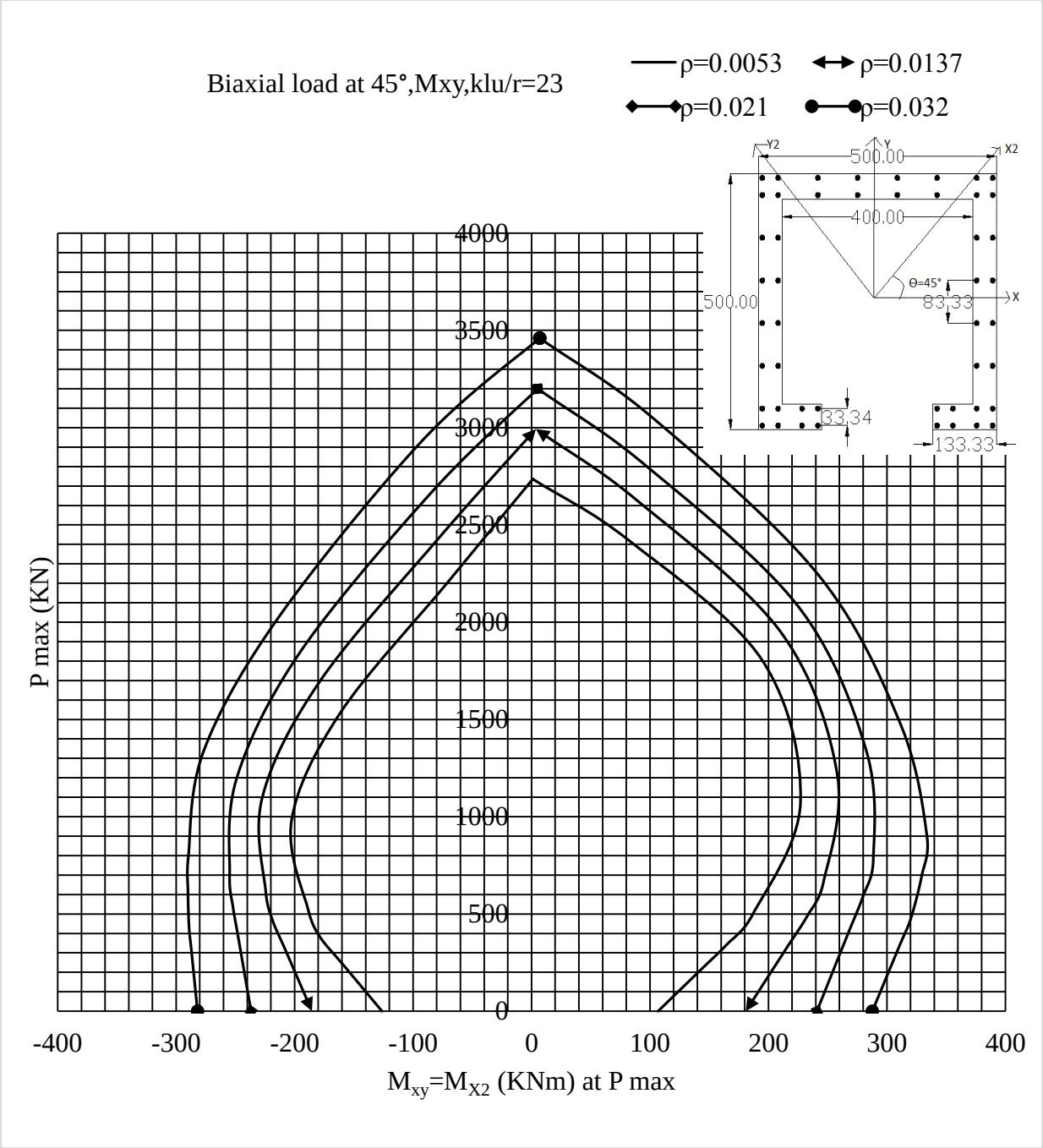

Figure A-12. P-M interaction diagrams of scaled down channel-shaped wall usning resultant moment for klu/r=23 loaded biaxially at 45°. Dimensions in mm.

Appendix B: Material properties used to model reinforced concrete column and walls

** Materials used for validation columns

*Material, name=concrete
*Elastic

(Young's modulus, Poisson's ratio)

37659, 0.2

*Concrete Damaged Plasticity

(Dilation angle, eccentricity, fb0/fc0, K_c ,viscosity parameter)

5., 0.1, 1.16, 0.67, 0.0001

*Concrete Compression Hardening

(Yield stress, inelastic strain)

18.6989, 0.

22.157, 1.16398e-05

25.5108, 2.25836e-05

28.7551, 3.64348e-05

31.8844, 5.33376e-05

34.893, 7.34459e-05

37.7748, 9.69242e-05

40.523, 0.000123948

43.1305, 0.000154707

45.5898, 0.000189402

47.8928, 0.00022825

50.0305, 0.000271484

51.9936, 0.000319355

53.772, 0.000372133

55.3545, 0.00043011

56.7294, 0.000493601

57.8838, 0.000562947

58.8037, 0.000638519

59.4741, 0.000720718

59.8784, 0.000809982

59.9987, 0.000906787

59.8154, 0.00101165

59.3071, 0.00112515

58.4502, 0.00124791

57.2189, 0.0013806

55.5848, 0.00152399

53.5164, 0.00167892

50.979, 0.0018463

47.9339, 0.00202716

44.3383, 0.00222264

40.1442, 0.00243401

*Concrete Tension Stiffening, type=DISPLACEMENT

(Tensile yield stress, displacement)

4.17949, 0.

3.74988, 0.01

*Concrete Compression Damage

(Damage parameter, inelastic strain)

0, 0

0, 1.16398e-05

0, 2.25836e-05

0, 3.64348e-05

0, 5.33376e-05

0, 7.34459e-05

0, 9.69242e-05

0, 0.000123948

0, 0.000154707

0, 0.000189402

0, 0.00022825

0, 0.000271484

0, 0.000319355

0, 0.000372133

0, 0.00043011

0, 0.000493601

0, 0.000562947

0, 0.000638519

0, 0.000720718

0, 0.000809982

0, 0.000906787

0.0030764, 0.00101165

0.0115485, 0.00112515

0.0258298, 0.00124791

0.0463511, 0.0013806

0.0735865, 0.00152399

0.10806, 0.00167892

0.15035, 0.0018463

0.201101, 0.00202716

0.261028, 0.00222264

0.33093, 0.00243401

*Concrete Tension Damage, type=DISPLACEMENT

(Damage parameter, displacement)

0, 0

0.102791, 0.01

*Material, name=longitudinal reinforcement

*Elastic

(Young’s modulus, Poisson’s ratio)

200000, 0.3

*Plastic

(Yield stress, plastic strain)

581.68, 0.

581.68, 0.0005

*Material, name=stirrup

*Elastic

(Young’s modulus, Poisson’s ratio)

200000, 0.3

*Plastic

(Yield stress, plastic strain)

340.578, 0

340.578, 0.0005

*Plastic

(Yield stress, plastic strain)

290.42, 0

290.42, 0.0005

*Plastic

(Yield stress, plastic strain)

652.109, 0

652.109, 0.0005

** Materials used for modeling rc walls

*Material, name=concrete

*Elastic

(Young’s modulus, Poisson’s ratio)

31476, 0.2

*Concrete Damaged Plasticity

(Dilation angle, eccentricity, fb0/fc0, viscosity parameter)

5., 0.1, 1.16, 0.67, 0.0001

*Concrete Compression Hardening

(Yield stress, inelastic strain)

6.25784, 0

9.12544, 1.00808e-05

11.8212, 2.4434e-05

14.347, 4.41892e-05

16.7045, 6.92907e-05

18.8954, 9.96837e-05

20.9215, 0.000135314

22.7844, 0.000176128

24.4858, 0.000222074

26.0274, 0.0002731

27.4106, 0.000329153

28.6372, 0.000390185

29.7086, 0.000456144

30.6265, 0.000526982

31.3924, 0.000602651

32.0077, 0.000683101

32.474, 0.000768287

32.7927, 0.00085816

32.9653, 0.000952677

32.9933, 0.00105179

32.8779, 0.00115545

32.6207, 0.00126363

32.2229, 0.00137627

31.686, 0.00149332

31.0113, 0.00161476

30.2, 0.00174053

29.2536, 0.0018706

28.1733, 0.00200492

26.9604, 0.00214346

25.6161, 0.00228616

24.1417, 0.00243301

22.5384, 0.00258394

20.8074, 0.00273894

18.9499, 0.00289795

*Concrete Tension Stiffening, type=DISPLACEMENT

(Tensile yield stress, displacement)

2.56496, 0

2.31907, 0.01

*Concrete Compression Damage

(Damage parameter, inelastic strain)

0, 0

0, 1.00808e-05

0, 2.4434e-05

0, 4.41892e-05

0, 6.92907e-05

0, 9.96837e-05

0, 0.000135314

0, 0.000176128

0, 0.000222074

0, 0.0002731

0, 0.000329153

0, 0.000390185

0, 0.000456144

0, 0.000526982

0, 0.000602651

0, 0.000683101

0, 0.000768287

0, 0.00085816

0, 0.000952677

0, 0.00105179

0.00369998, 0.00115545

0.0114954, 0.00126363

0.0235487, 0.00137627

0.0398189, 0.00149332

0.0602651, 0.00161476

0.0848475, 0.00174053

0.113526, 0.0018706

0.146263, 0.00200492

0.183018, 0.00214346

0.223753, 0.00228616

0.268432, 0.00243301

0.317017, 0.00258394

0.369472, 0.00273894

0.425759, 0.00289795

*Concrete Tension Damage, type=DISPLACEMENT

(Damage parameter, displacement)

0, 0

0.095865, 0.01

*Material, name=steel

*Elastic

(Young’s modulus, Poisson’s ratio)

200000, 0.3

*Plastic

(Yield stress, plastic strain)

420.881, 0

420.881, 0.0005

Appendix C: Sample illustrations for concrete compression damage and axial stress distribution of C-shaped wall with variation of eccentricities.

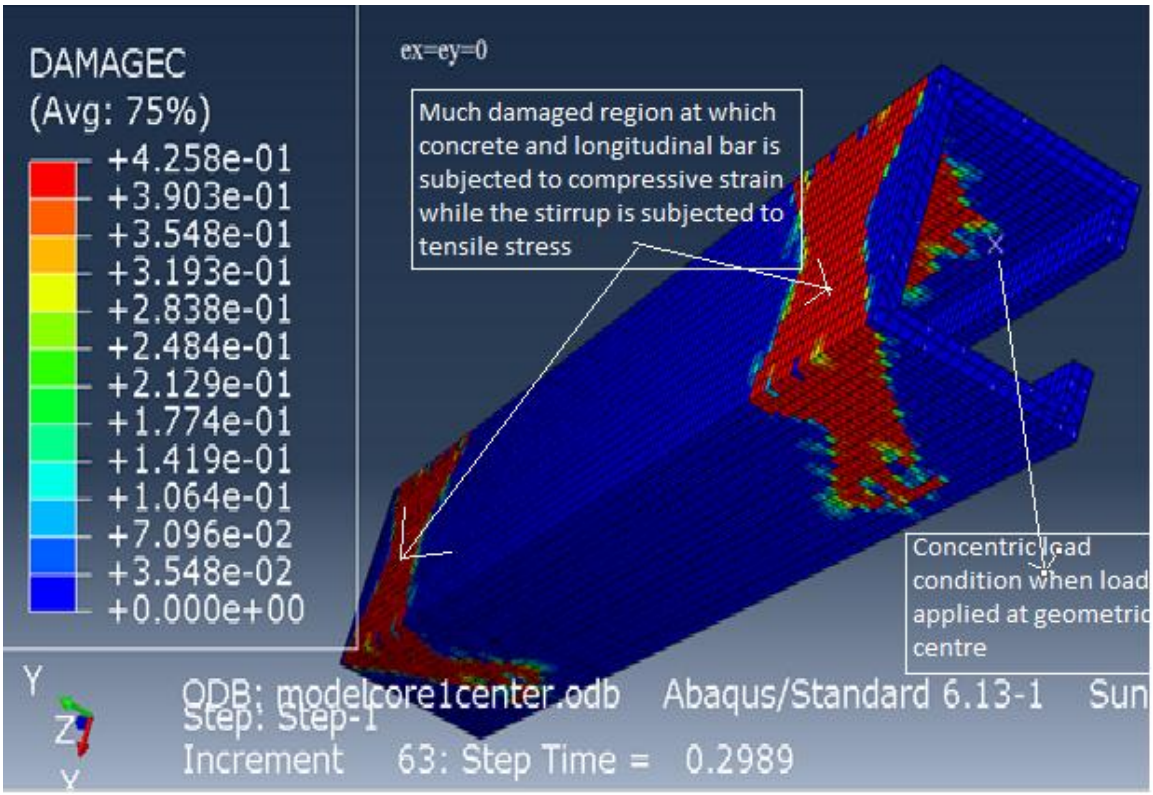

Figure C-1. Concrete compression damage of C-shaped reinforcement concrete wall at concentric load

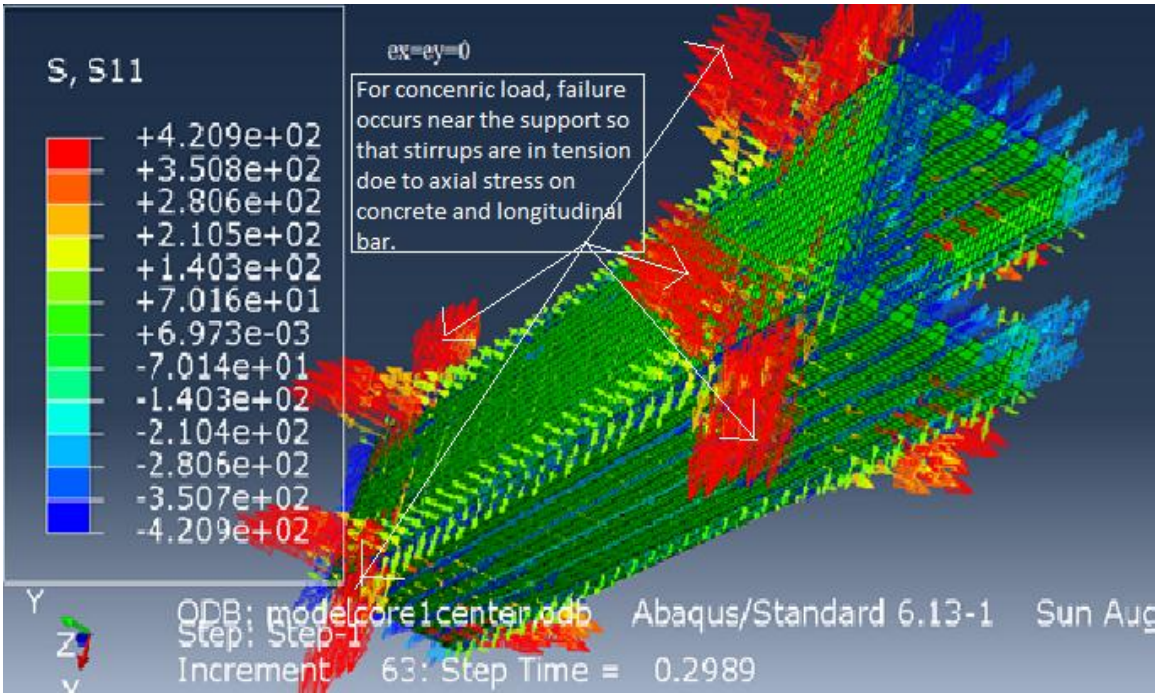

Figure C-2. Stress distribution of reinforcement steel of C-shaped wall at concentric load

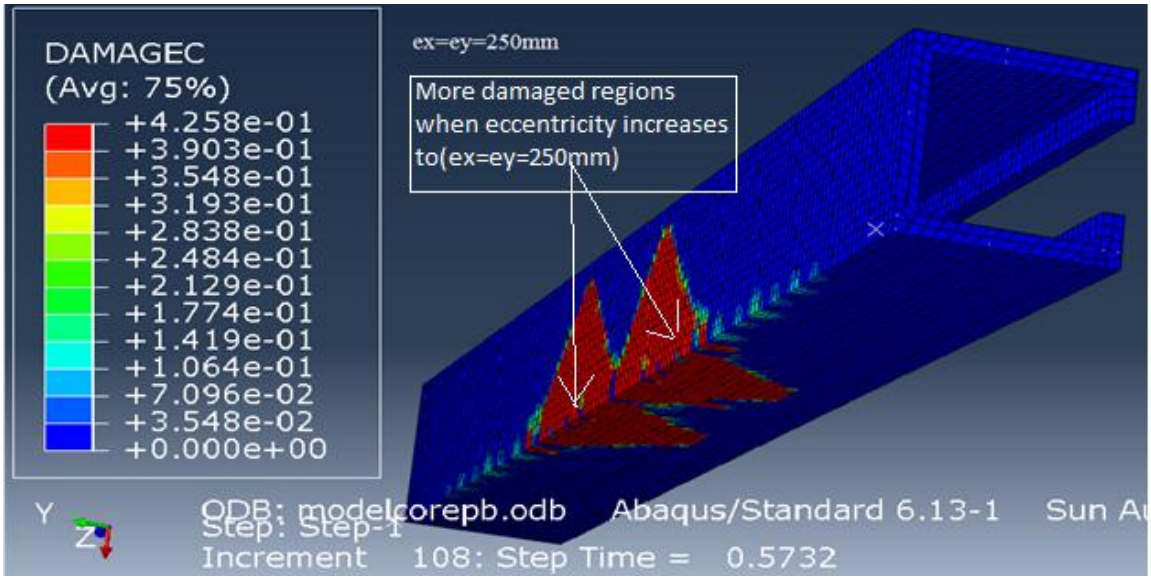

Figure C-3. Concrete compression damage of C-shaped reinforcement concrete wall at balanced failure.

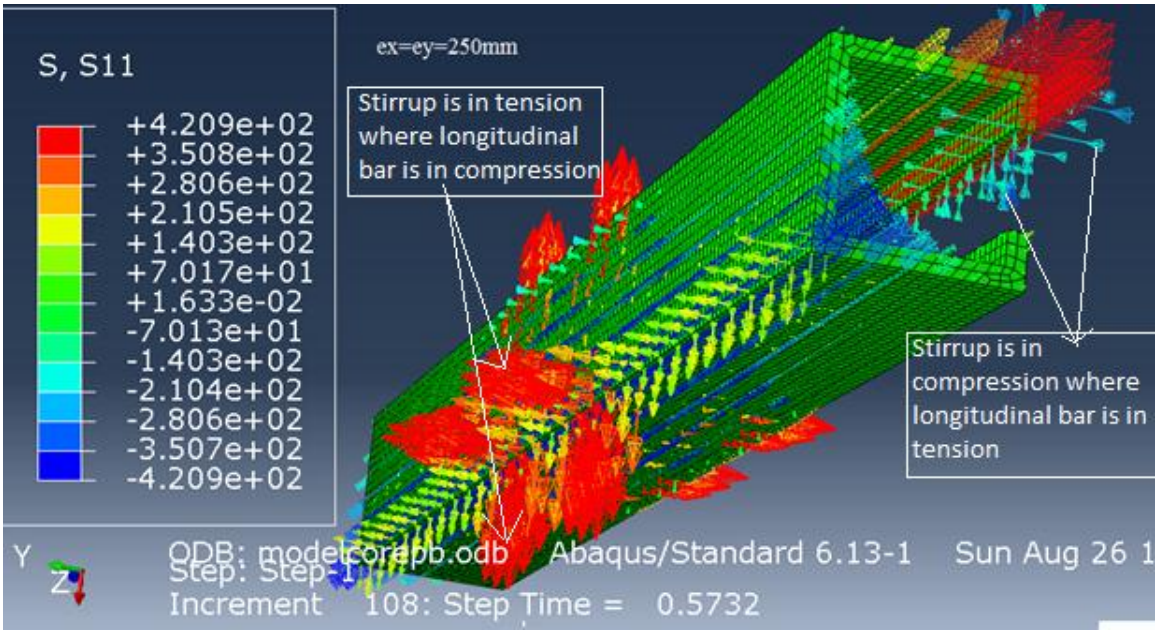

Figure C-4. Stress distribution of reinforcement steel of C-shaped wall at balanced failure.

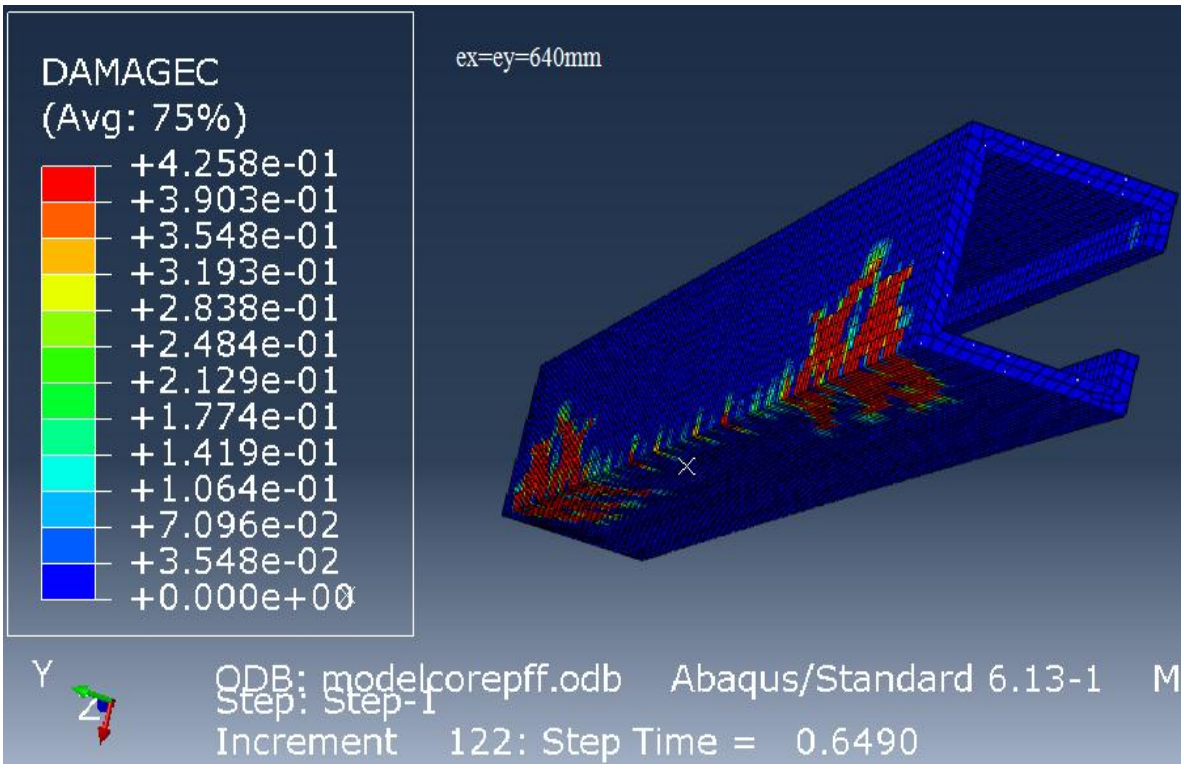

Figure C-5: Concrete compression damage of C-shaped reinforcement concrete wall at flexural failure.

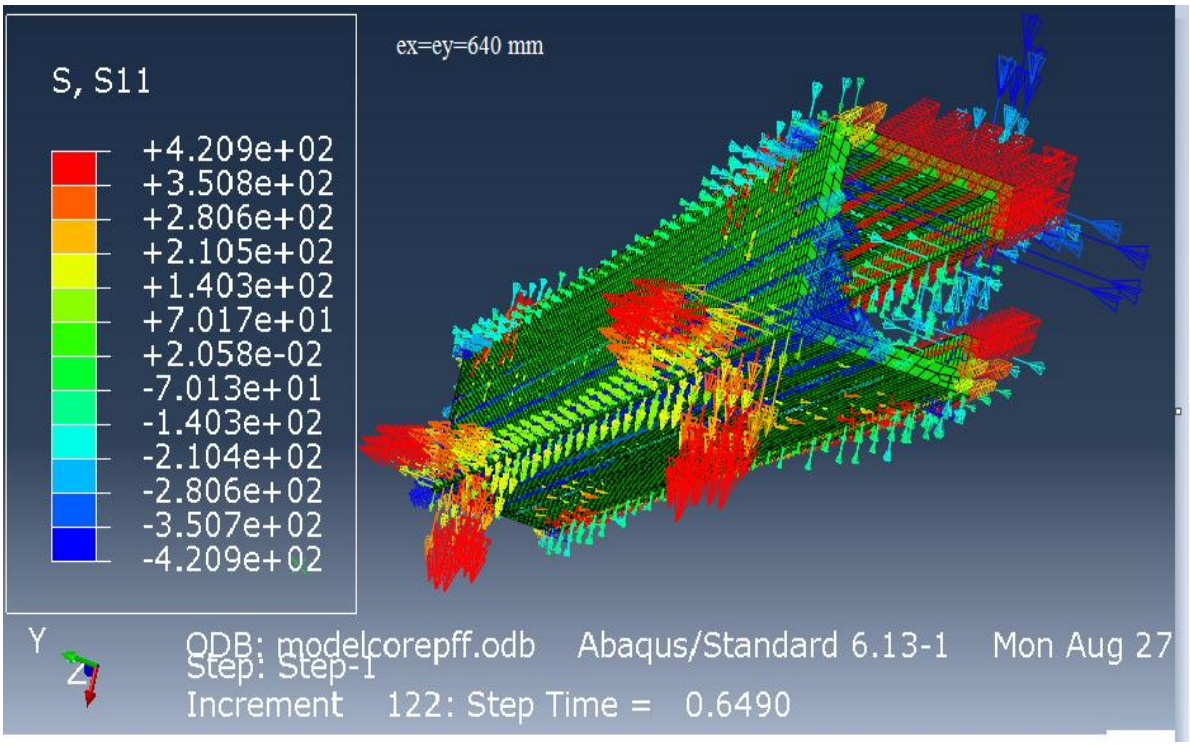

Figure C-6: Stress distribution of reinforcement steel of C-shaped wall at flexural failure.

Appendix D: Sample P-M interaction diagram plotting illustration for biaxial bending of L-shaped wall of klu/r=22 and ρ=0.032.

ex=ey (mm)	δx (mm)	δy (mm)	(δx) x(-1)	(δy) x(-1)	Pmax (N)	Pmax/ 1000 (KN)	(ex+δx)/ 1000(m)	(ey+δy)/ 1000(m)	(my=Pmax/1000)x ((ex+δx)/1000)(KNm)	P max (KN)	mx=(Pmax /1000)x ((ey+δy)/1000)(KNm)	P max KN)	Resultant moment(mxy)(KNm)	P max
0.00	1.27	1.36	-1.27	-1.36	7055129.00	7055.13	0.00	0.00	-8.99	7055.13	-9.59	7055.13	-13.15	7055.13
30.00	-7.48	-7.12	7.48	7.12	5413117.50	5413.12	0.04	0.04	202.90	5413.12	200.93	5413.12	285.55	5413.12
60.00	-10.39	-10.16	10.39	10.16	4086088.50	4086.09	0.07	0.07	287.63	4086.09	286.66	4086.09	406.08	4086.09
80.00	-12.31	-12.14	12.31	12.14	3445566.75	3445.57	0.09	0.09	318.05	3445.57	317.46	3445.57	449.37	3445.57
120.00	-15.29	-15.18	15.29	15.18	2503496.75	2503.50	0.14	0.14	338.71	2503.50	338.43	2503.50	478.81	2503.50
200.00	-19.55	-19.49	19.55	19.49	1473805.38	1473.81	0.22	0.22	323.57	1473.81	323.48	1473.81	457.54	1473.81
300.00	-22.77	-22.72	22.77	22.72	942508.81	942.51	0.32	0.32	304.22	942.51	304.17	942.51	430.19	942.51
500.00	-24.29	-24.26	24.29	24.26	534431.88	534.43	0.52	0.52	280.20	534.43	280.18	534.43	396.25	534.43
700.00	-27.28	-27.24	27.28	27.24	373131.09	373.13	0.73	0.73	271.37	373.13	271.36	373.13	383.77	373.13
1000.00	-35.02	-34.96	35.02	34.96	256830.78	256.83	1.04	1.03	265.82	256.83	265.81	256.83	375.92	256.83
									253.58	0.00	253.56	0.00	358.60	0.00